1-1-2015

Ab initio Quantum Chemistry Methods for Modeling Molecular Excited States Beyond Configuration Interaction Singles

Xinle Liu
University of Pennsylvania, liuxl89@gmail.com

Ab initio Quantum Chemistry Methods for Modeling Molecular Excited States Beyond Configuration Interaction Singles

Abstract
Electron transfer and energy transfer play a central role in photo-induced excited state chemical dynamics and are critical for understanding the fundamental processes in photosynthesis. Understanding electron and energy transfer at the molecular level is essential, since they must compete with deactivation processes back to the molecular ground state-- and deactivation releases any captured energies as wasted heat. Modeling electronic relaxation process is very challenging, however, for 2 reasons: i) Obtaining accurate potential energy surfaces (PESs) by solving the electronic Hamiltonian (only) is nontrivial, since all electrons are coupled together, which is essentially a many-body problem. It is even more difficult in the context of photochemistry, where the relevant molecules are typically big; ii) The Born-Oppenheimer Approximation of separating electronic and nuclear motion may be invalid, and thus one has to model nonadiabatic dynamics. This thesis is focused on the first problem above, i.e. solving the electronic Hamiltonian, where there is currently a lack of effective ab initio quantum chemistry methods, especially in the presence of charge transfer (CT) states.

Historically Configuration Interaction Singles (CIS) has been the standard method for modeling electronic excited states with qualitatively correct wavefunctions, but CIS is highly biased against charge transfer states-- which are very important for modeling photo-induced relaxation. Nevertheless, in this thesis, CIS proves to be a good starting point for improved ab initio quantum chemistry methods, that build in the correct molecular orbital optimization. These algorithms are labeled as: i) Orbital Optimized Configuration Interaction Singles (OO-CIS), ii) Variational Orbital Adapted Configuration Interaction Singles (VOA-CIS), and iii) Fully Variational Orbital Adapted Configuration Interaction Singles (FVOA-CIS).

Each of the three algorithms above represents an improvement upon its predecessor. i) OOCIS is able to recover perturbative corrections for CT states; ii) its variational extension VOA-CIS proves to be very effective for constructing globally smooth adiabatic PESs even with CT states; and iii) because it is fully variational, FVOA-CIS PESs are so smooth that it should allow analytic gradients. We believe these approaches will be widely used for future accurate electronic structure calculations.

Degree Type
Dissertation

Degree Name
Doctor of Philosophy (PhD)

Graduate Group
Chemistry

First Advisor
Joseph E. Subotnik

Keywords
ab initio, charge transfer, diabatization, excited states, orbital optimized, variational

Subject Categories
Chemistry | Physical Chemistry

AB INITIO QUANTUM CHEMISTRY METHODS FOR MODELING MOLECULAR EXCITED STATES BEYOND CONFIGURATION INTERACTION SINGLES

Xinle Liu

A DISSERTATION

in

Chemistry

Presented to the Faculties of the University of Pennsylvania

in Partial Fulfillment of the Requirements for the

Degree of Doctor of Philosophy

2015

Supervisor of Dissertation

Joseph E. Subotnik, Associate Professor of Chemistry

Graduate Group Chairperson

Gary A. Molander, Hirschmann-Makineni Professor of Chemistry

Dissertation Committee

Andrew M. Rappe	Professor of Chemistry and Materials Science and Engineering
Marsha I. Lester	Edmund J. Kahn Distinguished Professor
Charles L. Kane	Walter H. and Leonore C. Annenberg Professor in the Natural Sciences

To my family,

for their love and support

ACKNOWLEDGEMENT

First of all, I would like to express my sincere gratitude to my thesis advisor, Prof. Joseph Subotnik. His devotion and enthusiasm to science, innovative ideas, creative questions, giving us the great freedom to work on whatever we are interested in, doing all he can to help everyone achieving academic goals, have not only been my motivation for research, but also showed me how to be a successful mentor in academia.

I would also like to thank Prof. Andrew Rappe, Prof. Robin Hochstrasser, Prof. Marsha Lester and Prof. Charles Kane as my committee members. It has been a great pleasure presenting my research progress to them, which is also a fabulous opportunity learning from them, aside from sitting in their classes. I have benefited a lot from their insightful questions, helpful suggestions, terrific guidance for future directions, and their role models as first-class scientists.

Together with my collaborators, Dr. Yihan Shao, Dr. Shervin Fatehi, Dr. Brad S. Veldkamp, Dr. Ethan Alguire, Qi Ou, I have been making steady progress more than what I can achieve on my own. Many thanks to them for working patiently with me, and for the fruitful discussions.

The same goes for all other members in the Subotnik research group, Dr. Brain Landry, Dr. Kousik Samanta, Dr. Andrew Petit, Wenjun Ouyang, Wenjie Dou, for a very nice lab environment. I would also like to thank all my friends outside lab as well, Dr. Wenkai Zhang, Dr. Gaoyang Gou, Dr. Lai Jiang, Dr. Yubin Bai, Dr. Na Zhang, Dr. Zhaoxia Qian, Dr. Lu Gao, Dr. Shi Liu, Fan Zheng, Dr. Ruiteng Li, Hao Zhou, Dr. Yichao Lu, Zheng Shi, Dr. Fang Liu, Chun-wei Lin, Diomedes Saldana Greco, Yubo Qi, Dr. Jingmin Chen, Lisha Qiu and Wenhao Liu, for their friendship and having lots of fun together at graduate school. There are so many people helping me as well, after my moving away from Philadelphia, among them I would like to thank Dr. Jixia Dai, Dr. Qinglei Meng, Dr. Yanan Geng and

Dr. Sai Zhang sincerely.

Last but not the least, thanks to my parents, my brother and sister-in-law, without whom I can never imagine where I would otherwise be as a female, and with whom I am able to "lean in" steadily in my life.

ABSTRACT

AB INITIO QUANTUM CHEMISTRY METHODS
FOR MODELING MOLECULAR EXCITED STATES
BEYOND CONFIGURATION INTERACTION SINGLES

Xinle Liu

Joseph E. Subotnik

Electron transfer and energy transfer play a central role in photo-induced excited state chemical dynamics and are critical for understanding the fundamental processes in photosynthesis. Understanding electron and energy transfer at the molecular level is essential, since they must compete with deactivation processes back to the molecular ground state– and deactivation releases any captured energies as wasted heat. Modeling electronic relaxation process is very challenging, however, for 2 reasons: i) Obtaining accurate potential energy surfaces (PESs) by solving the electronic Hamiltonian (only) is nontrivial, since all electrons are coupled together, which is essentially a many-body problem. It is even more difficult in the context of photochemistry, where the relevant molecules are typically big; ii) The Born-Oppenheimer Approximation of separating electronic and nuclear motion may be invalid, and thus one has to model nonadiabatic dynamics. This thesis is focused on the first problem above, i.e. solving the electronic Hamiltonian, where there is currently a lack of effective *ab initio* quantum chemistry methods, especially in the presence of charge transfer (CT) states.

Historically Configuration Interaction Singles (CIS) has been the standard method for modeling electronic excited states with qualitatively correct wavefunctions, but CIS is highly biased against charge transfer states– which are very important for modeling photo-induced relaxation. Nevertheless, in this thesis, CIS proves to be a good starting point for improved *ab initio* quantum chemistry methods, that build in the correct molecular orbital

optimization. These algorithms are labeled as: i) Orbital Optimized Configuration Interaction Singles (OO-CIS), ii) Variational Orbital Adapted Configuration Interaction Singles (VOA-CIS), and iii) Fully Variational Orbital Adapted Configuration Interaction Singles (FVOA-CIS).

Each of the three algorithms above represents an improvement upon its predecessor. i) OO-CIS is able to recover perturbative corrections for CT states; ii) its variational extension VOA-CIS proves to be very effective for constructing globally smooth adiabatic PESs even with CT states; and iii) because it is fully variational, FVOA-CIS PESs are so smooth that it should allow analytic gradients. We believe these approaches will be widely used for future accurate electronic structure calculations.

TABLE OF CONTENTS

NOTATIONS

N_n:	Number of nuclei in a molecule
N_e, N:	Number of electrons in a molecule
N_B:	Number of basis functions
N_o:	Number of occupied orbitals
N_v:	Number of virtual orbitals
M_α:	Mass of nucleus α
m:	Mass of electrons
$\mathbf{R}_\alpha$:	Spatial coordinate of nucleus α
$\mathbf{r}$:	Spatial coordinate of an electron
$\mathbf{x} = (\mathbf{r}, \omega)$:	Coordinate of an electron (spatial and spin)
$E_n^{(\mathrm{k})}$:	kth order correction for E_n
$\lvert n^{(\mathrm{k})}\rangle$:	kth order correction for $\lvert n\rangle$
$\lvert\chi\rangle$:	Atomic Orbital (AO)
$\lvert\phi\rangle$:	Molecular Orbital (MO)
$C_{\mu p}$:	MO Coefficients
$\mathbf{U}$:	Unitary transformation matrix
$\lvert\Phi\rangle$:	Ground state wavefunction
	Adiabatic states
$\lvert\Psi\rangle$:	Electronically excited state wavefunction
$\lvert\Xi\rangle$:	Diabatic states
$\mu, \nu, \lambda, \sigma$:	Index for AOs
i, j, k, l:	Index for occupied MOs or electrons
a, b, c, d:	Index for virtual MOs
p, q, r, s:	Index for any MOs
I, J, K, L:	Index for excited states (adiabatic)
A, B:	Index for diabatic states
$\tilde{I}, \tilde{J}, \tilde{K}, \tilde{L}$:	Index for ground state or excited states
$a_p^\dagger$:	Creation Operator in $\lvert\phi_p\rangle$
a_p:	Annihilation Operator in $\lvert\phi_p\rangle$
$\langle pq\lvert rs\rangle$:	$\displaystyle\int \phi_p^*(\mathbf{x}_1)\, \phi_q^*(\mathbf{x}_2)\, \frac{1}{\lvert\mathbf{x}_1 - \mathbf{x}_2\rvert}\, \phi_r(\mathbf{x}_1)\, \phi_s(\mathbf{x}_2)\, d\mathbf{x}_1\, d\mathbf{x}_2$
$\langle pq \,\lvert\rvert\, rs\rangle$:	$\langle pq\lvert rs\rangle - \langle pq\lvert sr\rangle$
t:	CIS amplitudes
f:	Oscillator Strength
$A \pm B$:	Value (A) $\pm$ Standard Error (B)

LIST OF TABLES

LIST OF ILLUSTRATIONS

LIST OF ALGORITHMS

CHAPTER 1 : Introduction

1.1. Basic Quantum Chemistry Theory

1.1.1. Born-Oppenheimer Approximation

Modern quantum chemistry desires an accurate description of electronically excited states, especially for medium-sized or large organic molecules widely involved in photosynthesis. When chromophores absorb a photon in the UV-visible region, electrons can undergo an ultrafast (∼fs) excitation, triggering electron transfer and energy transfer within the molecule, or even with molecules in the vicinity. Modeling an accurate potential energy surface is challenging, due to the many-body interactions in the Hamiltonian Ref. [8], [9] and [10]. Assume we have a molecular system of N_n nuclei and N_e electrons, with their masses being M_α and m, and their charges being $Z_\alpha e$ and e respectively, then the Hamiltonian can be written as:

$$\begin{aligned}\hat{H} = \; & -\sum_{\alpha=1}^{N_n} \frac{\hbar^2}{2M_\alpha}\nabla_\alpha^2 - \sum_{i=1}^{N_e} \frac{\hbar^2}{2m}\nabla_i^2 \\ & + \sum_{\substack{\alpha=1 \\ \beta=1 \\ \alpha\neq\beta}}^{N_n} \frac{Z_\alpha Z_\beta e^2}{|\mathbf{R}_\alpha - \mathbf{R}_\beta|} - \sum_{\alpha=1}^{N_n}\sum_{i=1}^{N_e} \frac{Z_\alpha e^2}{|\mathbf{R}_\alpha - \mathbf{r}_i|} + \sum_{\substack{i=1 \\ j=1 \\ i\neq j}}^{N_e} \frac{e^2}{|\mathbf{r}_i - \mathbf{r}_j|}\end{aligned} \tag{1.1}$$

The first two terms correspond to the kinetic energies of nuclei and electrons respectively, while the last three terms represent potential energies. More specifically, they are interactions among nuclei, between nuclei and electrons, and among electrons that can be potentially strong. All these motions are coupled together, making it extremely difficult to solve for an *exact* solution to $\hat{H}$.

Fortunately, as is well known, the mass of electrons are much smaller than that of nuclei (ratio $\leq \frac{1}{1836}$), such that the motion of the former is typically much faster than the latter. The Born-Oppenheimer approximation assumes that the motions of electrons are so fast that they can respond instantaneously to any motion of the much heavier (and thus much slower) nuclei. In this way, one can separate the total Hamiltonian into two parts. One

is the motion of electrons corresponding to a stationary set of nuclear configuration $\{\mathbf{R}_\alpha\}$, at any instant of time. The set of eigenstates for the electrons Hamiltonian are the so-called *adiabatic* electronic states, which form a complete basis set for electronic motion; the eigenvalues of the electronic Hamiltonian are a set of potential energy surfaces (PESs), for the typically much slower motion for nuclei. The equation for electrons *only* is the following (where $\hat{H}_e$ is called the electronic Hamiltonian):

$$\hat{H}_e = -\sum_{i=1}^{N_e} \frac{\hbar^2}{2m}\nabla_i^2 + \sum_{\substack{i=1 \\ j=1 \\ i\neq j}}^{N_e} \frac{e^2}{|\mathbf{r}_i - \mathbf{r}_j|} - \sum_{\alpha=1}^{N_n}\sum_{i=1}^{N_e} \frac{Z_\alpha e^2}{|\mathbf{R}_\alpha - \mathbf{r}_i|} \tag{1.2}$$

and then the total Hamiltonian (nuclear plus electronic) reduces to:

$$\hat{H} = -\sum_{\alpha=1}^{N_n} \frac{\hbar^2}{2M_\alpha}\nabla_\alpha^2 + \sum_{\substack{\alpha=1 \\ \beta=1 \\ \alpha\neq\beta}}^{N_n} \frac{Z_\alpha Z_\beta e^2}{|\mathbf{R}_\alpha - \mathbf{R}_\beta|} + E_e \tag{1.3}$$

where E_e is the eigenvalue one gets when solving for $\hat{H}_e$, which constructs a potential energy surface for the nuclei. In the end, the total wavefunction (nuclear plus electronic) is a product of the electronic one and the nuclear one:

$$|\Psi(\{\mathbf{r}_i\};\{\mathbf{R}_\alpha\})\rangle = |\Psi_e(\{\mathbf{r}_i\}|\{\mathbf{R}_\alpha\})\rangle\,|\Psi_n(\{\mathbf{R}_\alpha\})\rangle \tag{1.4}$$

The advantage of separating the motion of electrons from that of nuclei is that, if the potential energy surface E_e is well separated from other potential energy surface, and if we assume that nuclei are so slow that they can be treated classically, then Eqn. 1.3 can be solved with Newtonian Mechanics if we replace the Laplacian $-\frac{\hbar^2}{2M_\alpha}\nabla_\alpha^2$ by the classical kinetic energy $\frac{P^2}{2M_\alpha}$. That being said, Eqn. 1.2 must always be solved from quantum mechanics. In fact, even solving Eqn. 1.2 *only* within chemical accuracy, has been the most challenging problem in quantum chemistry, due to the many-body interactions among electrons, which is the primary motivation for this thesis.

1.1.2. Mean Field Approximation

As mentioned in Sec. 1.1.1, Eqn. 1.2 is still a many-body problem, with all electronic motions still coupled together; as such, solving Eqn. 1.2 *exactly* is still very difficult. A further approximation is the mean field approximation. The main idea is to reduce a n-body problem to n 1-body problem with a good choice of external field as a replacement. Normally, the external field is the average or effective interaction of one electron with all other electrons.

A mean field approximation is able to reduce the n-body problem to n 1-body problem, and as such the problem one has to solve is simplified a lot. Moreover, all electrons are treated equivalently. As such, it has been widely used in modern quantum chemistry.

1.1.3. Slater Determinant and Hartree-Fock Approximation

With approximations in Sec. 1.1.1 and Sec. 1.1.2, solving Eqn. 1.2 can be simplified a lot. Note that it is also constrained by the Pauli Exclusion Principle, which means that a many-electron wavefunction must be antisymmetric with respect to the interchange of the coordinate $\mathbf{x} \equiv (\mathbf{r}, \omega)$, which accounts for not only the spatial coordinate $\mathbf{r}$, but also its spin coordinate ω.

$$|\Psi(\cdots \mathbf{x}_i \cdots \mathbf{x}_j \cdots)\rangle = -|\Psi(\cdots \mathbf{x}_j \cdots \mathbf{x}_i \cdots)\rangle \tag{1.5}$$

Thus from the conclusion of linear algebra, a many-body wavefunction had better reads as a determinant, then Eqn. 1.5 is satisfied trivially:

$$|\Psi(\mathbf{x}_1 \cdots \mathbf{x}_N)\rangle = \frac{1}{\sqrt{N!}} \begin{vmatrix} \chi_1(\mathbf{x}_1) & \cdots & \chi_i(\mathbf{x}_1) & \cdots & \chi_j(\mathbf{x}_1) & \cdots & \chi_N(\mathbf{x}_1) \\ \vdots & \ddots & \vdots & \ddots & \vdots & \ddots & \vdots \\ \chi_1(\mathbf{x}_i) & \cdots & \chi_i(\mathbf{x}_i) & \cdots & \chi_j(\mathbf{x}_i) & \cdots & \chi_N(\mathbf{x}_i) \\ \vdots & \ddots & \vdots & \ddots & \vdots & \ddots & \vdots \\ \chi_1(\mathbf{x}_j) & \cdots & \chi_i(\mathbf{x}_j) & \cdots & \chi_j(\mathbf{x}_j) & \cdots & \chi_N(\mathbf{x}_j) \\ \vdots & \ddots & \vdots & \ddots & \vdots & \ddots & \vdots \\ \chi_1(\mathbf{x}_N) & \cdots & \chi_i(\mathbf{x}_N) & \cdots & \chi_j(\mathbf{x}_N) & \cdots & \chi_N(\mathbf{x}_N) \end{vmatrix} \tag{1.6}$$

or, it can be written equivalently in a more compact way: $|\chi_1 \cdots \chi_i \cdots \chi_j \cdots \chi_N\rangle$. Starting with a given set of atomic orbitals (AOs) $\{|\chi_\mu\rangle\}$, one can write molecular orbitals (MOs) $\{|\phi_p\rangle\}$ as a linear combination of AOs, with a transformation matrix $C_{\mu p}$:

$$|\phi_p\rangle = C_{\mu p} \, |\chi_\mu\rangle \tag{1.7}$$

Hence, solving for MOs $\{\phi_p\}$ is equivalent to solve for the best MO Coefficient matrix $C_{\mu p}$.

Since the ground state is the most stable state for a given molecular system, one can get the best set of molecular orbitals (MOs) according to the variational principle. According to the Hartree-Fock theory, it would be equivalent to solve the eigenvalue problem for spin-orbitals below:

$$\hat{f} \, |\phi_p\rangle = \varepsilon_p \, |\phi_p\rangle \tag{1.8}$$

in which the fock operator $\hat{f}$ can be written as:

$$\hat{f} \quad = \hat{h} + \sum_{j \neq i} \hat{J} - \sum_{j \neq i} \hat{K} \tag{1.9}$$

Here, $\hat{h}$ is the one-electron term:

$$\hat{h}\,|i\rangle = \left(-\frac{\hbar^2}{2m}\nabla_i^2 - \sum_\alpha \frac{Z_\alpha e^2}{|\mathbf{R}_\alpha - \mathbf{x}_i|} \right) |i\rangle \tag{1.10}$$

while both $\hat{J}$ and $\hat{K}$ are two-electron operators, which captures the interactions between them. More specifically, $\hat{J}$ is the Coulombic repulsion term:

$$\hat{J}\,|i\rangle = \sum_{j\neq i} \int \phi_i^*(\mathbf{x}_i)\ \phi_j^*(\mathbf{x}_j)\ \frac{e^2}{|\mathbf{x}_i - \mathbf{x}_j|}\ \phi_i(\mathbf{x}_i)\ \phi_j(\mathbf{x}_j)\ d\mathbf{x}_j \tag{1.11}$$

while K is the exchange term, which has no classic analogue:

$$\hat{K}\,|i\rangle = \sum_{j\neq i} \int \phi_i^*(\mathbf{x}_i)\ \phi_j^*(\mathbf{x}_j)\ \frac{e^2}{|\mathbf{x}_i - \mathbf{x}_j|}\ \phi_j(\mathbf{x}_i)\ \phi_i(\mathbf{x}_j)\ d\mathbf{x}_j \tag{1.12}$$

Both for these two terms result from the mean field approximation shown in Sec. 1.1.2, accounting for interactions among electrons. Eqn. 1.8 can be solved iteratively until self-consistent, as such the Hartree-Fock method is also called SCF-HF method.

In the end, the ground state energy from Hartree-Fock theory reads as:

$$E_{\text{HF}} \quad = \sum_i h_{ii} + \frac{1}{2}\sum_{i\neq j} \langle ij \,||\, ij\rangle \tag{1.13}$$

with the following notations:

$$\langle pq|rs\rangle \equiv \int \phi_p^*(\mathbf{x}_1)\ \phi_q^*(\mathbf{x}_2)\ \frac{1}{|\mathbf{x}_1 - \mathbf{x}_2|}\ \phi_r(\mathbf{x}_1)\ \phi_s(\mathbf{x}_2)\ d\mathbf{x}_1\ d\mathbf{x}_2 \tag{1.14}$$

$$\langle pq \,||\, rs\rangle \equiv \langle pq|rs\rangle - \langle pq|sr\rangle \tag{1.15}$$

Hartree-Fock theory, is the traditional starting point both for correlated ground state methods as well as for electronically excited states. By definition, a mean field approximation only accounts for an average or effective term for interactions between electrons, and therefore HF ignores any instantaneous interactions, which can be potentially problematic when

accuracy is critical. Fortunately, there are many post-HF methods, attempting to capture those correlations and improve the accuracy systematically. The main goal of this thesis is to explore *ab initio* quantum chemistry methods that yield a hopefully good trade-off between computational cost and accuracy, for both the ground state and excited states.

Note that, although this thesis focuses on wavefunction based methods, other popular methods exist as well. Among them, density function theory (DFT) is widely used for studying crystal structures and properties. Instead of solving for wavefunctions, which require conditional probabilities and phases, DFT solves for electron density directly (at least in principle).

1.1.4. Second Quantization

In the matrix form of quantum mechanics, all physical observables can be written as Hermitian operators, and thus all expressions can be evaluated conveniently through second quantization, with the creation operator $a_p^\dagger$ and the annihilation operator a_p, defined in Eqns. 1.16 and 1.17.

The creation operator $a_a^\dagger$ creates an electron in orbital $|\chi_a\rangle$:

$$a_a^\dagger |\chi_i \cdots \chi_j\rangle = |\chi_a \chi_i \cdots \chi_j\rangle \tag{1.16}$$

while the annihilation operator a_k destroies an electron in orbital $|\chi_k\rangle$:

$$a_k |\chi_k \chi_i \cdots \chi_j\rangle = |\chi_i \cdots \chi_j\rangle \tag{1.17}$$

With Eqns. 1.16 and 1.17, together with the antisymmetric property of Slater determinants,

it is very straightforward to show the identities below:

$$a_p^\dagger a_q^\dagger + a_q^\dagger a_p^\dagger = 0 \tag{1.18}$$

$$a_p a_q + a_q a_p = 0 \tag{1.19}$$

$$a_p^\dagger a_q + a_q a_p^\dagger = \delta_{pq} \tag{1.20}$$

Eqn. 1.20 is an essential identity, which allows us to move creation operators $a_i^\dagger$ or annihilation operators a_a to the right side of a braket, and moving creation operators $a_a^\dagger$ or annihilation operators a_i to the left side of a braket, eventually generate trivial terms for any matrix elements.

As a simple example:

$$\begin{aligned} a_i a_a^\dagger \left|\chi_i\right\rangle &= (\delta_{ai} - a_a^\dagger a_i) \left|\chi_i\right\rangle \\ &= -a_a^\dagger \left|\ \right\rangle \\ &= -\left|\chi_a\right\rangle \end{aligned} \tag{1.21}$$

The simple example shown in Eqn. 1.21 shows that, the net effect of operator $a_a^\dagger a_i$ is to transform wavefunction $|\chi_i\rangle$ to $|\chi_a\rangle$, which is equivalent to exciting one electron from occupied orbital $|\chi_i\rangle$ to virtual orbital $|\chi_a\rangle$.

Through second-quantization, excitations become very intuitive and straightforward. In fact, almost all matrix elements in this thesis have been evaluated through second quantization. When developing wavefunction methods, one frequently finds analytic expressions with more than 10 operators sandwiched between non-interacting bra's and ket's. In such a case, deriving the analytic equations is extremely tedious. Therefore, I have written scripts to evaluate such calculations whenever necessary. Any scripting language dealing with regular expressions can do the job.

1.2. Wavefunction-Based Methods

I will now discuss methods to go beyond mean-field theory to compute ground and excited states accurately.

1.2.1. Variational Theory

Given a Hamiltonian (H) and a set of basis functions $\{|\Phi_i\rangle, i = 1, 2 \cdots N\}$, the basic idea of variational method is have guess a "trial" wavefunction Ψ, consisting of variational parameters $\{c_i\}$:

$$|\Psi\rangle \quad = \sum_i c_i |\Phi_i\rangle \tag{1.22}$$

The variational parameters $\{c_i\}$ can be optimized to minimize the energy:

$$\begin{aligned} E_{\text{trial}} &= \frac{\langle \Psi | H | \Psi \rangle}{\langle \Psi | S | \Psi \rangle} \\ &= \frac{\sum_{ij} c_i c_j \langle \Phi_i | H | \Psi_j \rangle}{\sum_{ij} c_i c_j \langle \Phi_i | S | \Psi_j \rangle} \\ &\equiv \frac{\sum_{ij} c_i c_j H_{ij}}{\sum_{ij} c_i c_j S_{ij}} \end{aligned} \tag{1.23}$$

To minimize the energy for each state, one can differentiate Eqn. 1.23, to solve for the parameters.

It is not difficult to show that the variational method is equivalent to the following linear equations:

$$\begin{pmatrix} H_{11} & H_{12} & \cdots & H_{1N} \\ H_{21} & H_{22} & \cdots & H_{2N} \\ \vdots & \vdots & \ddots & \cdots \\ H_{N1} & H_{N2} & \cdots & H_{NN} \end{pmatrix} \begin{pmatrix} c_1 \\ c_2 \\ \vdots \\ c_n \end{pmatrix} = E \begin{pmatrix} S_{11} & S_{12} & \cdots & S_{1N} \\ S_{21} & S_{22} & \cdots & S_{2N} \\ \vdots & \vdots & \ddots & \cdots \\ S_{N1} & S_{N2} & \cdots & S_{NN} \end{pmatrix} \begin{pmatrix} c_1 \\ c_2 \\ \vdots \\ c_n \end{pmatrix} \tag{1.24}$$

In the language of linear algebra, this is no more than a *generalized* diagonalization problem, for the pair of Hamiltonian matrix H and the overlap matrix S, with parameters $\{c_i\}$ being the wavefunction, and with E being the state energy. It is also called the "secular" equation in quantum chemistry:

$$|H - ES| = \begin{vmatrix} H_{11} - ES_{11} & H_{12} - ES_{12} & \cdots & H_{1N} - ES_{1N} \\ H_{21} - ES_{21} & H_{22} - ES_{22} & \cdots & H_{2N} - ES_{2N} \\ \vdots & \vdots & \ddots & \cdots \\ H_{N1} - ES_{N1} & H_{N2} - ES_{N2} & \cdots & H_{NN} - ES_{NN} \end{vmatrix} = 0 \tag{1.25}$$

Note that, in solving Eqn. 1.25, one computes not only the ground state but also a set of excited states that are orthogonal to each other. The end product is a variational approximation to the exact wavefunction and energy.

Variational method predict an upper bound for all states, and in practice, the method is robust and reliable– but the computational cost can be pretty expensive by diagonalizing a big matrix. If one cares only about the lowest lying n states, the Davidson algorithm is widely used to save the computational cost, as discussed in Sec. 5.2.2.

CIS. Configuration Interaction Singles (CIS) is probably the most widely used variational method in quantum chemistry, due to its simplicity. For a brief overview see Sec. 2.1.

1.2.2. Perturbation Theory

In what follows, it will be important that we have a familiar frame of reference for understanding perturbation theory.

Non-degenerate Perturbation Theory

Assume that one has already solved a well-defined problem with $\hat{H}_0$:

$$\hat{H}_0 \left|n^{(0)}\right\rangle = E_n^{(0)} \left|n^{(0)}\right\rangle \tag{1.26}$$

Now, if a small perturbation $\hat{H}_1$ applied, the total Hamiltonian is:

$$\hat{H} = \hat{H}_0 + \lambda \hat{H}_1, \qquad \lambda \ll 1 \tag{1.27}$$

Solving $\hat{H}$ from scratch

$$\hat{H} \left| n \right\rangle = E_n \left| n \right\rangle \tag{1.28}$$

would be very awkward and in fact it *not* necessary at all, since Eqn. 1.28 should be very similar to the original problem Eqn. 1.26, and more specifically $|n\rangle \approx |n^{(0)}\rangle$ in the limit of $\lambda \to 0$.

Now the eigenvectors $\{|n^{(0)}\rangle\}$ form a complete basis set, so any other wavefunction can be written as a linear combination, including those new eigenvectors $\{|n\rangle\}$ for $\hat{H}$. With a guess wavefunction and energy expression of:

$$\begin{cases} |n\rangle & = |n^{(0)}\rangle + \lambda |n^{(1)}\rangle + \lambda^2 |n^2\rangle + \cdots \\ E_n & = E_n^{(0)} + \lambda E_n^{(1)} + \lambda^2 E_n^2 + \cdots \end{cases} \tag{1.29}$$

we plug back into Eqn. 1.28:

$$\begin{aligned} \left(\hat{H}_0 + \lambda \hat{H}_1\right) \left(|n^{(0)}\rangle + \lambda |n^{(1)}\rangle + \lambda^2 |n^2\rangle + \cdots\right) = \\ \left(E_n^{(0)} + \lambda E_n^{(1)} + \lambda^2 E_n^2 + \cdots\right) \left(|n^{(0)}\rangle + \lambda |n^{(1)}\rangle + \lambda^2 |n^2\rangle + \cdots\right). \end{aligned} \tag{1.30}$$

By collecting different orders of λ^k $(k = 0, 1 \cdots)$, one rederives perturbation theory. More specifically, for $k = 0$ and 1, one gets:

$$\hat{H}_0 \left| n^{(0)} \right\rangle = E_n^{(0)} \left| n^{(0)} \right\rangle \tag{1.31}$$

$$\hat{H}_1 \left| n^{(0)} \right\rangle + \hat{H}_0 \left| n^{(1)} \right\rangle = E_n^{(0)} \left| n^{(1)} \right\rangle + E_n^{(1)} \left| n^{(0)} \right\rangle \tag{1.32}$$

Note that, for the zeroth-order approximation, Eqn. 1.31 is exactly the same as the original

problem $\hat{H}_0$ shown in Eqn. 1.26. The first-order approximation is defined by Eqn. 1.32, which is usually the key point of perturbation theory. This equation can be separated into $|n^{(1)}\rangle$ and $|n^{(0)}\rangle$:

$$\left(\hat{H}_0 - E_n^{(0)}\right)|n^{(1)}\rangle \;\; = \left(E_n^{(1)} - \hat{H}_1\right)|n^{(0)}\rangle \tag{1.33}$$

Projecting Eqn. 1.33 onto $\langle n^{(0)}|$ and $\langle m^{(0)}|\,(m \neq n)$ respectively, we find:

$$\begin{cases} 0 \;\; = E_n^{(1)} - \left\langle n^{(0)}\left|\hat{H}_1\right|n^{(0)}\right\rangle \\ \left(E_m^{(0)} - E_n^{(0)}\right)\langle m^{(0)}|n^{(1)}\rangle \;\; = -\left\langle m^{(0)}\left|\hat{H}_1\right|n^{(0)}\right\rangle \end{cases} \tag{1.34}$$

Or, equivalently:

$$\begin{cases} E_n^{(1)} \;\; = \left\langle n^{(0)}\left|\hat{H}_1\right|n^{(0)}\right\rangle \\ \langle m^{(0)}|n^{(1)}\rangle \;\; = -\dfrac{\left\langle m^{(0)}\left|\hat{H}_1\right|n^{(0)}\right\rangle}{E_m^{(0)} - E_n^{(0)}} \end{cases} \tag{1.35}$$

This implies:

$$\begin{cases} E_n^{(1)} \;\; = \left\langle n^{(0)}\left|\hat{H}_1\right|n^{(0)}\right\rangle \\ |n^{(1)}\rangle \;\; = \sum\limits_{m\neq n} -\dfrac{\left\langle m^{(0)}\left|\hat{H}_1\right|n^{(0)}\right\rangle}{E_m^{(0)} - E_n^{(0)}}\left|m^{(0)}\right\rangle \end{cases} \tag{1.36}$$

Eqn. 1.36 defines standard first-order Rayleigh-Schrodinger perturbation theory, through which one can estimate the effect of $\hat{H}_1$ in a very simple way, relative to the original problem, for both energy and wavefunction corrections.

There are a few drawbacks to this approach, however.

1. So far we have talked only about non-degenerate perturbation theory, which breaks down when states get close in energy, as can be easily seen in Eqn. 1.36. Whenever there are any degeneracies ($E_m^{(0)} = E_n^{(0)}$), the eigenstates are *not* unique, and the interactions among those states can *not* be neglected, so the assumption of $|n\rangle \approx$

$\left|n^{((0))}\right\rangle$ breaks down, and Eqn. 1.36 is not valid any more. In this case, non-degenerate perturbation theory is entirely *not* reliable, and degenerate perturbation theory has to be applied. The same is almost always true for near-degeneracies ($E_m^{(0)} \approx E_n^{(0)}$) as well.

2. At first order, there is no interaction between corrections to each individual state:

   (a) In the context of photochemistry, the energy corrections for charge transfer (CT) states are typically much bigger than the corrections for non-CT states. Therefore, with perturbation theory, one is not really confident about the new state ordering.

   (b) The new set of wavefunctions are no longer orthogonal.

3. Whenever λ gets big, a first order approximation is likely insufficient. In this case, one can certainly go to the second order or even higher order when necessary, but the computational cost grows quickly.

Degenerate Perturbation Theory

As shown in Eqn. 1.36, the energy difference between zeroth order eigenstates appears in the denominator, and this factor implies a break down whenever states get close energetically.

Mathematically, let the block Hamiltonian matrix be as follows:

$$\begin{pmatrix} \ddots & \vdots & \ddots & \vdots & \ddots \\ \cdots & H_{ii} & \cdots & H_{ij} & \cdots \\ \ddots & \vdots & \ddots & \vdots & \ddots \\ \cdots & H_{ji} & \cdots & H_{jj} & \cdots \\ \ddots & \vdots & \ddots & \vdots & \ddots \end{pmatrix} \tag{1.37}$$

in the basis $|\Psi_k\rangle, k = \{\cdots i \cdots j \cdots\}$. Perturbation theory will fail when the off-diagonal elements are much bigger than the diagonal differences.

In such a case, the only reliable way forward is to block diagonalize the Hamiltonian among those degenerate or nearly degenerate states, which hopefully lifts all the frustrating degeneracies. Thereafter, one can apply non-degenerate perturbation theory safely for those new states. This "block diagonalization" is also called degenerate perturbation theory. In practice, the variational method is often simpler to apply than degenerate perturbation theory.

1.3. Adiabatic Representation and Diabatic Representation

According to Sec. 1.1.1, adiabatic states are the eigenvectors obtained by diagonalizing the molecular electronic Hamiltonian at a given nuclear geometry. Thus, adiabatic states are the stationary states for electrons evolving in time, and they have usually been the most convenient representation for quantum chemistry.

However, the nuclear derivative coupling

$$\langle \Phi_I \left| \nabla_{\mathbf{R}} \right| \Phi_J \rangle \tag{1.38}$$

is typically non-zero, so adiabatic states are *not* fully stationary. And, in the context of non-adiabatic processes, adiabatic states need not be appropriate. For example, when photo-excited systems undergo different electron or energy transfer processes, the initial and final states of those processes are not always adiabatic states ($\{|\Phi_J\rangle, J = 1, 2 \cdots\}$). As another example, one can find the adiabatic states in the gas phase are unstable in a condensed phase system when solvent is present. In general, in many large systems, the derivative couplings to nuclear motion can be significant, and lead to a complete failure of the Born-Oppenheimer approximation. For all these reasons, the adiabatic states from an electronic structure calculation may not be meaningful.

As an alternative to adiabatic states, diabatic states ($\{|\Xi_A\rangle, A = 1, 2 \cdots\}$) are historically

defined to be electronic states with zero coupling to the nuclear motion:

$$\langle \Xi_A \left| \nabla_{\mathbf{R}} \right| \Xi_B \rangle = 0 \tag{1.39}$$

and for many circumstances, diabatic states are appropriate initial and final electronic states for chemical dynamics (e.g., when Marcus theory [11] applies), thus the diabatic representation is more meaningful. Even though the constraint of zero derivative coupling may be impossible to achieve [12], the notion of nearly diabatic states is very helpful in quantum chemistry and has a very rich history [13, 14, 15].

1.3.1. Diabatization Methods

Though diabatic states have been defined according to Eqn. 1.39, usually strictly diabatic states do not exist, and one can only minimize derivative couplings. In practice, there are many other definitions for approximate diabatization as well, roughly categorized as three approaches [16]:

1. According to the formal definition one can find the unitary transformation to apply to adiabatic states to generate diabatic states, and one can form such a transformation so as to minimizes the derivative coupling term. The main drawback for this method is that one requires explicit calculation of derivative coupling, which is usually very expensive.

2. Instead of minimizing derivative couplings explicitly, one can also try minimizing them implicitly by imposing desirable mathematical constraints on a set of diabatic states. The block-diagonalization and the fourfold way are two popular approaches. The former relies on some target reference diabatic states, and attempts to minimize the distance (in wavefunction space) between target and reference states. The latter introduces diabatical molecular orbitals, extending the idea of "configurational uniformity" to "molecular orbital uniformity".

3. A third, and more physically intuitive, approach for characterizing diabatic states is to use a physical observable, e.g. dipole moment $\vec{\mu}$, rather than focus on the wavefunctions or transformations directly. One of the most widely used algorithm is the Generalized Mulliken-Hush (GMH) [17], which was initially developed specifically for electron transfer problems. Boys diabatization method, as introduced below, is equivalent to GMH for the two-state problem.

1.3.2. Localized Diabatic States

Localized diabatization is an important tool for generating nearly diabatic states. The motivation behind localized diabatization is to construct electronic states that function as the initial and final states of electron and energy transfer processes. In brief, to generate a set of localized diabatic states, one rotates together a set of adiabatic states via a unitary transformation $\mathbf{U}_{JA}$:

$$|\Xi_A\rangle = \sum_J |\Phi_J\rangle \, \mathbf{U}_{JA}. \tag{1.40}$$

All localized diabatization techniques are defined via a rotation matrix $\mathbf{U}$. Current available methods are Generalized Mulliken Hush (GMH) [17], Fragment Charge Difference(FCD) [18], Fragment Energy Difference(FED) [19, 20, 21], Constrained DFT (CDFT) [22], Boys localization [23], ER localization [24], *etc.* For a review of localized diabatization and the implicit assumptions therein, see Ref. [23].

In this thesis, Sec. 4.1.1, we will use Boys localization, which is a computationally cheap generalization of the Cave/Newton GMH approach [17]. The physical motivation for the Boys algorithm is that, for CT systems, charges are stabilized and localized by a linear electric field from some solvent molecule or other auxiliary field. In practice, just like Boys localization of orbitals [24, 25, 26], Boys localized diabatization suggests that diabatic charge

centers should be moved as far apart as possible, thereby maximizing the quantity below:

$$\begin{aligned} f_{\text{Boys}}(\mathbf{U}) &= f_{\text{Boys}}(\{\Xi_A\}) \\ &\equiv \sum_{AB} \left| \langle \Xi_A \left| \vec{\mu} \right| \Xi_A \rangle - \langle \Xi_B \left| \vec{\mu} \right| \Xi_B \rangle \right|^2 . \end{aligned} \tag{1.41}$$

It has been shown that Boys localized diabatic states indeed have very small derivate couplings as expected [27, 28].

1.4. Outline of this Dissertation

The goals of this thesis are primarily to explore electronic structure calculations of excited states for modeling photosynthesis and less importantly, to calculate the couplings between these states. We now provide an outline of our contributions to this goal.

1.4.1. Chapter 2

In Ref. [29], Subotnik showed that configuration interaction singles (CIS) has a systematic bias against charge-transfer (CT) states, wherein the computed vertical excitation energies for CT states are disproportionately too high (by 1-2 eV) – as compared with non-CT states. In Chapter 2, we show that this CIS error can be corrected approximately by performing a single Newton-Raphson step to reoptimize orbitals, thus establishing a new set of orbitals which better balances ground and excited state energies. The computational cost of this correction is exactly that of one coupled-perturbed Hartree-Fock (CPHF) calculation, which is effectively the cost of the CIS calculation itself. In other words, for twice the computational cost of a standard CIS calculation, or roughly the same cost as a TDHF calculation, one can achieve a balanced, size-consistent description of CT versus non-CT energies, ideally with the accuracy of a much more expensive doubles CIS(D) calculation.

1.4.2. Chapter 3

Post-CIS corrections do exist but most often, if they are computationally inexpensive, these methods rely on perturbation theory. At the same time, inexpensive *variational* post-CIS

methods would be ideal since modeling electronic relaxation usually requires globally smooth potential energy surfaces (PESs) and there will inevitably be regions of near electronic degeneracy. With that goal in mind, in Chapter 3 we present a new method entitled variationally orbital optimized CIS (VOA-CIS). We show that VOA-CIS yields a uniform improvement to CIS, rebalancing the energies of CT states versus non-CT states within the same framework. Furthermore, VOA-CIS finds energetic corrections for CT states that are even larger than those predicted by CIS(D). The computational cost of VOA-CIS depends strongly on the number of excited states requested (n), but otherwise should be proportional to the cost of CIS itself.

1.4.3. Chapter 4

Chapter 4 provides the necessary benchmarking for the VOA-CIS method introduced in Chapter 3. On the one hand, we show that in the ground-state geometry, VOA-CIS performs comparably to CIS(D) at predicting relative excited state energies. On the other hand, far beyond CIS(D) or any other perturbative method, VOA-CIS correctly rebalances the energy of charge-transfer (CT) states versus non-CT states, while simultaneously producing smooth PESs–including the important case of avoided crossings. In fact, through localized diabatization of VOA-CIS excited states, one can find a set of reasonable diabatic states modeling CT chemical dynamics.

1.4.4. Chapter 5

In Chapter 5 we propose one final variational method, Fully Variational Orbital Adapted Configuration Interaction Singles (FVOA-CIS), as a potential improvement upon VOA-CIS. We show that FVOA-CIS is generally consistent with its predecessor VOA-CIS, but it is uniformly more robust and accurate than the latter, in the presence of avoided crossings and conical intersections. We also show that, if we use the molecular orbitals from TDDFT with hybrid density functionals (as opposed to HF), the FVOA-CIS PESs are smoother, and a smaller number of excited states is needed. Future benchmarking will be necessary

to validate the general applicability of the method, but preliminary data look reasonably encouraging.

1.4.5. Chapter 6

Chapter 6 is a brief summary and overview of future directions for *ab initio* quantum chemistry methods.

CHAPTER 2 : The Orbital Optimized Configuration Interaction Singles Method

This chapter is reprinted from [Liu, Fatehi, Shao, Veldkamp, and Subotnik, *J. Chem. Phys.* **136**, 161101, 2012].

2.1. Introduction

Configuration interaction singles (CIS) is the simplest and most intuitive approach for constructing excited electronic states. A CIS wave function has the form of $|\Psi_{\text{CIS}}\rangle = \sum_{ia} t_i^a |\Phi_i^a\rangle$, and it depends on two sets of variables: (i) the choice of occupied ("i") and virtual ("a") orbitals, and (ii) the choice of amplitudes or singles excitations ("t_i^a"). In a standard calculation, the choice of orbitals is dictated by a Hartree-Fock (HF) calculation to ensure orthogonality to the ground-state, and the amplitudes are chosen variationally by diagonalizing the Hamiltonian in the basis of single excitations $\mathbf{A}$:

$$\mathbf{A} \equiv \left\langle \Phi_i^a | H | \Phi_j^b \right\rangle \qquad \sum_{jb} A_{iajb} t_j^b = E_{\text{CIS}} t_i^a \tag{2.1}$$

Although it is well-known that CIS does not recover accurate vertical excitation energies from the ground state [31], CIS is often good enough to predict accurate rates of electronic excitation transfer between non-CT excited states [32, 33]. By implication, this means that CIS often does a decent job of predictingrelative energies between non-CT excited states.Other attractive features of CIS include: (i) it is variational; (ii) it is computationally cheap; (iii) it recovers the correct $-1/r$ asymptotic behavior of CT states that comes about because of the Coulombic attraction between electron attachments and detachments [34].

For all of the reasons above, our research group has attempted to use CIS theory to consider electron transfer events between excited states, though we have had little success. As we showed in a recent publication [29], even though CIS recovers the correct $-1/r$ asymptotic behavior of CT states, CIS excitation energies are highly biased against CT states, shifted usually by 1-2 eV. Thus, the relative energies between CT and non-CT states are unreliable, and quite often the very ordering of CT and non-CT excited states is incorrect with CIS.

Now, the standard alternative to CIS for large systems is time-dependent density functional theory [35] (TD-DFT), a method that typically obtains better vertical excitation energies than CIS for non-CT states. Unfortunately, however, standard TD-DFT fails miserably for

CT states because it does not recover the correct $-1/r$ asymptotic behavior [34], which leads to CT excitation energies that are often many eV too low (and getting worse for larger systems) [36, 37, 38, 39, 40]. This failure of TD-DFT stems from the approximate (adiabatic) exchange-correlation functional [41, 42], and Tozer and co-workers [43, 44] have argued that TD-DFT errors can be correlated in general with a measure of charge-transfer (though this is not always true [45]). To correct the CT problem in TD-DFT, cutting-edge research in quantum chemistry is creating new long-range corrected (LRC) TD-DFT functionals that add in exact Hartree-Fock exchange at long distances by partitioning the Coulomb operator [46, 47, 48, 49]. LRC functionals are a creative approach to blend together DFT functionals (that underestimate CT state energies) with CIS theory (for which CT state energies are overestimated, but with the correct asymptotic behavior). In the future, it will be interesting to see whether LRC-TD-DFT functionals can give a correct and robust description of both CT and non-CT excited state energies. As with all DFT development, there is no systematic way to improve accuracy in general.

Rather than exploring TD-DFT, the goal of this chapter is to provide a simple approach for correcting CIS energies to give a balanced description of CT versus non-CT states. While the accuracy of CIS can always be improved by using an expanded configuration interaction subspace (i.e., including doubles, à la CISD or CIS(D) [2, 50], etc.), we will show below that one can find the correct balance between CT and non-CT states simply by reoptimizing orbitals. We emphasize that we do not address here the intrinsically poor vertical excitation energies of CIS, which arise from not including electron-electron correlation. Instead, here we intend only to improve relative excitation energies, with the aim in mind of using CIS to model electron transfer between excited states in the future.

2.2. Theory

CIS wave functions are optimized with respect to amplitudes – $\partial E_{\mathrm{CIS}}/\partial t_i^a = 0$ – but CIS wave functions are certainly not optimized with respect to choice of orbitals. Using standard analytical gradient theory [51, 52], one can parameterize the space of orbital rotations using

the anti-symmetric generator of the orthogonal group. Starting with a set of atomic orbitals $\{\chi_\mu\}$ and a fixed initial set of orthonormal molecular orbitals, $\left\{\phi_i^0\right\}$, $\phi_i^0 = \sum_\mu \chi_\mu C_{\mu i}^0$, all possible choices of molecular orbitals are parameterized by orbital coefficients $\mathbf{C}$:

$$C_{\mu p} = \sum_q C_{\mu q}^0 \left(e^{\mathbf{\Theta}}\right)_{qp} \quad \mathbf{\Theta} = \sum_{p>q} \theta_{pq} J_{pq} \tag{2.2}$$

$$\left(\mathbf{J}_{pq}\right)_{rs} = -\delta_{pr}\delta_{qs} + \delta_{ps}\delta_{qr} \tag{2.3}$$

Using the standard definition of the Fock matrix F_{pq}, the CIS energy has the form

$$E_{\mathrm{CIS}} = E_{\mathrm{HF}} + \sum_{abi} t_i^a t_i^b F_{ab} - \sum_{aij} t_i^a t_j^a F_{ij} + \sum_{aibj} t_i^a t_j^b \langle aj||ib\rangle \tag{2.4}$$

Differentiating with respect to θ_{pq}, we find that $\partial E_{\mathrm{CIS}}/\partial\theta_{ij}(0) = \partial E_{\mathrm{CIS}}/\partial\theta_{ab}(0) = 0$, while

$$\begin{aligned} Y_{ai} \equiv \left.\frac{\partial E_{\mathrm{CIS}}}{\partial\theta_{ai}}\right|_{\mathbf{\Theta}=0} = \quad & 2\sum_{jb} t_j^a t_j^b F_{ib} - 2\sum_{jbc} t_j^b t_j^c \langle ca||bi\rangle \\ & +2\sum_{jb} t_j^b t_i^b F_{aj} + 2\sum_{jkb} t_j^b t_k^b \langle ji||ka\rangle \\ & +2\sum_{jkb} t_j^a t_k^b \langle ik||jb\rangle - 2\sum_{jbc} t_i^b t_j^c \langle bj||ac\rangle \neq 0 \end{aligned} \tag{2.5}$$

We will show below that Y_{ai} is much larger for CT states than for non-CT excited states. While this result in itself is not surprising, the scale of the energy difference *is* rather surprising: looking at $\mathbf{Y}$ alone is often enough to discern a CT state from a non-CT state.

Given this result, one is tempted to correct standard CIS states by accounting for orbital optimization. The simplest correction is to take a Newton-Raphson step. Thus, we expand the excitation energy to second order,

$$E_{\mathrm{CIS}}(\mathbf{\Theta}) = E_{\mathrm{CIS}}(0) + Y_{ai}\theta_{ai} + \sum_{aibj} \frac{1}{2} \left.\frac{\partial^2 E_{\mathrm{CIS}}}{\partial\theta_{ai}\partial\theta_{bj}}\right|_{\mathbf{\Theta}=0} \theta_{ai}\theta_{bj} \tag{2.6}$$

and searching for the optimal $\mathbf{\Theta}$, we find:

$$\theta_{ai}^{\text{opt}} = -\sum_{bj} \left(\frac{\partial^2 E_{\text{CIS}}}{\partial\theta_{ai}\partial\theta_{bj}} \right)^{-1} Y_{bj} \tag{2.7}$$

$$E_{\text{CIS}}^{\text{opt}} \approx E_{\text{CIS}}(0) - \sum_{aibj} \frac{1}{2} Y_{ai} \left(\frac{\partial^2 E_{\text{CIS}}}{\partial\theta_{ai}\partial\theta_{bj}}\bigg|_{\mathbf{\Theta}=0} \right)^{-1} Y_{bj} \tag{2.8}$$

Now, unfortunately, this approach has two drawbacks. First, the method requires us to invert the second-derivative matrix individually for each excited state, rather than all at once. Second, there is no guarantee that $\frac{\partial^2 E_{\text{CIS}}}{\partial\theta_{ai}\partial\theta_{bj}}$ will be or should be a positive definite matrix, and as such, the method may be unstable. To that end, a reasonable solution is to replace the second-derivative in Eqns. 2.6- 2.8 with the HF second-derivative; our intuition here is that for larger displacements in the choice of orbitals (i.e. large $\mathbf{\Theta}$), the HF term in Eqn. 2.4 dominates. Thus, our final expression for the orbital-optimized OO-CIS energy correction is

$$\theta_{ai}^{\text{opt}} = -\sum_{bj} \left(\frac{\partial^2 E_{\text{HF}}}{\partial\theta_{ai}\partial\theta_{bj}} \right)^{-1} Y_{bj} \tag{2.9}$$

$$E_{\text{CIS}}^{\text{opt}} \approx E_{\text{CIS}}(0) - \sum_{aibj} \frac{1}{2} Y_{ai} \left(\frac{\partial^2 E_{\text{HF}}}{\partial\theta_{ai}\partial\theta_{bj}}\bigg|_{\mathbf{\Theta}=0} \right)^{-1} Y_{bj} \tag{2.10}$$

which corresponds to a first-order (in Θ) perturbative wavefunction:

$$|\Psi_{\text{CIS}}^{\text{opt}}\rangle \approx |\Psi_{\text{CIS}}\rangle + \sum_{ai} t_i^a \theta_{ai}^{\text{opt}} |\Psi_{\text{HF}}\rangle - \sum_{aibj} t_i^a \theta_{bj}^{\text{opt}} \left|\Phi_{ij}^{ab}\right\rangle \tag{2.11}$$

In the next section, we will show that Eqn. 2.10 yields a strong correction for CT states that is in approximate agreement with CIS(D) [2, 50] in the limit of long-range charge transfers. Conveniently, Eqn. 2.10 can be solved using only one z-vector call [53] to invert $\frac{\partial^2 E_{\text{HF}}}{\partial\theta_{ai}\partial\theta_{bj}}$ for all excited states at once.

2.3. Results: PYCM

To test the theory above, we have studied the PYCM molecule from Ref. [29] (shown in the inset of Fig. 2.1). For a set of 500 different nuclear geometries, we have computed the first 12 excited states, amongst which there is almost always at least one CT state: the electron donor is the dimethyl alkene group and the electron acceptor is the dicyano group. Electronic absorption experiments have shown that the CT state should be the lowest-lying excited state [54], but CIS calculations in vacuum drastically overestimate the vertical excitation energy of this CT state, ranking the CT state always between the third and seventh excited state, in disagreement with experiment. Of course, in solution, a CT state would be stabilized by the surrounding solvent molecules – which we ignore in our calculation – but solvent effects are not large enough to account for the discrepancy. In Ref. [29], we showed that CIS(D) gives a strong correction, lowering the energy of the CT state (making it the first or second excited state), and that correction is to a good approximation proportional to the excited state dipole moment. If OO-CIS is a valid theory, we expect that it should behave similarly. We now present three pieces of evidence in the method's favor.

As our first piece of evidence, in Fig. 2.1 we show that the orbitals are indeed far less optimized for CT-states as compared with non-CT states, just as we asserted above. We have plotted a histogram of the trace of $\mathbf{Y}^T\mathbf{Y}$ (Eqn. 2.5), separated according to the relative dipole moment of the excited states ($|\vec{\mu}_{\mathrm{rel}}|$. Non-CT states are colored blue, and CT states are colored dark red. Of our 6000 calculations (500×12), we identify 498 CT states, all of which have relatively large norms for Y_{ai}.

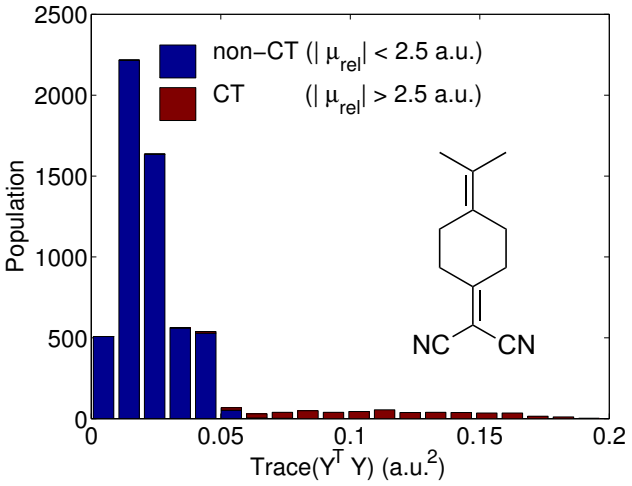

Figure 2.1: Histogram of Trace($\mathbf{Y}^T\mathbf{Y}$) for 6000 excited state PYCM calculations (500 geometries $\times$ 12 excited states/ geometry.). See Eqn. 2.5. Here, we have 498 CT states (defined as $|\vec{\mu}_{\rm rel}| > 2.5$ a.u.). Notice that Y_{ai} almost always has a larger norm for CT states compared to non-CT states: the very smallest value for a CT states is 0.03 and the largest value for a non-CT state is 0.07. This demonstrates the HF orbitals are poor for CT states calculated with CIS. Inset: Molecular structure for 2-(4-(propan-2-ylidene)cyclohexylidene)malononitrile (PYCM).

Next, in Fig. 2.2, we present a scatter plot of both $\Delta E_{\text{CIS(D)}} = E_{\text{CIS(D)}} - E_{\text{CIS}}$ and $\Delta E_{\text{OO-CIS}} = E_{\text{OO-CIS}} - E_{\text{CIS}}$ versus the magnitude of the relative dipole moment of each excited state, $|\vec{\mu}_{\text{rel}}| = |\vec{\mu} - \vec{\mu}_{\text{HF}}|$. For non-CT states (on the left-hand side), $\Delta E_{\text{CIS(D)}}$ follows no obvious pattern, and can be positive or negative. For OO-CIS, the energy correction is always negative, because the HF Hessian is positive definite, but the energy correction is very small for non-CT states. By contrast, for CT states (on the right-hand side of Fig. 2.2), both CIS(D) and OO-CIS are proportional to the dipole moment, with nearly the same slope! Thus, our OO-CIS approach recovers the CIS(D) correction roughly for strong CT states, up to a constant shift in energy; according to OO-CIS, the CT state is usually the first, second, or third excited state.

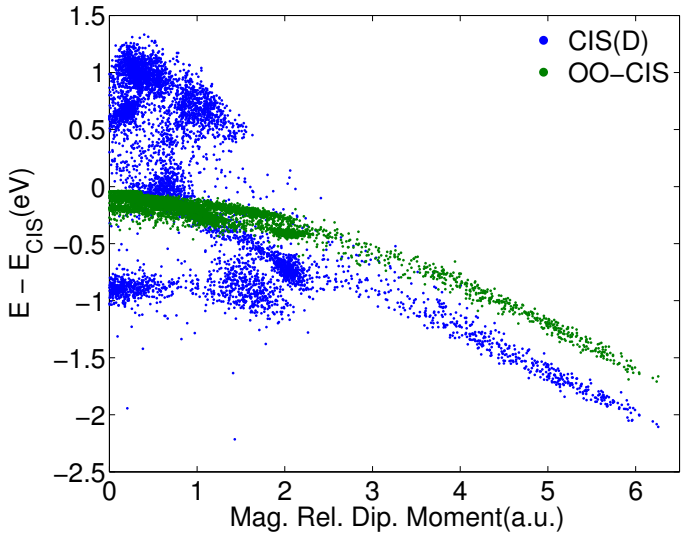

Figure 2.2: A scatter plot of energy correction $\Delta E \equiv E - E_{\mathrm{CIS}}$ versus the magnitude of dipole moment relative to the ground state $|\vec{\mu}_{\mathrm{rel}}| \equiv |\vec{\mu} - \vec{\mu}_{\mathrm{gs}}|$, from CIS(D) and OO-CIS. Note the near agreement between the OO-CIS and CIS(D) for CT states.

Finally, to strengthen our argument, we present in Fig. 2.3 a scatter plot of $\Delta E_{\text{OO-CIS}}$ versus $\Delta E_{\text{CIS(D)}}$, showing the cross-correlations between the OO-CIS and CIS(D) energy corrections. We color points differently according to their OO-CIS correlation energy: (*i*) states with $\Delta E_{\text{OO-CIS}} > -0.46$ eV (corresponding roughly to non-CT states, $|\vec{\mu}_{\text{rel}}| < 2.5$ a.u.) are colored blue; (*ii*) states with $-0.46\text{ eV} > \Delta E_{\text{OO-CIS}} > -1.22\text{ eV}$ (355 points corresponding roughly to weak CT states, $2.5\text{ a.u.} < |\vec{\mu}_{\text{rel}}| < 4.5$ a.u.) are colored green; (*iii*) states with $-1.22\text{ eV} > \Delta E_{\text{OO-CIS}}$ (135 points corresponding roughly to strong CT states, $|\vec{\mu}_{\text{rel}}| > 4.5$ a.u.) are colored red. While the correction energies appear uncorrelated for non-CT states, they become highly correlated for CT states. In fact, a linear fit of these points shows a slope of 0.79 for the red and green points, and a slope roughly 0.96, much closer to 1, for the red dots alone. In total, this data indicates that, for at least one molecule with CT excited states, OO-CIS gives a very meaningful energy correction, quite comparable to CIS(D).

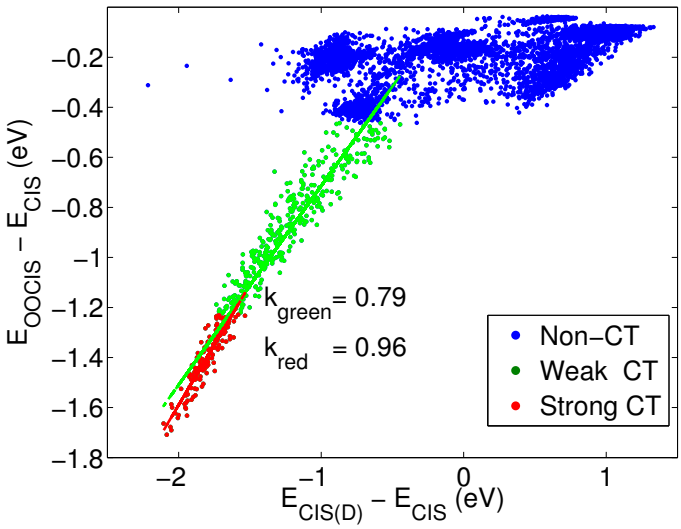

Figure 2.3: A scatter plot of energy corrections $\Delta E_{\text{OO-CIS}} \equiv E_{\text{OO-CIS}} - E_{\text{CIS}}$ versus $\Delta E_{\text{CIS(D)}} \equiv E_{\text{CIS(D)}} - E_{\text{CIS}}$. See text for exact definition of non-CT, weak CT, and strong CT states. Note the near agreement between the OO-CIS and CIS(D) for CT states. The fitted slopes are 0.79 for the green line (weak CT states) and 0.96 for the red line (strong CT states).

2.4. Discussion and Conclusions

The data above demonstrates that orbital optimization is crucial for correcting the relative energies of CT versus non-CT excited states. This fact suggests many novel avenues for exploration. First, it will be crucial in the future to implement and analyze the more rigorous corrections in Eqns. 2.7 and 2.8, where the step size in orbital space is determined by the second derivative of the CIS energy (rather than the HF energy). Preliminary evidence suggests that Eqn. 2.8 may yield larger corrections (in absolute value) for CT state energies as compared with Eqn. 2.10, but that the CIS Hessian may not always be positive definite. Is it reasonable to expect that excited states must correspond to minima, or are saddle points also physical? Second, one may wonder if similar treatments of orbital optimization can be applied to TD-DFT; the CT problem is not yet completely solved in the framework of TD-DFT, and orbital optimization may yield new insight. Third and finally, OO-CIS wave functions are of the form in Eqn. 2.11, and are thus orthonormal only to first order, and orthogonal to the ground-state only to zeroth order. Future research must analyze the properties of these wavefunctions beyond energetics. Moreover, do the doubles corrections found in Eqn. 2.11 match explicitly the doubles corrections found in CIS(D), which are clearly necessary to describe CT states [29]?

In summary, we have shown that a simple one-step orbital optimization (Eqn. 2.10) yields a meaningful correction to CIS excitation energies for CT states, comparable in fact to a CIS(D) correction. The approach is clearly size-consistent and the computational cost of this correction is minimal: inverting $\frac{\partial^2 E_{\mathrm{HF}}}{\partial\theta_{ai}\partial\theta_{bj}}$ has the same cost (approximately) as the CIS calculation itself, which is an order of magnitude cheaper than CIS(D). Thus, for only twice the computational cost of standard CIS, or exactly the same cost as TDHF, the OO-CIS approach rebalances the relative excitation energies of CT versus non-CT CIS states. Because this cost is so minimal, we expect Eqn. 2.10 will likely become a standard component of all future CIS calculations.

CHAPTER 3 : The Variatonal Orbital Adapted Configuration Interaction Singles Method

This chapter is reprinted from [Liu, Ou, Alguire, and Subotnik, *J. Chem. Phys.* **138**, 221105, 2013] and [Liu and Subotnik, *J. Chem. Theory Comp.* **10**, 1004, 2014].

3.1. Introduction

Our research group desperately needs practical, inexpensive wavefunction methods for modeling excited states: such methods must be (*i*) inexpensive and applicable to large molecules and (*ii*) accurate enough to capture excited state crossings (which are essential for understanding electronic relaxation).

Configuration Interaction singles (CIS) is perhaps the simplest approach to electronic excited states. One assumes that an excited state wavefunction is a linear combination of single excitations on top of the ground state. On the plus side, CIS is variational, size-consistent, and most of the time, CIS-wavefunctions are qualitatively correct (in terms of detachment and attachment plots [50]). On the negative side, CIS energies are simply not accurate and one cannot ascertain relative excited state energies from a CIS calculation alone: the CIS ansatz captures too little electron correlation and thus represents too great a simplification of the excited state wavefunctions for chemical accuracy. One cardinal failure of CIS is its notorious overestimation of charge-transfer(CT) excited state energies by 1-2 eV [29].

The goal of this chapter is to introduce a new and powerful method that builds a variational wavefunction on top of zeroth-order CIS wavefunction [55]. The format of this chapter will be as follows. In Sec. 3.2, we review existing post-CIS excited state methods and motivate our new VOA-CIS approach. In Sec. 3.3, we provide the theoretical framework for VOA-CIS as well as the computational details for extracting VOA-CIS wavefunctions and energies. Sec. 3.4 shows its numerical results for PYCM ground state, and twisted ethylene, and Sec. 3.5 is a brief summary, which also suggests benchmarking for the new method as shown in Chapter 4.

3.2. Background: Post-CIS Methods

3.2.1. CIS(D)

The simplest post-CIS excited state methodology is CIS(D). CIS(D) [2] proposes a perturbative improvement to CIS, modeled roughly after CIS-MP2 [56]. Whereas CIS-MP2 applies standard perturbation theory in the entire doubles and triples space $\left\{\left|\Phi_{ij}^{ab}\right\rangle, \left|\Phi_{ijk}^{abc}\right\rangle\right\}$, CIS(D) applies standard perturbation theory only in the doubles space; for the triples space, CIS(D) hypothesizes a first-order wavefunction correction via an intuitive ansatz, rather than strictly applying formal perturbation theory: CIS(D) proposes that the amplitudes for triply excited excitations are the products of CIS singles excitations with ground-state MP2 double excitations. The validity of this hypothesis can be tested numerically. In the end, the CIS(D) correction can be broken up into three parts: one component from the doubles manifold, and two components from the triples manifold– one "disconnected" and one "connected" component. The disconnected component cancels exactly with the ground-state MP2 energy, and the resulting two terms make up the vertical excitation energy. The final CIS(D) energy is size-consistent (unlike CIS-MP2) and the overall cost of the method is $O(N^5)$.

Although CIS(D) reduces the computational cost of CIS-MP2 from $O(N^6)$ to $O(N^5)$, as N gets big, the amount of work increases quickly. Luckily, in recent years, through the implementation of the resolution-of-the-identity (RI) approximation [57, 58], the CIS(D) prefactor has been reduced greatly, and currently the method is applicable to the calculation of vertical excitation energies in small to medium-sized molecules; local pair-natural orbital approaches can further reduce the cost [59]. That being said, CIS(D) still cannot be implemented to help solve most problems in electronic relaxation. Beyond the failure of CIS(D) to capture enough electron-electron correlation energy for CT states [29], the biggest culprit is the perturbative nature of the CIS(D) ansatz itself. In general, electronic relaxation (as mediated by phonons or nuclear motion) occurs at nuclear geometries where several electronic states come close together in energy; this is the entire basis of classical

Marcus theory [60, 61]. At such geometries, however, the use of perturbation theory is usually not valid: the zeroth order wavefunctions can still be strongly interacting and, in such cases, the resulting CIS(D) wavefunctions and energy corrections will be unreliable. Thus, in the end, CIS(D) can be used to model only those electronic states that are well-separated energetically; the method also fails if the $S_0 - S_1$ gap becomes too small and there is strong mixing between ground and excited states. Note that these limitations apply to all perturbative excited state methods.

3.2.2. CIS(D_n) and CC2

As a non-degenerate perturbative method, CIS(D) cannot deal with near-degeneracies. Among the set of post-CIS excited state methods, CIS(D_n) [62] is a quasi-degenerate improvement to CIS(D). CIS(D_n) was designed around the principle of "perturb and then diagonalize". The CIS(D_n) correction is found by diagonalizing a perturbative approximation to the second-order response matrix for the MP2 ground state.

Within the CIS(D_n) framework, one always approximates the doubles-doubles block of the response matrix by excitations of the diagonal Fock matrix. If this is the only enforced approximation, diagonalization of the response matrix is entitled CIS(D_∞), which closely resembles [63] the CC2 [64] method. Otherwise, one can expand the self-energy of the doubles-doubles block in a Taylor series, and with truncation one generates CIS(D_0) and CIS(D_1). Formally, CIS(D_0) and CIS(D_1) require diagonalization of a dressed matrix with size $N_{ov} \times N_{ov}$, just like CIS; CIS(D_∞) requires diagonalization of a matrix of size $N_{ov}^2 \times N_{ov}^2$ (through several tricks help). In practice, full CIS(D_0) and CIS(D_1) are significantly more expensive than CIS(D) calculations.

Overall, the CIS(D_n) suite of algorithms are a powerful means to investigate avoided crossings between excited states, but they suffer from several drawbacks:

- The computational cost can be prohibitive. Recently, progress has been made to reduce the cost of CIS(D_0) through an empirically scaled opposite-spin (SOS) ap-

proximation [1]. For CC2 methods, local approximations with density fitting have also been made [65], as have pair natural orbital approaches [66].

- For $n > 0$, the CIS(D_n) effective Hamiltonian is not Hermitian, and thus the method can fail at near-degeneracies, especially near conical intersections where imaginary frequencies are possible [63]. To improve upon CC2 near a true degeneracy, the algebraic diagrammatic construction (ADC) method [67] symmetrizes the response matrix and thus one must diagonalize only a Hermitian matrix.

- The CIS(D_n) approach will not be effective when the $S_0 - S_1$ energy gap becomes too small, or when doubly excited states are important.

3.2.3. ADC(2)

A natural alternative to CIS(D_∞) (or CC2) with the flavor of configuration interaction is the algebraic diagrammatic construction (ADC) method [67]. (For a more complete set of ADC(2) references, see Ref. [68]) As mentioned above, the ADC(2) method symmetrizes the CC2 response matrix and thus one must diagonalize only a Hermitian matrix; thus, the method is applicable near avoided crossings as well as conical intersections. Importantly, ADC(2) yields a means to calculate electronic matrix elements between excited states [69] which is useful for electronic dynamics [70]. Unfortunately, the cost of the method is approximately the cost of a CC2 calculation, which can be prohibitive for large systems, even though local approximations are possible [66]. $S_1 - S_0$ crossings will also be difficult to converge (as with any single reference ground-state theory).

Lastly, it must be noted that one can go beyond strict ADC(2) via the ADC(2)-x algorithm [71] that includes all off-diagonal terms in the doubles-doubles block of the effective Hamiltonian. Thus, ADC(2)-x allows for the possibility of doubly excited states, but the cost of ADC(2)-x grows accordingly (as N^6, on the order of EOM-CCSD). Overall, ADC is a promising approach for generating the excited states necessary for describing electronic relaxation, but computational cost remains an obstacle (and $S_1 - S_0$ crossings are a potential

problem).

3.2.4. CISD

According to the standard quantum chemistry dogma, the formal answer to all problems in electronic structure theory is full-CI. However, full-CI requires diagonalization of the Hamiltonian at all levels of excitation. As such, full-CI has an exponentially large cost and is practical only for very small molecules. For medium-sized or large molecules, if one is keen on configuration interaction, one must settle for truncated-CI– which is still variational but unfortunately not size-consistent. The accuracy of truncated CI deteriorates as the number of electrons increases, though corrections for recovering size-consistency are well-known for CISD [72].

Now, it is important to recognize that CISD's size-consistency problem for excited states can be partially removed by excluding the HF ground-state from the Hamiltonian diagonalization. In such a case, intuitively, if we have two infinitely separated fragments A and B, excitations localized to fragment A (set #1) are entirely decoupled from excitations localized to fragment B (set #2). The only problematic complication is that we can find a third set (set #3) of excited states with excitations on both fragments A and B. However, this third set of excitations is entirely decoupled from sets #1 and #2 and thus, by inspection, one can pick out excited states with size-consistent wavefunctions and energies. For more details, see Sec. 3.6.2 in the appendix.

Despite this glimmer of hope, however, we must emphasize that straight CISD necessarily produces poor excitation energies. On the one hand, if the HF state is excluded, excitation energies are always too low – after all, only the excited states are stabilized with correlation energy. On the other hand, if we include the HF state, CISD is known to overstabilize the ground state [73] and yield erroneously large excitation energies (see also Fig. 4.1 below). This failure of CISD results from the fact that the ground and excited states are not treated equivalently: while the ground state couples strongly to the doubles space and gains a great

deal of dynamical correlation, a CIS excited state wavefunction will not relax sufficiently without inclusion of the corresponding triples space. In the end, the variational benefits of full CISD must be weighed against the distorted CISD absolute vertical excitation energies. (For a discussion of multi-reference configuration interaction in the context of the VOA-CIS algorithm below, please see the Appendix.)

3.2.5. Perturbative OO-CIS

Using all of the background above, over the past few years our research group has been working to develop our own post-CIS excited state methods, introduced in Chapter 2. Given that CIS states are strongly coupled to the space of double excitations (on the one hand), but including entire doubles space *a la* CISD is counterproductive (on the other hand), our original intuition was that a meaningful post-CIS excited state wavefunctions could be obtained by partial orbital optimization. In particular, our hope was that reasonably accurate excited state energies could be obtained by optimizing the MOs for each specific excited state, rather than always using the same SCF orbitals that were optimized for the ground state. Moreover, as long as the orbital changes were small, each excited state would keep its identity and the algorithm would remain stable. The end product of this line of thinking was an algorithm entitled perturbative orbital optimized CIS (OO-CIS), as shown in Chapter 2 [30].

Here, we would redefine the Y and θ matrix, shown in Eqns. 2.5 and 2.7, as a generalization of the original OO-CIS method, for later use in this chapter:

$$\begin{aligned} -\frac{1}{2}Y_{ai}^{IJ} &\equiv +\sum_{bcjk} t_k^{cI} \left\langle \Phi_k^c \middle| \hat{H}\ a_a^\dagger a_i \middle| \Phi_j^b \right\rangle\ t_j^{bJ} \qquad (3.1) \\ &= +\sum_{bcj} \Big(t_i^{cI} t_j^{bJ} \langle cj \,||\, ab \rangle + t_j^{cI} t_j^{bJ} \langle ci \,||\, ba \rangle \Big) \\ &\quad +\sum_{bjk} \Big(t_k^{aI} t_j^{bJ} \langle ij \,||\, bk \rangle + t_k^{bI} t_j^{bJ} \langle ij \,||\, ka \rangle \Big) \\ \theta_{ai}^{IJ} &\equiv -\frac{Y_{ai}^{IJ}}{\epsilon_a - \epsilon_i + E^J - E^I} \qquad (3.2) \end{aligned}$$

In practice, OO-CIS has some appealing properties. First, although we invoke orbital optimization in spirit for each CIS state, all optimization is actually performed with the initial SCF orbitals; this approach is completely free from cherry picking orbitals in an active space. Second, the algorithm is incredibly fast and low-demanding.

Despite these attributes, however, the OO-CIS method is still perturbative (like CIS(D)), and we have found empirically that it yields significant improvement only for charge-transfer states (and, even then, the CT correction is not large enough). Lastly, because the excited states are non-orthogonal to the ground state, transition moments might be difficult to extract. Ideally, one would like an excited state approach with the speed of OO-CIS but the accuracy of a balanced variational calculation (which can treat $S_I - S_J$ crossings for all I, J).

3.3. Variational Orbital Adapted CIS (VOA-CIS)

With the previous background material in mind, we now describe the VOA-CIS approach. In the spirit of CIS(D_n) (and also CIS(2) [74]), our intention is to perturb-then-diagonalize, rather than vice versa; however, unlike the case of CIS(D_n), we will formally use the full Hamiltonian matrix rather than an approximate response matrix. Thus, the VOA-CIS approach can be decomposed into two primary steps. First, will generate a basis of wavefunctions in the spirit of a *generalized* OO-CIS approach. On the one hand, it is computationally cheap to generate perturbative wavefunctions through orbital optimization; on the other hand, we believe that orbital optimization should capture the most important doubles correction for excited states. Second, we diagonalize the Hamiltonian in the basis of all perturbed wavefunctions, thus yielding variational energies and eigenvectors. All Hamiltonian matrix elements can be evaluated through second-quantization and, in simplified form, the matrix elements are given in Eqns. 3.12, 3.13 and 3.14 in Sec. 3.3.2.

We will now discuss these steps in more detail. In the end, the notation for our algorithm can be cast in the form VOA-CIS-C(n, m); in what follows, we will explain the meaning of

C, n and m.

m	C		
	O	G	X
1	$\left\|\Psi^{JJJ}\right\rangle$ $(2n)$	$\|\Phi_{\text{HF}}\rangle, \left\|\Psi^{JJJ}\right\rangle$ $(1+2n)$	$\|\Phi_{\text{HF}}\rangle,$ $\left\|\Psi^{JJJ}\right\rangle$ $(1+2n)$
2	$\left\|\Psi^{JKK}\right\rangle (n+n^2)$	$\|\Phi_{\text{HF}}\rangle, \left\|\Psi^{JKK}\right\rangle (1+n+n^2)$	$\|\Phi_{\text{HF}}\rangle, \left\|\Psi^{JKK}\right\rangle, \left\|\Psi^{GKK}\right\rangle (1+2n+n^2)$
3	$\left\|\Psi^{JKL}\right\rangle (n+n^3)$	$\|\Phi_{\text{HF}}\rangle, \left\|\Psi^{JKL}\right\rangle (1+n+n^3)$	$\|\Phi_{\text{HF}}\rangle, \left\|\Psi^{JKL}\right\rangle, \left\|\Psi^{GKL}\right\rangle$ $(1+n+n^2+n^3)$

Table 3.1: Additional basis functions included alongside the zeroth order CIS wavefunctions ($\{\left|\Psi^I_{\text{CIS}}\right\rangle\}$) for VOA-CIS-C($n$, m). $I, J, K, L = \{1, 2 \cdots n\}$. In parentheses is the total number of basis wavefunctions (N_B) for each option.

3.3.1. Choosing the VOA-CIS Basis

We will define N_B as the size of the VOA-CIS basis.

Size of CIS Subspace (n)

In choosing a set of basis functions for diagonalization, the first and most immediate question is the number of requested excited states. Very often, photochemical experiments can be interpreted by considering the dynamics of the lowest 10 excited states. This fortunate circumstance forms the basis for the entire VOA-CIS algorithm. Effectively, the VOA-CIS approach uses CIS as a means of generating a set of many-electron excited states as an "active" space. We define n as the number of CIS states which must be calculated initially (i.e., $N_B = n$), and the smaller n is, the faster the VOA-CIS algorithm will be. Although our algorithm will not be independent of n, luckily, from our experience [55], VOA-CIS excited state wavefunctions and absolute energies do not change greatly with n; n can be chosen robustly. At the same time, though, the VOA-CIS ground-state will change dramatically as n gets very large and the VOA-CIS energy approaches the CISD limit; see the energy diagram in Fig. 4.1. This difference in behavior as a function of n will actually be exploited later.

Additional parameters we use are m and C. Roughly speaking, m is an indication of how many doubles we have for perturbed wavefunctions, while C tells how the ground state should be balanced against the excited states . The details are shown below.

Size of Doubles Space (m)

Having picked an initial size for the CIS subspace n ($N_B = n$), we must next address the number of double excitations to be included in the (post-CIS) VOA-CIS basis. As mentioned above, we will select candidate doubles excitations using a *generalized* OO-CIS framework, with the following mathematical structure: $\left\{ \left|\Psi^{IJK}\right\rangle \equiv -\sum_{bj} \theta_{bj}^{IJ}\, a_b^\dagger a_j \left|\Psi_{\text{CIS}}^K\right\rangle \right\}$. See Eqn. 3.2 for a definition of θ; recall that I is the index of the CIS state from which the

doubles are generated. In general, there are three nested options for choosing the number of such double excitations:

1. $\{\left|\Psi^{III}\right\rangle\}$ (m= 1): For the $m = 1$ case, VOA-CIS adds n doubly excited wavefunctions to the basis, on top of the original n CIS wavefunctions (N_B+= n). These n wavefunctions are exactly the same as the first order wavefunctions one constructs by allowing for orbital relaxation in perturbative OO-CIS. See equation Eqn. 2.8 above.

2. $\{\left|\Psi^{IJJ}\right\rangle\}$ (m= 2): For the $m = 2$ case, VOA-CIS adds n^2 doubly excited wavefunctions to the basis, on top of the original n CIS wavefunctions (N_B+= n^2). These n^2 wavefunctions include all wavefunctions proposed in the $m = 1$ case. Now, the basic idea is to expand each of the n excited CIS states in a basis of doubly excited states that can be generated by single excitations from those same n excited states. This gives n^2 different combinations of the form $\{\left|\Psi^{IJJ}\right\rangle\}$. The $m = 2$ subspace is a clear improvement over the $m = 1$ subspace because, at an avoided crossing, excited states will begin to mix and thus, in order to capture electron-electron correlation correctly, we must allow for mixing between the doubly-excited configurations generated from different CIS states.

3. $\{\left|\Psi^{IJK}\right\rangle\}$ (m= 3): For the $m = 3$ case, VOA-CIS adds n^3 doubly excited wavefunctions to the basis, on top of the original n CIS wavefunctions (N_B+= n^3). These n^3 wavefunctions include all wavefunctions proposed in the $m = 2$ case, but there is no physical basis for including all $\{\left|\Psi^{IJK}\right\rangle\}$ (m= 3) in the VOA-CIS basis. Instead, the only justification that can be given is mathematical: notice that the $m = 3$ basis is well-defined even at a point of exact degeneracy between two CIS states. The same conclusion is not true for the $m = 1$ or $m = 2$ subspaces.

Treatment of Ground State (C)

The final question that must be addressed for the VOA-CIS basis is our treatment of the ground state. On the one hand, for an exactly size-consistent algorithm, one should exclude

the ground state from the basis. (See the Appendix for a proof.) On the other hand, without including the ground state, a post-CIS algorithm cannot construct meaningful wavefunctions and energies whenever the ground state is energetically close to the first excited state (which is not uncommon far from the equilibrium geometry). Facing this dilemma, we believe that most often the correct choice is to include the ground-state, while also comparing results with the case of ground-state exclusion.

In the end, just as for the choice of double spaces, we can define three nested possible routes by which VOA-CIS can treat the ground state. These options are defined through the parameter C:

1. $C = O$: When considering the ground-state, the simplest option is to ignore the ground state and not include the Hartree-Fock determinant in the VOA-CIS basis. Thus, N_B is unchanged. We label this option 'O'. In this case, one recovers exact size-consistency.

2. $C = G$: Vice versa, the next simplest option is simply to include the HF determinant in the basis, which we label the 'G' option (N_B+= 1). The 'G' option is especially important when the $S_0 - S_1$ energy gap gets small and ground-excited state mixing is unavoidable. In such cases, it make sense to forgo exact size-consistency for the sake of reasonable energetics around an avoided crossing. Moreover, Ref. [55] showed that, in the case of twisted ethylene, VOA-CIS excitation energies are not changed greatly by including the HF determinant. In fact, VOA-CIS-G excitation energies are well-balanced; unlike CISD, the VOA-CIS-G ground state is not overstabilized relative to the excited states and VOA-CIS yields reliable absolute excitation energies.

3. $C = X$: We label our third and final option for treating the ground state with the letter 'X'. For this option, we include not only the Hartree-Fock determinant in our basis, but we also include the doubly excited determinants generated by the interaction of the HF state with single excitations on top of CIS states.

Mathematically, just as one CIS state can be expanded in a basis of orbital optimized CIS states, so too can the HF ground state be expanded in a basis of orbital optimized CIS states. Thus, just as was done previously, one can define a set of doubly excited determinants $\{\left|\Psi^{GJK}\right\rangle\}$ to relax the HF ground state. These doubly-excited determinants are defined analogously to Eqns. 3.1 and 3.2 through the intermediate quantities Y^{GJ} and θ^{GJ}:

$$-\frac{1}{2}Y_{ai}^{GJ} \equiv \left\langle \Phi_{\rm HF} \left| H a_a^\dagger a_i \right| \Psi_{\rm CIS}^J \right\rangle = \sum_{bj} t_j^{bJ} \left\langle ij \,||\, ab \right\rangle \tag{3.3}$$

$$\theta_{ai}^{GJ} = -\frac{Y_{ai}^{GJ}}{\epsilon_a - \epsilon_i + E_{\rm CIS}^J - E_{\rm HF}} \tag{3.4}$$

In Sec. 4.2.2, we will show that this 'X' option is closely related to the TDHF formalism.

- For the case of $m = 1$, the 'X' option is redundant; the electronic bases in VOA-CIS-G(n, 1) and VOA-CIS-X(n, 1) are exactly the same (N_B+= 1).
- For the case $m = 2$, we include all $\{\left|\Psi^{GJJ}\right\rangle\}$, and so we set N_B+= n;
- For the case $m = 3$, we include all $\{\left|\Psi^{GJK}\right\rangle\}$, and so we set N_B+= n^2.

Synopsis

In the end, there are as many as 9 (or really 8) different flavors of VOA-CIS. Henceforward, we will use the notation VOA-CIS-C(n, m), as defined in Table 3.1. *A priori*, it would appear difficult to predict the optimal algorithm. Luckily, according to our experience, for large enough n, the relative energies among excited states remain almost unchanged for all choices. That being said, though, choosing the absolutely best *ground-state* option can be tricky and absolute excitation energies can change with method options. Thus far, if we seek the best absolute potential energy surfaces – including geometries far from equilibrium – VOA-CIS-G(n, 2) seems to be the best choice.

3.3.2. Matrix Elements for VOA-CIS

Having constructed a well-defined basis for excited state wavefunctions, we must now diagonalize the Hamiltonian. The necessary matrix elements for the Hamiltonian (H), overlap (S) and dipole ($\vec{\mathbf{R}} \equiv (X, Y, Z)$) operators are quite similar. Of course, the matrix elements for S and $\vec{\mathbf{R}}$ are simpler than those for H in that the former are purely single-electron operators. All necessary matrix elements are given in Eqns. 3.12, 3.13 and 3.14. For convenience, we use several convenient intermediate quantities defined below: in Eqns. 3.5- 3.11, M can be of any size while A, B, C and D are all of size $N_v \times N_o$:

$$\mathcal{L}^{vo}_{pq}(A) \equiv \sum_{ai} \langle pi \,||\, qa \rangle \, A_{ai} \tag{3.5}$$

$$\mathcal{L}^{vv}_{pq}(M) \equiv \sum_{ab} \langle pb \,||\, qa \rangle \, M_{ab} \tag{3.6}$$

$$\mathcal{L}^{oo}_{pq}(M) \equiv \sum_{ij} \langle pj \,||\, qi \rangle \, M_{ij} \tag{3.7}$$

$$\begin{aligned} \mathcal{F}_{ai}(A) \equiv & \quad \mathcal{L}^{vo}_{ai}(A) \\ & + \sum_{b} F_{ab} A_{bi} - \sum_{j} A_{aj} F_{ji} \end{aligned} \tag{3.8}$$

$$\mathcal{K}_{ab}(A, B) = \mathcal{L}^{vv}_{ab}(AB^T) - \mathcal{L}^{oo}_{ab}(B^T A) \tag{3.9}$$

$$\mathcal{K}_{ij}(A, B) = \mathcal{L}^{vv}_{ij}(AB^T) - \mathcal{L}^{oo}_{ij}(B^T A) \tag{3.10}$$

$$\mathcal{M}(A, B, C, D) \equiv D \cdot \left(AB^T C + CB^T A \right) \tag{3.11}$$

$$
\begin{aligned}
\left\langle \Phi_{\mathrm{HF}} \left| H \right| \Phi_{\mathrm{HF}} \right\rangle &= E_{\mathrm{HF}} \\
\left\langle \Psi^I_{\mathrm{CIS}} \left| H \right| \Psi^J_{\mathrm{CIS}} \right\rangle &= \delta_{IJ} E^J_{\mathrm{CIS}} \\
\left\langle \Psi^{\tilde{I}JK} \left| H \right| \Psi^{\tilde{I}'J'K'} \right\rangle &= \sum_{abij} \theta^{\tilde{I}J}_{bj} \theta^{\tilde{I}'J'}_{ai} \left\langle \Psi^K \left| a^\dagger_j a_b H a^\dagger_a a_i \right| \Psi^{K'} \right\rangle \\
&= +(t^K \cdot t^{K'})(\theta^{IJ} \cdot \theta^{I'J'}) E_{\mathrm{HF}} \qquad +(t^K \cdot \theta^{I'J'})(\theta^{IJ} \cdot t^{K'}) E_{\mathrm{HF}} \\
&\quad -\mathcal{M}(\theta^{IJ}, \theta^{I'J'}, t^K, t^{K'}) E_{\mathrm{HF}} \\
&\quad +(t^K \cdot \mathcal{F}(t^{K'}))(\theta^{IJ} \cdot \theta^{I'J'}) \qquad +(t^K \cdot t^{K'})(\theta^{IJ} \cdot \mathcal{F}(\theta^{I'J'})) \\
&\quad +(t^K \cdot \theta^{I'J'})(\theta^{IJ} \cdot \mathcal{F}(t^{K'})) \qquad +(\mathcal{F}(t^K) \cdot \theta^{I'J'})(\theta^{IJ} \cdot t^{K'}) \\
&\quad -\mathcal{M}(\theta^{IJ}, \theta^{I'J'}, t^K, \mathcal{F}(t^{K'})) \qquad -\mathcal{M}(\theta^{IJ}, t^{K'}, t^K, \mathcal{F}(\theta^{I'J'})) \\
&\quad -\mathcal{M}(\theta^{IJ}, \theta^{I'J'}, \mathcal{L}^{vo}_{vo}(t^K), t^{K'}) \qquad -\mathcal{M}(t^K, t^{K'}, \mathcal{L}^{vo}_{vo}(\theta^{IJ}), \theta^{I'J'}) \\
&\quad +\theta^{IJ} \cdot \left(\mathcal{K}_{vv}(t^{K'}, t^K)\, \theta^{I'J'} \right) \qquad -\theta^{IJ} \cdot \left(\theta^{I'J'} \mathcal{K}_{oo}(t^{K'}, t^K) \right) \\
&\quad +\theta^{IJ} \cdot \left(\mathcal{K}_{vv}(\theta^{I'J'}, t^K)\, t^{K'} \right) \qquad -\theta^{IJ} \cdot \left(t^{K'} \mathcal{K}_{oo}(\theta^{I'J'}, t^K) \right)
\end{aligned} \tag{3.12}
$$

$$
\begin{aligned}
\left\langle \Phi_{\mathrm{HF}} \left| H \right| \Psi^L_{\mathrm{CIS}} \right\rangle &= 0 \\
\left\langle \Phi_{\mathrm{HF}} \left| H \right| \Psi^{\tilde{I}JK} \right\rangle &= \sum_{ai} \theta^{\tilde{I}J}_{ai} \left\langle \Phi_{\mathrm{HF}} \left| H a^\dagger_a a_i \right| \Psi^K \right\rangle \\
&= \sum_{abij} \theta^{\tilde{I}J}_{ai} t^{bK}_j \left\langle ij \,||\, ab \right\rangle \\
&= \theta^{\tilde{I}J} \cdot \left(\mathcal{L}^{vo}_{ov}(t^K) \right)^T \\
\left\langle \Psi^L_{\mathrm{CIS}} \left| H \right| \Psi^{\tilde{I}JK} \right\rangle &= \theta^{\tilde{I}J} \cdot \left(-2 Y^{LK} \right)
\end{aligned}
$$

$$
\begin{aligned}
\langle \Phi_{\rm HF} | X | \Phi_{\rm HF} \rangle &= X_{\rm HF} \\
\langle \Psi^I_{\rm CIS} | X | \Psi^J_{\rm CIS} \rangle &= \delta_{IJ} X^I_{\rm HF} + t^I \cdot \left(X_{vv} t^J - t^J X_{oo} \right) \\
\left\langle \Psi^{\tilde{I}JK} | X | \Psi^{\tilde{I}'J'K'} \right\rangle &= \sum_{abij} \theta^{\tilde{I}J}_{bj} \theta^{\tilde{I}'J'}_{ai} \left\langle \Psi^K \left| a^\dagger_j a_b X a^\dagger_a a_i \right| \Psi^{K'} \right\rangle \\
&= +(t^K \cdot t^{K'})(\theta^{IJ} \cdot \theta^{I'J'}) X_{\rm HF} + (t^K \cdot \theta^{I'J'})(\theta^{IJ} \cdot t^{K'}) X_{\rm HF} \\
&\quad -\mathcal{M}(\theta^{IJ}, \theta^{I'J'}, t^K, t^{K'}) X_{\rm HF} \\
&\quad -\mathcal{M}(\theta^{IJ}, \theta^{I'J'}, t^K, (X_{vv} t^{K'} - t^{K'} X_{oo})) \\
&\quad -\mathcal{M}(\theta^{IJ}, t^{K'}, t^K, (X_{vv} \theta^{I'J'} - \theta^{I'J'} X_{oo})) \\
&\quad +(t^K \cdot (X_{vv} t^{K'} - t^{K'} X_{oo}))(\theta^{IJ} \cdot \theta^{I'J'}) \\
&\quad +(t^K \cdot t^{K'})(\theta^{IJ} \cdot (X_{vv} \theta^{I'J'} - \theta^{I'J'} X_{oo})) \\
&\quad +(t^K \cdot \theta^{I'J'})(t^K \cdot (X_{vv} \theta^{I'J'} - \theta^{I'J'} X_{oo})) \\
&\quad +((X_{vv} t^K - t^K X_{oo}) \cdot \theta^{I'J'})(t^{K'} \cdot \theta^{IJ}) \\
\langle \Phi_{\rm HF} | X | \Psi^L_{\rm CIS} \rangle &= t^L \cdot X_{vo} \\
\left\langle \Phi_{\rm HF} | X | \Psi^{\tilde{I}JK} \right\rangle &= 0 \\
\left\langle \Psi^L_{\rm CIS} | X | \Psi^{\tilde{I}JK} \right\rangle &= \left(t^L \cdot \theta^{\tilde{I}J} \right) \left(t^K \cdot X_{vo} \right) + \left(t^L \cdot t^K \right) \left(\theta^{\tilde{I}J} \cdot X_{vo} \right) \\
&\quad -\mathcal{M}(t^L, t^K, X_{vo}, \theta^{\tilde{I}J})
\end{aligned}
\tag{3.13}
$$

$$
\begin{aligned}
\langle \Phi_{\rm HF} | S | \Phi_{\rm HF} \rangle &= 1 \\
\langle \Psi^I_{\rm CIS} | S | \Psi^J_{\rm CIS} \rangle &= \delta_{IJ} \\
\left\langle \Psi^{\tilde{I}JK} | S | \Psi^{\tilde{I}'J'K'} \right\rangle &= \sum_{abij} \theta^{\tilde{I}J}_{bj} \theta^{\tilde{I}'J'}_{ai} \left\langle \Psi^K \left| a^\dagger_j a_b S a^\dagger_a a_i \right| \Psi^{K'} \right\rangle \\
&= +(t^K \cdot t^{K'})(\theta^{IJ} \cdot \theta^{I'J'}) + (t^K \cdot \theta^{I'J'})(\theta^{IJ} \cdot t^{K'}) \\
&\quad -\mathcal{M}(\theta^{IJ}, \theta^{I'J'}, t^K, t^{K'}) \\
\langle \Phi_{\rm HF} | S | \Psi^L_{\rm CIS} \rangle &= 0 \\
\left\langle \Phi_{\rm HF} | S | \Psi^{\tilde{I}JK} \right\rangle &= 0 \\
\left\langle \Psi^L_{\rm CIS} | S | \Psi^{\tilde{I}JK} \right\rangle &= 0
\end{aligned}
\tag{3.14}
$$

In Alg. 3.1 and Alg. 3.2, we provide a flowchart for how we have calculated VOA-CIS to date. Though this algorithm is not yet optimal or parallelized, it offers the reader a taste of

how easy VOA-CIS energies and wavefunctions are to compute. In this flowchart, we define N_θ to be the number of $\theta^{\tilde{I}J}$s.

Algorithm 3.1 VOA-CIS algorithm [7]

1: **for** I= $1:n$ **do** ▷ Calculate Y^{IJ}, θ^{IJ}

2: **for** J= $1:n$ **do**

3: $A = t^I; B = t^J$

$$\begin{aligned} -\frac{1}{2}Y_{ai}^{IJ} = &+\sum_b \mathcal{L}_{ab}^{voT}(B)A_{bi} - \sum_j A_{aj}\mathcal{L}_{ji}^{voT}(B) + \mathcal{L}_{ai}^{vv}(AB^T) - \mathcal{L}_{ai}^{oo}(B^TA) \\ \theta_{ai}^{IJ} = &-\frac{Y_{ai}^{IJ}}{E_{\text{CIS}}^J - E_{\text{CIS}}^I + \epsilon_a - \epsilon_i} \end{aligned}$$

4: **end for**

5: **end for**

6:

7: **for** J= $1:n$ **do** ▷ Calculate Y^{GJ}, θ^{GJ}

$$\begin{aligned} -\frac{1}{2}Y_{ai}^{GJ} &= \left(\mathcal{L}_{ia}^{vo}(t^J)\right)^T \\ \theta_{ai}^{GJ} &= -\frac{Y_{ai}^{GJ}}{E_{\text{CIS}}^J - E_{\text{HF}} + \epsilon_a - \epsilon_i} \end{aligned}$$

8: **end for**

9: $N_\theta = n^2 + n$

10: $N_B = n + 1 + n^2 + n^3$

11:

12: **for** $\tilde{I}J$= $1:N_\theta$ **do** ▷ Normalize $\theta^{\tilde{I}J}$

13: $\theta^{\tilde{I}J} = \theta^{\tilde{I}J} / \left|\theta^{\tilde{I}J}\right|$

14: **end for**

15:

16: **for** I= $1:n$ **do** ▷ Save expensive matrices

17: Save $\mathcal{L}_{ai}^{vo}(t^I)$, $\mathcal{F}_{ai}(t^I)$

18: **end for**

19: **for** $\tilde{I}J$= $1:N_\theta$ **do**

20: Save $\mathcal{L}_{ai}^{vo}(\theta^{\tilde{I}J})$, $\mathcal{F}_{ai}(\theta^{\tilde{I}J})$

21: **end for**

Algorithm 3.2 VOA-CIS algorithm (cont) [7].

for I= $1:n$ **do**
  for J= $1:n$ **do**
    A= $t^I; B = t^J$
    Save $\mathcal{K}_{ab}(t,t) = \mathcal{L}^{vv}_{ab}(AB^T) - \mathcal{L}^{oo}_{ab}(B^TA)$
    Save $\mathcal{K}_{ij}(t,t) = \mathcal{L}^{vv}_{ij}(AB^T) - \mathcal{L}^{oo}_{ij}(B^TA)$
  end for
end for
for $\tilde{I}J= 1:N_\theta$ **do**
  for K= $1:n$ **do**
    A= $\theta^{\tilde{I}J}; B = t^K$
    Save $\mathcal{K}_{ab}(\theta,t) = \mathcal{L}^{vv}_{ab}(AB^T) - \mathcal{L}^{oo}_{ab}(B^TA)$
    Save $\mathcal{K}_{ij}(\theta,t) = \mathcal{L}^{vv}_{ij}(AB^T) - \mathcal{L}^{oo}_{ij}(B^TA)$
  end for
end for
▷ Construct the Hamiltonian
for $|\Psi_1\rangle \in \{\ |\Phi_{\text{HF}}\rangle, \left|\Psi^L_{\text{CIS}}\right\rangle, \left|\Psi^{IJK}\right\rangle\ \}$ **do**
  for $|\Psi_2\rangle \in \{\ |\Phi_{\text{HF}}\rangle, \left|\Psi^L_{\text{CIS}}\right\rangle, \left|\Psi^{IJK}\right\rangle\ \}$ **do**
    Save H_{12}, S_{12}, $\vec{\mathbf{R}}_{12}$
  end for
end for
▷ $\{H, S, \vec{\mathbf{R}}, N_B\}$
$Hv = SvE \rightarrow \{v_i, E_i\}$, $i = 1, 2 \cdots N_B$
$\{v_i\} \rightarrow \{\vec{\mathbf{R}}_i$, Oscillator Strength $f_i\}$

for i= $1:N_B$ **do** ▷ Loop over $\{v_i\}$
  Mapping: $|\Psi_{\text{VOA-CIS}}\rangle \rightarrow |\Psi_{\text{CIS}}\rangle$ with max overlap
end for

3.4. Results

The VOA-CIS algorithm was implemented using a developers' version of the Q-Chem software package [75]. In the following calculations, the basis set was 6-31G* basis set together with the rimp2-cc-pvdz auxiliary basis set. We present results for two molecules: 2-(4-(propan-2-ylidene)cyclohexylidene)malononitril (PYCM, shown in inset of Fig. 3.1(f)) and twisted ethylene (C_2H_4).

3.4.1. PYCM

Experimentally, the absorption spectrum of PYCM shows a strong non-CT band at 5.4 eV and a CT band at 4.6 eV in hexane [54]. At the ground-state geometry, CIS predicts that the CT state is the 7th state, while CIS(D) correctly predicts the CT state is the first excited state. From SOS-CIS(D_0) both the lowest-lying two excited states have a large dipole moment, indicting both are a mixture of the CT state and non-CT state. Because the non-CT decays radiationlessly, Verhoeven *et al* predicted [54] a crossing between the CT and non-CT as a function of the torsional motion along the double bond of the ethylenic-CN group. VOA-CIS confirms such a crossing, and this will be presented in Chapter 4.

In this communication, we will focus exclusively on the potential energy surface near the ground-state geometry. Previously [29], we have generated 500 geometries from a ground-state classical trajectory, and we consider the first 12 excited states, each with roughly 1 CT state apiece, for a total of 6000 data points. In this region of configuration space, with no torsional motion, we do not expect to see any crossings between the CT and non-CT state. Strangely, however, CIS does predicts such crossings. When faced with such an unexpected crossing, CIS(D) encounters adiabatic CIS states that are incorrectly mixtures of CT and non-CT states; as such, CIS(D) does the best that it can, and it gives a correction lying anywhere from big to small. As such, according to CIS(D), the CT state is not consistently the lowest excited state.

By contrast, VOA-CIS does not predict such a crossing. In Fig. 3.1(a)- (d), we plot the

VOA-CIS energy correction versus CIS(D) energy correction for different combinations of parameters in VOA-CIS-$C(n,\ m)$. The red dots are from CT states, while blue dots are from non-CT ones. To construct $\Delta E_{\text{VOA-CIS}}$, we mapped each CIS eigenstate to the VOA-CIS eigenstate with maximum overlap. The data is striking: unlike CIS(D), VOA-CIS always finds a sharp boundary for ΔE between non-CT and CT states and does not mix CT and non-CT states. The $m = 2$ and $m = 3$ corrections give an even more consistent correction than $m = 1$. (By comparing (c) with (b), we see that adding in the ground-state can shift all the excitation energies up.) Our data is summarized in (e) which shows a histogram of energy corrections for CIS(D) and VOA-CIS-G(12, 2). The former has a wide and continuous distribution, while the latter yields a bimodal distribution– with one sharp peak for CT states (≈ -2 eV) and another for non-CT ones (≈ 0 eV).

Turning to dipole moments, in (f), we plot the relative dipole moments of the excited states, $|\vec{\mu}_{\text{rel}}| = |\vec{\mu}_{\text{ex}} - \vec{\mu}_{\text{gs}}|$, comparing VOA-CIS-G(12, 2) with CIS. Whereas CIS predicts $|\vec{\mu}_{\text{rel}}|$ values that change continuously from non-CT through weak CT states to strong CT states, again VOA-CIS predicts a completely bimodal distribution of dipole moments: there are CT states with large dipole moments and there are non-CT states with small dipole moments. As such, VOA-CIS yields an extremely intuitive picture of the valence excited states.

In the end, this PYCM data suggests that, by rediagonalizing the Hamiltonian matrix instead of applying perturbation theory, VOA-CIS is not limited by the failure of CIS for treating CT states.

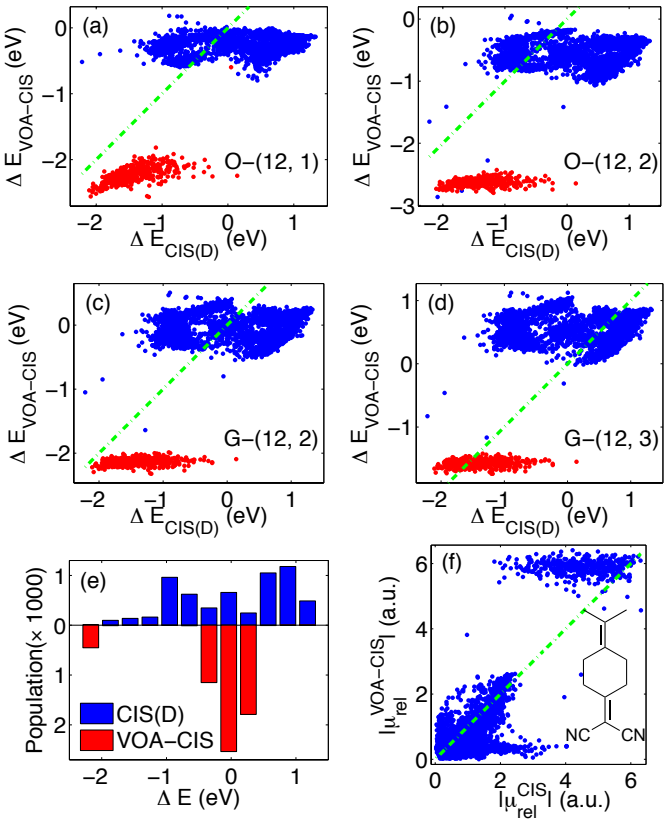

Figure 3.1: In (a)- (d), we plot the VOA-CIS energy correction versus the CIS(D) energy correction, with different VOA-CIS options for m and C, for 6000 excited states PYCM calculations (500 geometries $\times$ 12 states/ geometry). Data points with $|\vec{\mu}_{\rm rel}|$ bigger than $4\,a.u.$ are colored red (for CT states); non-CT states are colored blue. (e) shows a histogram of energy corrections from both CIS(D) and VOA-CIS-$G(12,\,2)$. In (f), we plot the VOA-CIS-$G(12,\,2)$ $|\vec{\mu}_{\rm rel}| \equiv \left|\vec{\mu}^{\text{VOA-CIS-}G(12,\,2)} - \vec{\mu}_{\rm gs}^{\text{VOA-CIS-}G(12,\,2)}\right|$ versus $|\vec{\mu}_{\rm rel}^{\rm CIS}| \equiv \left|\vec{\mu}^{\rm CIS} - \vec{\mu}_{\rm gs}^{\rm HF}\right|$. The insert is the PYCM structure. All the green lines are $y = x$ for reference. Note that all VOA-CIS combinations find a clear separation between CT and non-CT states, while CIS(D) does not.

3.4.2. Twisted Ethylene

Twisted ethylene is a paradigmatic example of an avoided crossing [76]: at 90°, the π and π^* orbitals come together in energy. As a result there are three low-lying singlet states, with roughly π^2, $\pi\pi^*$, and $(\pi^*)^2$ character [3]. To assess the VOA-CIS approach, we plot in Fig. 3.2 the relative energy of the first few excited states along the torsional angle τ from 60° to 120°, with geometries from Ref. [5].

In Fig. 3.2, (a)-(c), we plot low-lying excitation energies from VOA-CIS-G(n, 2) with $n = 5, 6, 7$ and 14. Note how a new excited state appears in our model Hamiltonian as n goes from 5 to 7; this is the doubly excited $(\pi^*)^2$ state and its appearance suggests that VOA-CIS can predict some doubly excited states (though perhaps only serendipitously). Observe also that increasing the basis beyond $n = 7$ yields no big changes (see $n = 14$). Altogether, this implies in order to get an accurate description of the first n' states, the parameter n in VOA-CIS-C(n, m) does not have to be much bigger than n'.

In (d), we plot VOA-CIS-X(14, 3) data versus SF-XCIS [5] data (shown in red). SF-XCIS effectively introduces a $\pi - \pi^*$ active space and should be extremely accurate for this problem. The figure suggests that VOA-CIS finds accurate relative energies among the excited states, (although VOA-CIS overestimates the ground states by roughly 0.5 eV compared to SF-XCIS). In (e), we plot the CIS/E_{HF} and CIS(D)/MP2 data, which totally miss the doubly excited state and ignore coupling with the ground-state. SOS-CIS(D_0) is almost the same to CIS(D) results, with a maximum difference of 0.2 eV for those two states. From this data, we tentatively conclude that VOA-CIS is stable near avoided crossings, with the added benefit that doubly-excited states are possibilities.

In (f), we plot the dependence of VOA-CIS-X(n, 3) energies upon the number of states n (for the $\tau = 80°$ geometry). S_0 is the ground state, while $S_i (i = 1, 2)$ is the ith excited state. On the far right, we plot CISD data (which is equivalent to VOA-CIS-X(∞, 3)). Note that (i) VOA-CIS energies does not depend strongly on n and (ii) VOA-CIS excited state

energies are close to CISD energies for $n = 15$, but the ground-state energy is still far away. This is likely a feature of our method, because CISD is known to wildly overestimate vertical excitation energies (by over-stabilizing the ground state [73]). For instance, compare the CISD data ($E_1^{\text{ex}} \equiv E_{S_1} - E_{S_0} = 7.7$ eV) with the SF-XCIS data (which includes triples, $E_1^{\text{ex}} = 3.4$ eV) and our VOA-CIS-X(14,3) data ($E_1^{\text{ex}} = 3.2$ eV). Altogether, (f) suggests that we can get reasonable potential energy surface for n not too big or too small.

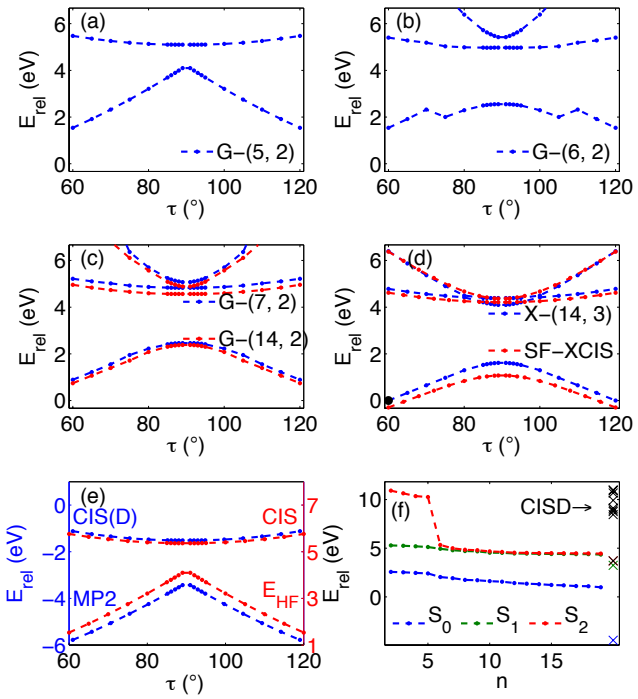

Figure 3.2: In parts (a)- (d), we plot VOA-CIS energies for ethylene along the torsional angle τ, with different VOA-CIS options. Red in (d) is SF-XCIS [5] active-space result. CIS/E_{HF} and CIS(D)/MP2 are plotted in (e). (f) shows the VOA-CIS-$X(n, 3)$ energy as a function of n at $\tau = 80°$, compared with CISD data (x's). All energies are relative to the ground state at $\tau = 60°$ in (d) (black solid dot). Note that VOA-CIS is able to find the low-lying doubly excited state.

3.5. Conclusions and Caveats

VOA-CIS-$C(n,\ m)$ is a variational, black-box approach for solving excited state problems without choosing active space orbitals. The only parameters in our approach are the number of CIS states n and the number of doubles added $\sim n^m$. Thus far, there appears to be little dependence on the number of states n, provided n is not too small. This is crucial because the cost goes up quickly with n. In our experience, $m = 2, 3$ convincingly outperforms $m = 1$ when treating state crossings. In all cases, VOA-CIS gives a strong energy correction for CT states, far stronger than is found with perturbation theory. Thus far, the strongest drawback to VOA-CIS is that the method appears to underestimate Rydberg excitation energies, though this may not be crucial for photochemistry [77] especially in the condensed phase [78].

Intensive benchmarking of VOA-CIS is crucial and will be reported in Chapter 4. At worst, VOA-CIS is a cheap algorithm to generate approximate CISD energies from an expansion in the doubles space. At best, VOA-CIS is an inexpensive approach for valence CISD energy calculations–where static and dynamic correlation are balanced and vertical excitation energies are not exaggerated. For these reasons, we are currently working on an optimal VOA-CIS algorithm. Because VOA-CIS requires only $O(n^2 N_o N_v)$ memory (e.g., to represent $\theta_{ai}^{\tilde{I}J}$) and the number of important excited states is often small (e.g., $n \leq 10$), a VOA-CIS algorithm should be highly parallelizable and quite affordable for big molecules. If such an algorithm can be implemented, VOA-CIS methods will have a strong impact on excited state calculations, where new methods are sorely needed.

3.6. Appendix

3.6.1. Matrix Elements from Second-Quantization

For completeness, we now give the formula for the doubles-doubles block of the VOA-CIS algorithm. Eqn. 3.15 can be used to derive Eqn. 3.12 in the text above.

$$\left\langle \Psi^I_{\rm CIS} \left| a^\dagger_j a_b \ \hat{H} \ a^\dagger_a a_i \right| \Psi^J_{\rm CIS} \right\rangle = t^{dI}_l \left\langle \Phi^{dI}_l \left| a^\dagger_j a_b \ \hat{H} \ a^\dagger_a a_i \right| \Phi^{cJ}_k \right\rangle t^{cJ}_k =$$

$$\begin{array}{llll}
+\delta_{ab}\delta_{ij}t^{cI}_k t^{cJ}_k E_{\rm HF} & -\delta_{ab}t^{cI}_i t^{cJ}_j E_{\rm HF} & -\delta_{ij}t^{aI}_k t^{bJ}_k E_{\rm HF} & +t^{aI}_i t^{bJ}_j E_{\rm HF} \\
+\delta_{ab}\delta_{ij}t^{dI}_k t^{cJ}_k f_{dc} & -\delta_{ab}\delta_{ij}t^{cI}_l t^{cJ}_k f_{kl} & +\delta_{ab}t^{cI}_i t^{cJ}_k f_{kj} & -\delta_{ab}t^{dI}_i t^{cJ}_j f_{dc} \\
-\delta_{ab}t^{cI}_k t^{cJ}_k f_{ij} & +\delta_{ab}t^{cI}_l t^{cJ}_j f_{il} & -\delta_{ij}t^{aI}_k t^{cJ}_k f_{bc} & +\delta_{ij}t^{cI}_k t^{cJ}_k f_{ba} \\
-\delta_{ij}t^{dI}_k t^{bJ}_k f_{da} & +\delta_{ij}t^{aI}_l t^{bJ}_k f_{kl} & +t^{aI}_i t^{cJ}_j f_{bc} & -t^{aI}_i t^{bJ}_k f_{kj} \\
-t^{cI}_i t^{cJ}_j f_{ba} & +t^{dI}_i t^{bJ}_j f_{da} & +t^{aI}_k t^{bJ}_k f_{ij} & -t^{aI}_l t^{bJ}_j f_{il} \\
+\delta_{ab}\delta_{ij}t^{dI}_l t^{cJ}_k \langle dk \,||\, lc\rangle & +\delta_{ab}t^{dI}_i t^{cJ}_k \langle dk \,||\, cj\rangle & +\delta_{ab}t^{dI}_k t^{cJ}_k \langle di \,||\, jc\rangle & +\delta_{ab}t^{cI}_l t^{cJ}_k \langle ik \,||\, jl\rangle \\
+\delta_{ab}t^{dI}_l t^{cJ}_j \langle di \,||\, cl\rangle & +\delta_{ij}t^{dI}_k t^{cJ}_k \langle bd \,||\, ac\rangle & +\delta_{ij}t^{aI}_l t^{cJ}_k \langle bk \,||\, cl\rangle & +\delta_{ij}t^{cI}_l t^{cJ}_k \langle bk \,||\, la\rangle \\
+\delta_{ij}t^{dI}_l t^{bJ}_k \langle dk \,||\, al\rangle & & & \\
+t^{aI}_i t^{cJ}_k \langle bk \,||\, jc\rangle & +t^{cI}_i t^{cJ}_k \langle bk \,||\, aj\rangle & +t^{dI}_i t^{cJ}_j \langle bd \,||\, ca\rangle & +t^{dI}_i t^{bJ}_k \langle dk \,||\, ja\rangle \\
+t^{aI}_k t^{cJ}_k \langle bi \,||\, cj\rangle & +t^{cI}_k t^{cJ}_k \langle bi \,||\, ja\rangle & +t^{dI}_k t^{bJ}_k \langle di \,||\, aj\rangle & +t^{aI}_l t^{cJ}_j \langle bi \,||\, lc\rangle \\
+t^{aI}_l t^{bJ}_k \langle ik \,||\, lj\rangle & +t^{cI}_l t^{cJ}_j \langle bi \,||\, al\rangle & +t^{dI}_l t^{bJ}_j \langle di \,||\, la\rangle &
\end{array} \tag{3.15}$$

3.6.2. Size-Consistency of VOA-CIS Method

In the text above, we claimed that the VOA-CIS algorithm provided a size-consistent approach provided that the ground state was not included in the rediagonalized Hamiltonian. To show this, we will now demonstrate explicitly that VOA-CIS-m(O, n) ($m = 1, 2$) is size-consistent. In other words, suppose that we are given two molecular fragments A and B that are infinitely far away from each other in space. For an excitation on fragment A, we must prove that $E_{AB}(A^*) = E_A(A^*)$, where "AB" signifies a calculation with both frag-

ments included and "A" signifies a calculation with only the one fragment. To prove this statement, consider the AB calculation. Note that there can be no charge transfer excited states between fragments A and B because of their infinite separation. Let I and J be local excitations on A and B respectively. According to Eqn. 3.1, we then find that θ^{IJ} (which is proportional to Y^{IJ}) will be 0: this follows because all interfragment two-electron integrals must vanish. θ^{IJ}_{ai} can be nonzero only if excitations I, J are located on the same fragment (say A), and the molecular orbitals a, i are also localized to that same fragment (A).

Now, for the $m = 1, 2$ options, all doubly excited wavefunctions have the form $\left|\Psi^{IJJ}\right\rangle = \sum_{bj} \theta_{bj} a_b^\dagger a_j \left|\Psi^J_{\text{CIS}}\right\rangle$. Thus, all doubly excited configurations require that both excitations be on the same fragment (again A). Finally, note that in the Hamiltonian to be rediagonalized, localized excitations on A and B cannot couple to each other at all– either directly or indirectly (because we have removed the ground-state). From this logic, we may conclude that excited states on A will not mix with excited states on B, and thus, we must have $E_{AB}(A^*) = E_A(A^*)$, i.e. size-consistent excitation energies. One final word is necessary about size-consistency.

For the $m = 3$ option, the doubly-excited configurations have the form:

$\left|\Psi^{IJK}\right\rangle = \sum_{bj} \theta_{bj} a_b^\dagger a_j \left|\Psi^K_{\text{CIS}}\right\rangle$. In this case, one does allow for the possibility of excitations on both fragments, since CIS state K could be localized to fragment B, while CIS states I, J could be localized to fragment A. Nevertheless, it is easy enough to show that, after diagonalizing the Hamiltonian, we will find three distinct and nonmixing classes of excited states: those with excitations exclusively on A, those with excitations exclusively on B, and those with excitations on both A and B. The first two sets will have size-consistent energies and be meaningful. This situation is the exact scenario described in Sec. 3.2.4 above.

3.6.3. Connection to Multireference Configuration Interaction and Neeses Spectroscopy Oriented Configuration Interaction

In Sec. 3.2.4 above, we discussed the limitations of bare CISD. Of course, there are many effective multi-reference CI (MRCI) approaches towards generating excited states that outperform CISD and generate strong absolute and relative excitation energies [79]. While such MRCI methods are not post-CIS approaches, in general MRCI algorithms are very powerful techniques (though often expensive). Recently, Neese has proposed a spectroscopy oriented configuration interaction approach (SORCI) to excited states built on top of a CASSCF calculation for treating large molecules. At the heart of the SORCI algorithm, working in a meaningful set of average natural orbitals, the SORCI algorithm prescribes: (i) one perform a CASSCF calculation, (ii) one truncates the CASSCF wavefunctions to a smaller set of reference configurations, (iii) one generates excitations into a predefined strongly interacting subspace, and (iv) finally one rediagonalizes the Hamiltonian. (A perturbative correction for dynamic correlation is also added.) Using SORCI, one can generate quite accurate excited states for a very broad variety of molecules, small and large, for small enough configuration interactions. Nevertheless, the caveat for SORCI is that one must first choose an active space for CASSCF and second invoke several thresholds for choosing average natural orbitals, truncating the relevant reference states, and defining a strongly interacting subspace. For these reasons, the method is not "black box".

In the end, Neeses SORCI approach can not be mapped onto the model we propose in this chapter (if we replace a CASSCF calculation by a CIS calculation). The reasoning is as follows. The VOA-CIS approach generates a set of doubly excited configurations in the form of a linear combination via perturbation theory. By contrast, SORCI performs no such contraction; instead, SORCI uses one threshold to generate a set of truncated reference states and a second threshold to generate a strongly interacting subspace. Thus, SORCI requires the diagonalization of a matrix of dynamic size (depending on thresholds); whereas, VOA-CIS requires the diagonalization of a matrix of static size. In general, for reasonable

thresholds, we can expect that VOA-CIS will be less accurate but also significantly less expensive than a typical SORCI calculation.

CHAPTER 4 : Benchmarking the VOA-CIS Method

This chapter is reprinted from [Liu and Subotnik, *J. Chem. Theory Comp.* **10**, 1004, 2014].

As shown in the last chapter, we would prefer a variational approach similar to OO-CIS, this is the origin for the VOA-CIS approach. Similar to the spirit of CIS(D_n) (and also CIS(2) [74]), our approach is to perturb and then diagonalize, rather than vice versa though more common. Chapter 3 shows preliminary data for the success of VOA-CIS methods, this chapter we show more results out of VOA-CIS to verify its validity.

In Sec. 4.1, we benchmark VOA-CIS excited states versus results from high-level approaches in excited state theory and experimental data. In Sec. 4.2 we present a brief and pictorial discussion of how and why VOA-CIS works, and its close connection with Time-Dependent HF (TDHF) [80, 81]. We conclude in Sec. 4.3 with a summary of the VOA-CIS approach and a look toward future extensions, theoretical and computational.

4.1. Results

The VOA-CIS algorithm was implemented in a developmental version of the Q-Chem [75] software package. We will now describe the results of applying the VOA-CIS algorithm to a broad range of photoexcitable organic molecules.

4.1.1. PYCM

Absorption

Over the years, our research group has focused a great deal of attention on the molecule in Fig. 4.1 (abbreviated PYCM for 2-(4-(propan-2-ylidene)cyclohexylidene)malononitril) [82]. Experimentally, PYCM has a low-lying CT absorption peak at 36,800 cm^{-1} (4.56 eV), where the donor (D) is the methylene group and the acceptor (A) is the dicyano group. Above the the CT state, there is also a local $A \rightarrow A^*$ excitation absorption peak on the cyano groups at 43,900cm^{-1} (5.44 eV) (both in n-hexane at 20°C) [54].

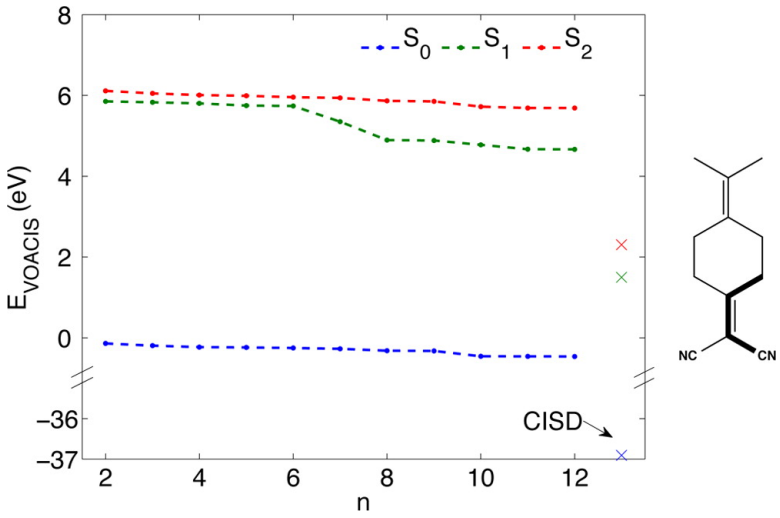

Figure 4.1: Comparison of VOA-CIS-G(n, 2) energies with (approximate) CISD energies [6] at the ground state geometry, for the first three singlet states, relative to the original E_{HF}. On the right is the PYCM molecular structure, with the dihedral angle τ shown with bold bonds. Note that VOACIS excitation energies are close to experimental values and relatively insensitive to n for n not too big and not too small ($n \in [8, 12]$). Here, S_1 is the CT state and finds a big correction with $n = 8$. By contrast, note that CISD excitation energy are grossly unphysical (with $E_1 - E_0 = 38.41$ eV!)

In Fig. 4.1, we plot the dependence of the VOA-CIS energies (VOA-CIS-G(n, 2)) on the number of states n. All calculations were performed at the ground state geometry with the 6-31G* basis set (optimized with MP2), and we plot energies for the ground state and the first two excited states. S_1 is the CT state and S_2 is the locally excited state. On the right hand side of Fig. 4.1, we identify (approximate) CISD energies [6]. Recall that CISD energies are equivalent to VOA-CIS energies for $n = \infty$. Similar to our previous results for ethylene in Ref. [55], in Fig. 4.1 we find again that CISD vastly overstabilizes the ground state; the vertical excitation energy of S_1 is a whopping 38.41 eV according to CISD.

By contrast, VOA-CIS-G(12, 2) yields far more balanced excitation energies than straight CISD, with S_1 having an excitation energy of 5.12 eV, which compares well with experiment (4.56 eV). Moreover, our results are not highly dependent on n; we believe the energy of the S_1 state changes sharply at $n = 7$ only because the CT state is the seventh excited state according to CIS (but the CT state is the first excited state according to VOACIS). Finally, notice that VOA-CIS-G(12, 2), VOA-CIS-O(12, 2) find very similar energies here for S_0, S_1, and S_2, relative to the original ground-state energy E_{HF}: $-0.46, 4.66$ and 5.69 eV versus $0.00, 4.66$ and 5.66 eV. Altogether, on the basis of its reasonable excitation energies and its weak dependence on n, we find this data very encouraging and supportive of our claim that meaningful excited state energies can be found by diagonalizing only a sub-block of the CISD matrix.

Smooth PES and Emission

Regarding emission, experimentally the lower-lying PYCM CT state decays with measurable fluorescence, while the non-CT excited state decays exclusively radiationlessly. Verhoeven *et al* [54] have postulated that these experimental signatures can be explained by breaking the ethylenic double bond connecting cyclohexane to the dicyano groups. More specifically, they have proposed an avoided crossing between the S_1 and S_2 excited states along the torsional angle (τ). According to the Verhoeven picture, the S_1 excited state lives in a weak local minimum that can radiate to the ground state, while the S_2 state undergoes an

ultrafast *cis-trans* isomerization back to the ground state after photoexcitation. See Fig. 7 in Ref. [54].

To simulate this putative relaxation process, we have investigated the PES of PYCM as follows. First, we performed a geometry optimization for the first excited state (S_1) at the CIS level. Although we had no confidence in the accuracy of the CIS method to generate excitation energies, we reasoned that if twisting a double bond were really a robust feature of PYCM, then CIS approach should find an optimal structure with the ethylenic groups pointed out of plane; indeed, our results confirmed such a geometry. Second, apart from the dihedral angle τ shown in Fig. 4.1, (i.e. the dihedral angle along the cyclohexane-dicyano group double bond), we froze all the other geometrical coordinates in PYCM. At equilibrium τ is 0°. Then, we calculated the PESs along τ to learn about electronic relaxation, and we found a small barrier for the S_1 state between $\tau = 0°$and $\tau = 90°$.

In Fig. 4.2, we plot VOA-CIS energies (left-hand side) and relative dipole moments ($|\vec{\mu}_{\rm rel}| \equiv |\vec{\mu}_{\rm ex} - \vec{\mu}_{\rm g}|$, right-hand side) as a function of the torsional angle τ, for a few different VOA-CIS parameter options. We plot the first 4 singlet states, $S_0 - S_3$, with S_0 being the ground state. From the dipole moment plot, one can see that the CT state $\left|\mathrm{D}^+\mathrm{A}^-\right\rangle$ changes adiabatic surface as a function of τ, moving smoothly from S_1 (red) to S_2 (green) as τ goes from 0° to 90°. Conversely, the locally excited state $|\mathrm{DA}^*\rangle$, changes adiabat as well, moving smoothly from S_2 to S_1. In Fig. 4.3, these VOA-CIS findings are confirmed by EOM-CCSD [83] data, where we show that both methods (VOA-CIS-G(12, 2) and EOM-CCSD) yield very similar *absolute* dipole moments for S_1. From the energy plot, we compute that the corresponding avoided crossing occurs when τ is around 40°. Thus, VOA-CIS captures PYCM's experimental features described above, and in the process highlights the power of a variational method near an avoided crossing.

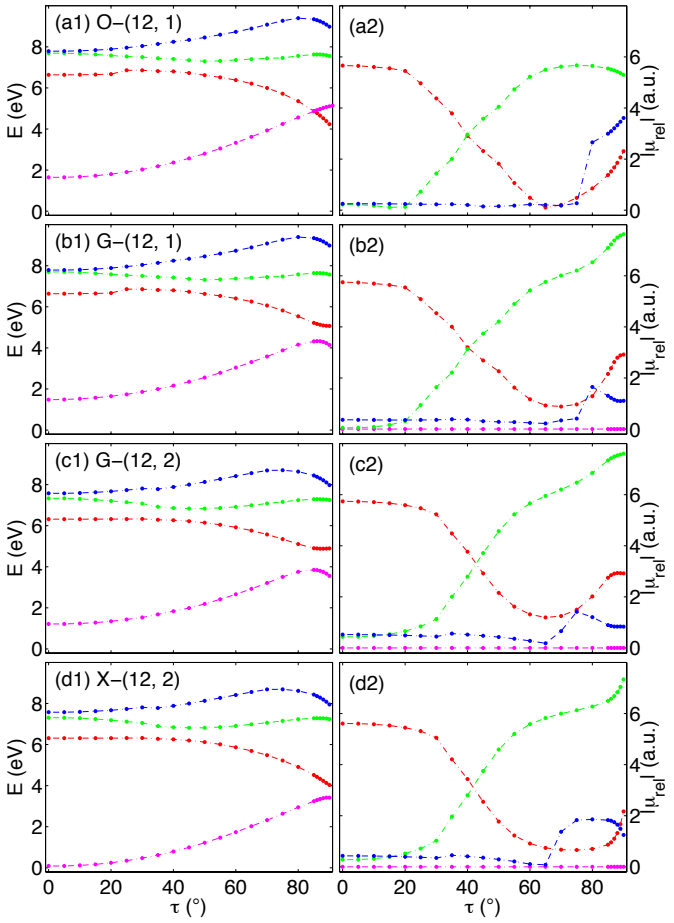

Figure 4.2: VOA-CIS-C(12, m) energies and corresponding dipole moments (relative to the ground state) $|\vec{\mu}_{\text{rel}}| \equiv |\vec{\mu} - \vec{\mu}_{\text{gs}}|$ as a function of torsional angle τ for PYCM. Each color represents a singlet state $S_i, i \in [0, 3]$. Note that in subfigure (a) (VOA-CIS-O(n, m)) the ground state is not included in the basis; thus, the HF energy is used for S_0.

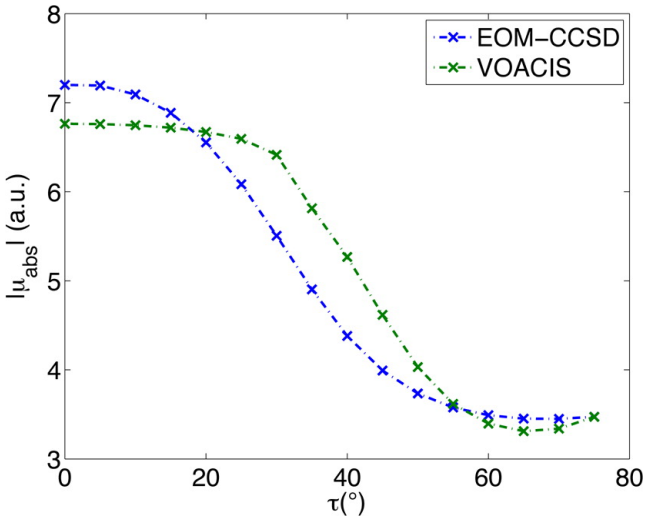

Figure 4.3: $|\vec{\mu}_{\text{abs}}|\,(a.u.)$ for S_1 as a function of torsional angle τ, for EOM-CCSD and VOA-CIS-G(12, 2) for PYCM. Note that both methods find very similar geometries for the avoided crossing as a function of τ.

To underscore the importance of a variational method, we provide a comparison with CIS(D) in Fig. 4.4(a) Here, although CIS(D) finds the correct excited states in the $\tau = 0$ and $\tau = 90$ limits, because the method is perturbative at bottom, CIS(D) PESs and dipole moments are not smooth (and in fact, completely distorted) along the τ coordinate. In part (b), we show results from SOS-CIS(D_0) the scaled-opposite version of the CIS(D_0). Recall that the CIS(D_n) suite of methods were designed to handle quasi-degenerate excited states. As expected, SOS-CIS(D_0) curves are much smoother than CIS(D) curves. However, numerically, we find that SOS-CIS(D_0) excitation energies are problematic. In particular, at the equilibrium geometry $\tau = 0°$, which should be far away from the crossing, SOS-CIS(D_0) predicts that the $\left|D^+A^-\right\rangle$ and the $|DA^*\rangle$ diabatic states should be strongly mixed together in the S_1 and S_2 adiabatic states, according to the dipole moments. Thus, SOS-CIS(D_0) would appear to not stabilize CT states enough. As a side note, we showed in Ref. [55] that CIS(D) also does not stabilize CT states enough, though CIS(D) does better than SOS-CIS(D_0) and much better than straight CIS.

Fig. 4.4 (c) and (d) present time-dependent DFT (TDDFT) results, using the exchange-correlation functionals B3LYP [84] and ωB97x [47] respectively. The former shows a large gap (~ 2 eV) for S_1 and S_2 at $\tau = 0°$, which is significantly larger than any other method (and the experimental data, 0.88 eV as well). Moreover, the predicted crossing of diabatical states is incorrectly around 70°. These errors are likely a reflection of the well-known failure of TD-DFT for CT states [34, 36, 37, 38, 39, 40] when there is no long-range correction [46, 47, 48, 49, 85, 86, 87, 88, 89, 90, 91, 92, 93].

By including long-range exchange, ωB97x [47] performs much better than B3LYP in generating balanced CT vs. non-CT excited states, and it locates an avoided crossing near 30° (in agreement with EOM-CCSD and VOA-CIS).

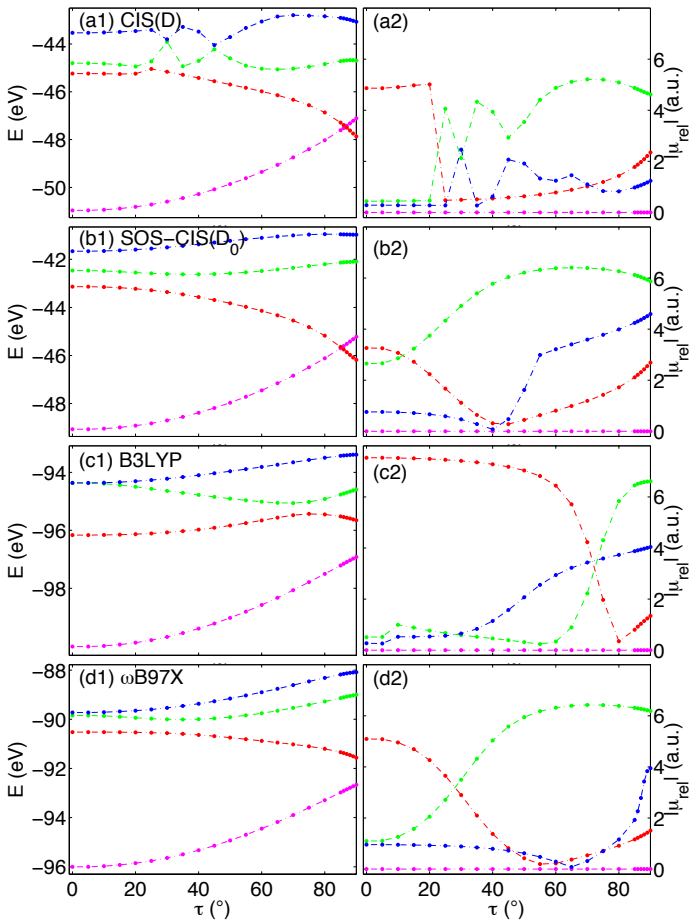

Figure 4.4: CIS(D), SOS-CIS(D_0) and TDDFT(B3LYP and ωB97x) energies and corresponding dipole moments (relative to the ground state) $|\vec{\mu}_{\text{rel}}| \equiv |\vec{\mu} - \vec{\mu}_{\text{gs}}|$ as a function of torsional angle τ for PYCM. Each color represents a singlet state $S_i, i \in [0, 3]$.

Finally, around $\tau = 90°$, we found an intersection between S_1 and S_0. Avoided crossings between ground and excited states are common for systems that decay vibronically, and as for all near degeneracies, an accurate energetic description can be made only by invoking a variational electronic structure method. For PYCM, at the $S_0 - S_1$ crossing, it is a locally excited state $|\mathrm{DA}^*\rangle$ that is mixed together with the ground state.

For a faithful and smooth representation of a crossing, one must treat all ground and excited states on equal footing. Note, however, that all methods in Fig. 4.4 ignore $S_0 - S_1$ mixing and, as such, one often finds erroneous potential energy surfaces (e.g., $S_0 - S_1$ conical intersections with the wrong topology). Among the suite of VOA-CIS methods, VOA-CIS-O(n, m) has the exact same problem; in fact, VOA-CIS-O(n, m) predicts that S_1 can have a lower energy than the ground state energy E_{HF}. Fortunately, using VOA-CIS-G(n, m) or VOA-CIS-X(n, m) we can safely include the ground state wavefunction while barely changing with relative energies among the excited states. This fortunate state of affairs reflects the beauty of VOA-CIS as a variational method.

Diabatization with Boys Localization

Having calculated smooth adiabatic potential energy surfaces through the VOA-CIS algorithm, one can make a preliminary analysis of electronic relaxation processes through diabatization. In the Appendix, we briefly review Boys localization as a tool for generating localized diabatization. Using Boys localized diabatization, in Fig. 4.5 we plot the energies and relative dipole moments from VOA-CIS-G(12, 2), for both adiabatic states (S_1 and S_2) and their corresponding diabatic states for the PYCM molecule (again, as a function of the torsional angle τ). States $1, 2$ and a, b represent adiabatic and diabatic states respectively. As would be expected in an avoided crossing, the energies of diabatic states a and b do cross near $\tau = 40°$. Moreover, in part (b), the dipole moments show that diabatic state a is indeed the CT state, characterized by a large dipole moment; whereas state b is a non-CT excited state. Thus, Boys-localized diabatic VOA-CIS is in agreement with the experimentalist's picture of PYCM, and we may conclude that the VOA-CIS algorithm gives us a meaningful

starting point for studying electronic relaxation.

Lastly, beyond individual surface energies, Fig. 4.5 provided us with a plot of the diabatic coupling h_{ab} (in part (a)) as a function of τ. According to the Condon approximation [11], one assume that h_{ab} is a constant at all geometries. From the figure, however, we see that h_{ab} increases smoothly with τ, so that the absolute value of h_{ab} at $\tau = 80^\circ$ is roughly twice as big as the value at $\tau = 0^\circ$. This form of the diabatic coupling will be important for calculating the physical relaxation time for PYCM.

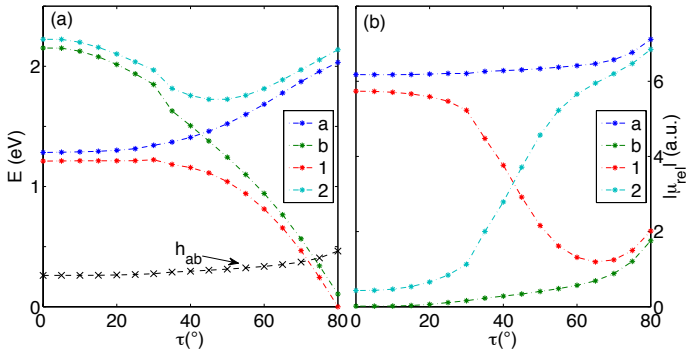

Figure 4.5: (a) VOA-CIS-G(12, 2) energy relative to E_1 at $\tau = 80°$ and (b) $|\vec{\mu}_{\text{rel}}|$ relative to the ground state, as a function of torsional angle τ for PYCM, for both adiabatic(labeled as $1, 2$) and diabatic(labeled as a, b) states. In part (a), diabatic coupling h_{ab} is also shown.

4.1.2. Benchmark Molecules

As another test of the VOA-CIS method, we study the 28 small to medium-sized molecules recently benchmarked by the Thiel group [4]. This rich set of organic test molecules includes unsaturated aliphatic hydrocarbons, aromatic hydrocarbons and heterocycles, carbonyl molecules (including aldehydes, ketones and amides) and nucleobases. The relevant excited states are usually of valence character, though several Rydberg states are also included; nominally, all vertical excitations can be classified as either $\sigma \rightarrow \pi^*$, $\pi \rightarrow \pi^*$ or $n \rightarrow \pi^*$. In Ref. [4], the Thiel group provided singlet and triplet energies, as calculated by a variety of different methods, including CASPT2, CC2, CCSD and CC3.

In this work, we have performed VOA-CIS calculation for all singlet excited states considered by Thiel *et al* [4], specifically 104 calculations. We restricted ourselves to singlets because we do not yet have functional VOA-CIS triplet code. All calculations were performed with the TZVP basis set and we used the geometries as provided in Ref. [4]. Using the symmetry of each electronic state, we were able to compare our VOA-CIS data with all other electronic structure data in Table 4.4 in the Sec. 4.4.1.

Method #1 for Quantifying Accuracy: Absolute Error

In order to compare VOA-CIS data quantitatively versus the Thiel benchmarked data, two different approaches seem intuitive. On the one hand, we can use absolute errors. To be precise, assume we have two sets of energies obtained from different methods, one labeled std for reference, and the other labeled trial for our new data. For the mth ($m = 1, 2 \cdots 28$) molecule, assuming we get n_m states, and for each state j, we can define an *absolute* error for that state:

$$\mathrm{Err}_{m,j} = E^{\mathrm{trial}}_{m,j} - E^{\mathrm{std}}_{m,j} \quad (j = 1, 2 \cdots n_m)$$

With this in mind, we can estimate the overall quality of the VOA-CIS method by computing a mean absolute error relative to the standard reference energy. In other words, fore each

molecule m, we compute the mean absolute value $\mathrm{Err}_{m,j}$:

$$\mathrm{Err}_m^a \equiv \frac{\sum_{j=1}^{n_m} |\mathrm{Err}_{m,j}|}{n_m} \tag{4.1}$$

Method #2 for Quantifying Accuracy: Relative Error

Beyond absolute energy errors, another option is to analyze the VOA-CIS method through relative energy errors. Because VOA-CIS was designed to optimize orbitals and thus rebalance relative vertical excited state energies (rather than absolute vertical energies), we might expect to see better performance for relative energies according to VOA-CIS. In fact, for a few cases, we find that VOA-CIS tends to underestimate excitation energies – for instance, in Sec. 4.1.4 we will show that VOA-CIS consistently underestimates absolute vertical excitation energies of Rydberg states. Nevertheless, even with Rydberg states present, the method VOA-CIS does find much more accurate relative excited state energies than absolute excited state energies. With that in mind, we can define a simple measure of the relative error of VOA-CIS for molecule m as :

$$\mathrm{Err}_m^b \equiv \sqrt{\frac{\sum_{i,j=1}^{n_m} \left(\mathrm{Err}_{m,i} - \mathrm{Err}_{m,j}\right)^2}{n_m^2}} \tag{4.2}$$

(Since n_m can be 1, it is not convenient to define the denominator in Eqn. 4.2 as $n_m(n_m-1)$ as would be standard for a variance calculation.)

Notice that, if there were two sets of excitation energies with the following form,

$$y_{m,j} = x_{m,j} + c_m, \quad j = 1, 2 \cdots n_m.$$

then Err_m^a would give the overall shift $|c_m|$, while Err_m^b is exactly 0, according to the definitions above. For this reason, it is clear that Err^a and Err^b offer two important and

complementary means of assessing the validity of the VOA-CIS algorithm.

Results

In Fig. 4.6 and Fig. 4.7, we plot Err^a and Err^b respectively for the 28 different molecules in Thiel benchmark set. Now unfortunately, as the Thiel group emphasizes, it is not usually possible to conclude which reference method is the most accurate among the list of CC2, CC3, EOM-CCSD, CASPT2 and post-processed experimental data As such, in Figs. 4.6 and 4.7, we compare VOA-CIS versus all possible references, and we do the same for CIS and CIS(D). Both VOA-CIS and CIS(D) vastly outperform CIS, and most of the time, VOA-CIS closely follows CIS(D), suggesting that the latter two methods are nearly comparable. While CIS(D) does perform slightly better than VOA-CIS at vertical excitation energies, this discrepancy is not very surprising: CIS(D) includes all doubles and even triples at some level of perturbation theory, while VOA-CIS includes only a small subset of the doubles space. At the same time, by being a variational method, VOA-CIS works very well far away from the ground-state geometry, where CIS(D) fails. Furthermore, the Thiel benchmark set does not include any charge transfer complexes, where CIS(D) is unreliable [55].

Future work in this arena might well benefit by further extending the basis of the VOA-CIS Hamiltonian into the triples manifold, in order to give the method additional energetic accuracy. Currently, the VOA-CIS-G Hamiltonian is very small (dimension $n^2 \times n^2$ roughly), and improvements in the VOA-CIS algorithm may well be possible with only minimal cost.

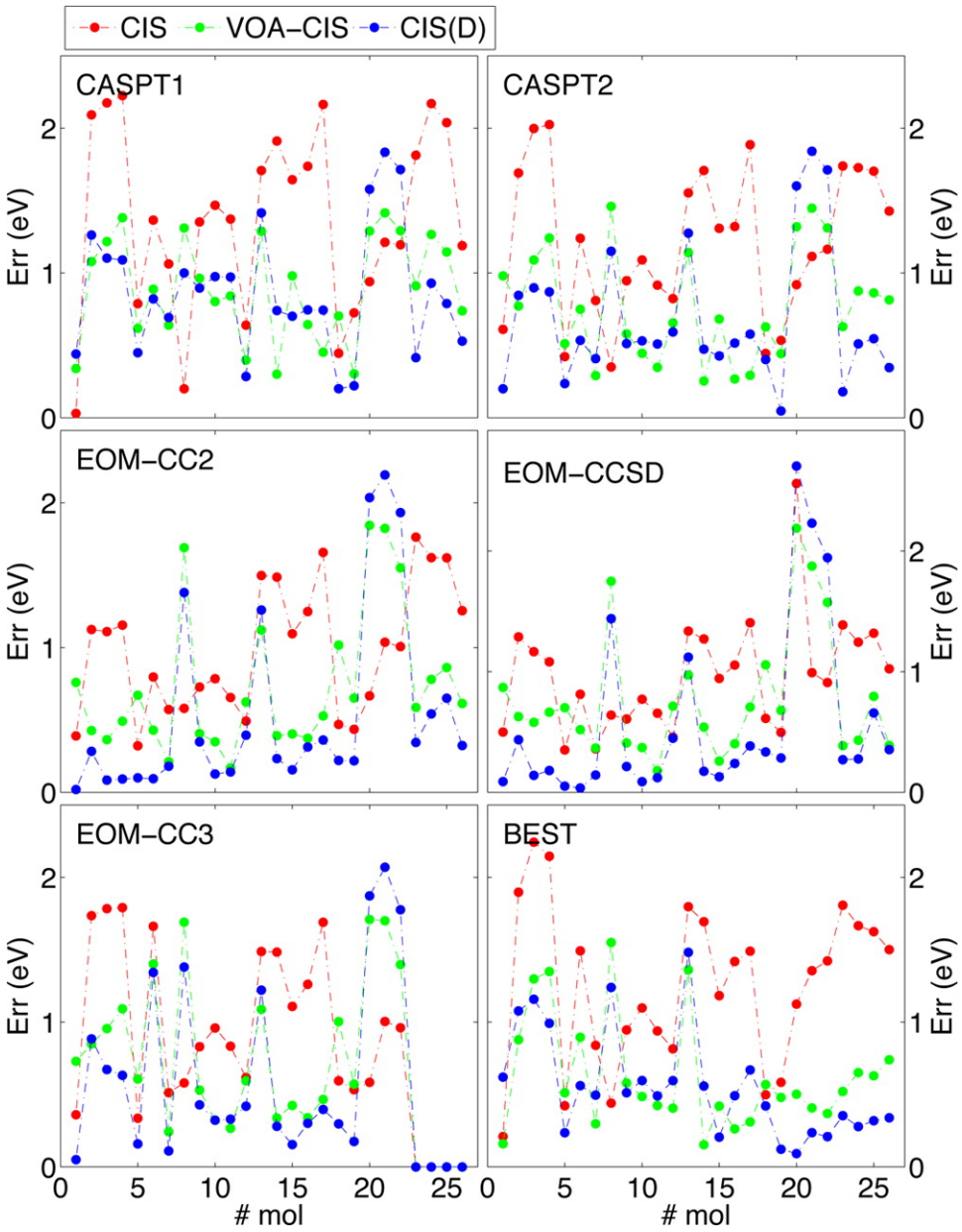

Figure 4.6: *Absolute* errors (Err^a) of CIS, VOA-CIS-G(12, 2) and CIS(D) as compared with different "standard" methods. "Best" here refers to the numerical values which Thiel *et al* have judged most accurate [4].

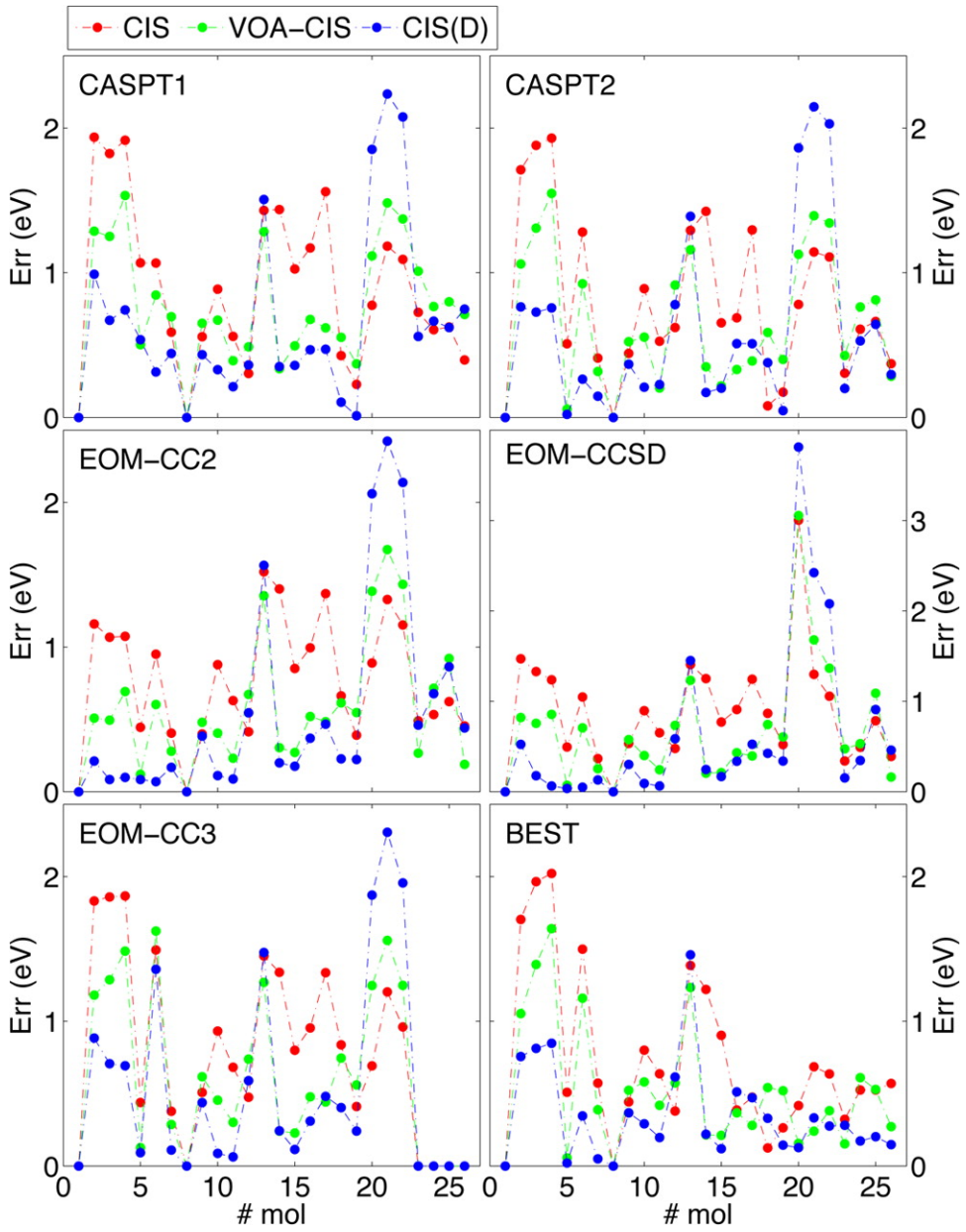

Figure 4.7: *Relative* errors (Err^b) of CIS, VOA-CIS-G(12, 2) and CIS(D) as compared with different "standard" methods. "Best" here refers to the numerical values which Thiel *et al* have judged most accurate.

4.1.3. CH_2O

For our final two test cases, we choose small organic molecules where Rydberg states are embedded in valence states. As the reader will see, these cases present difficulties for the VOA-CIS algorithm. We begin with formaldehyde.

Because of a plethora of Rydberg states mixed with valence states, for accurate results on formaldehyde, one is forced to use a large basis replete with diffuse functions and then one must hope for a balanced measure of the energies of valence states versus Rydberg states. When using a big basis set 6-311(2+, 2+)G(d, p), EOM-CCSD almost recovers experimental data; for the standard suite of post-CIS methods out there (CIS(D), CIS(D_0), SOS-CIS(D_0)), each successive method improves on the accuracy of its predecessor [1].

In Table 4.1 and Table 4.2, we present energies and oscillator strengths respectively, for CIS, TDHF, VOA-CIS-G(14, m) with $m = 1, 2, 3$, EOM-CCSD and experimental data. Experimental state assignments are from Ref. [1]. VOACIS and CIS excited states were matched up according to wavefunction overlap. In the case of VOA-CIS, we find that our results closely follow experimental data, with the exception of the S_1 state. For the most part, where experimental evidence is available, the difference between VOA-CIS and experiment is within 0.2 eV, much smaller than typical CIS data.

These are encouraging features of the VOA-CIS algorithm. For this problem, we find that VOA-CIS can actually address Rydberg states quite well (and with a much cheaper cost than EOM-CCSD). Nevertheless, the reader should note that VOA-CIS and EOM-CCSD oscillator strengths are quite different, often by a factor of 2.

#	E_{CIS}	E_{TDHF}	E_1	E_2	E_3	$E_{\mathrm{EOM\text{-}CCSD}}$	E_{Exp}	state
1	4.48	4.30	3.56	3.51	3.58	3.95	4.07	V
2	8.64	8.63	7.03	7.05	7.12	7.06	7.11	R
3	9.37	9.36	7.78	7.91	7.98	7.89	7.97	V
4	9.46	9.08	8.78	8.81	8.91	10.00	-	R
5	9.67	9.42	8.85	9.01	9.08	8.00	-	R
6	9.67	9.59	7.90	8.02	8.05	-	8.14	V
7	9.78	9.78	8.07	8.19	8.26	8.23	8.37	R
8	10.61	10.61	8.87	9.02	9.12	9.07	8.88	R
9	10.87	10.86	9.13	9.28	9.37	9.38	-	R
10	10.89	10.86	9.22	9.34	9.43	9.27	-	R

Table 4.1: Comparison of excitation energies for CH_2O from various *ab initio* methods with experimental data. Note the almost perfect recovery of experimental data from VOA-CIS except for the first state. $E_m, m \in \{1, 2, 3\}$ corresponds to VOA-CIS-G(12, m). Nuclear geometries are optimized with MP2/6-31G* (following Ref. [1]); EOM-CCSD and experimental data are also from Ref. [1]. Valence (V) and Rydberg (R) state assignments are from Ref. [2].

#	f_{CIS}	f_{TDHF}	f_1	f_2	f_3	$f_{\text{EOM-CCSD}}$
1	0.0000	0.0000	0.0000	0.0000	0.0000	0.0000
2	0.0227	0.0216	0.0096	0.0115	0.0123	0.0160
3	0.0467	0.0456	0.0390	0.0357	0.0397	0.0376
4	0.2606	0.2219	0.1335	0.1414	0.1312	0.2217
5	0.0005	0.0003	0.0001	0.0000	0.0000	0.0482
6	0.0160	0.0203	0.0338	0.0358	0.0318	-
7	0.0000	0.0000	0.0000	0.0000	0.0000	0.0000
8	0.0143	0.0138	0.0023	0.0018	0.0023	0.0115
9	0.0023	0.0025	0.0004	0.0006	0.0000	0.0330
10	0.0059	0.0033	0.0674	0.0516	0.0417	0.0193

Table 4.2: Comparison of oscillator strengths for CH_2O from various *ab initio* methods. $f_m, m \in \{1, 2, 3\}$ corresponds to VOA-CIS-G(12, m). Nuclear geometries are optimized with MP2/6-31G* (following Ref. [1]).

4.1.4. C_2H_4

For our final test case, we now show a clear failure of the VOA-CIS approach: the molecule ethlyene. Following the work of Martinez *et al* [94, 95], many researchers have studied the photochemistry of C_2H_4; after photoexcitation, the molecule is quickly funneled through a conical intersection where it pyramidalizes while also breaking a double bond to yield a *cis-trans* isomerization. Ethylene photoisomerization is a prototypical model system for photochemistry.

For ethylene, even more so than formaldehyde, at many geometries the lowest-lying states are dominated by Rydberg states (rather than valence states). In fact, at the equilibrium geometry the lowest lying few states are all Rydberg states (R($3s$), R($3p_x$), R($3p_y$) and R($3p_z$)) for C_2H_4, except for one valence state $\pi \rightarrow \pi^*$ [3]. For the most part, the Rydberg states were ignored by early nonadiabatic dynamics calculations [77] that focus on valence states instead; at the same time, however, the electronic structure community recognizes ethylene as a difficult test case for electronic structure precisely because of valence-Rydberg mixing.

With this in mind, we have sought to test the VOA-CIS method on ethylene, and to check whether we can find accurate potential energy surfaces. In Ref. [55], we reported strong results for twisted ethylene, where our results matched up well with MRCI results; but for a twisted geometry, all low-lying excited states for ethylene are valence states. In this chapter, in Table 4.3 we report results for ethylene at the ground-state geometry, where most Rydberg state compete lie energetically below any valence states.

Unfortunately, from Table 4.3, we find that the VOA-CIS method does poorly in this case. In particular, we find that Rydberg states are strongly stabilized by the VOA-CIS method, while (perhaps unsurprisingly) the ground state does not gain much correlation energy by orbital relaxation of Rydberg states. As a result, the VOA-CIS vertical excitation energies in Table 4.3 are all too low (by 1.0 to 1.5 eV). Even the CIS results agree much better with

the experiment than VOA-CIS. Lastly, and worst of all, VOA-CIS does not find the correct relative energies for this example. Over all, this molecule highlights that VOA-CIS is not a good option for electronic structure problems dominated by Rydberg states. Luckily, our interest is in condensed phase chemistry, and Michl has argued convincingly that Rydberg states will not be important in most solvents [78].

#	E_{CIS}	E_1	E_2	E_3	E_{exp}	state
1	7.12	5.84	5.83	6.13	7.11	R($3s$)
2	7.71	6.47	6.49	6.79	7.80	R($3p_y$)
3	7.74	6.98	7.05	7.37	7.60	V
4	7.86	6.47	6.48	6.77	8.01	R($3p_z$)
5	8.09	6.74	6.79	7.11	8.29	R($3p_x$)

Table 4.3: Comparison of excitation energies for C_2H_4. $E_m, m \in \{1, 2, 3\}$ corresponds to VOA-CIS-G(12, m). Nuclear geometries are optimized with MP2/6-31G* (following Ref. [1]). Experimental data also from Ref. [1]. Valence (V) and Rydberg (R) state assignments are from Ref. [3].

4.2. Discussion

Having demonstrated the strengths of the VOA-CIS algorithm (as well as its limitations), we now want to address two subtle points about how the VOA-CIS algorithm works, which may also give insight into its performance.

4.2.1. Visualizing the θ Matrix for Orbital Relaxation

The VOA-CIS algorithm finds an improved balance between CT and non-CT excited states via orbital relaxation. To that end, one can ask a very simple question: what is the nature of that orbital relaxation for the case of a CT excited state? To answer this question, in Fig. 4.8, we visualize the attachment-detachment densities [50] of the t matrix, together with the θ_{ai}^{II} matrix associated with a CT CIS state ($\left|\Psi_{\text{CIS}}^{I}\right\rangle$). In other words, for the latter we consider the electronic density of the state $|\Psi\rangle = \sum_{ai} \theta_{ai}^{II} a_a^\dagger a_i \left|\Psi_{\text{HF}}\right\rangle$. In analogy with standard CIS densities, the attachment-detachment densities for θ_{ai}^{II} are:

$$D_{ij}^{\text{det}} = \sum_{a} \theta_{ai}^{II} \theta_{aj}^{II} \tag{4.3}$$

$$A_{ab}^{\text{att}} = \sum_{i} \theta_{ai}^{II} \theta_{bi}^{II} \tag{4.4}$$

From Fig. 4.8, one can easily infer that, in the case of a CT excited state, according to VOA-CIS, orbital relaxation remains entirely local. Thus, even though a CT state is characterized by one bare electron moving a long distance from detachment to attachment, VOA-CIS predicts that the subsequent energetic drop in energy caused by electron-electron correlation is due to local orbital relaxation. This local nature of electronic shielding is consistent with the simple He_2 example studied in Ref. [29], and suggests that local correlation approaches [96] on top of CIS might even be possible.

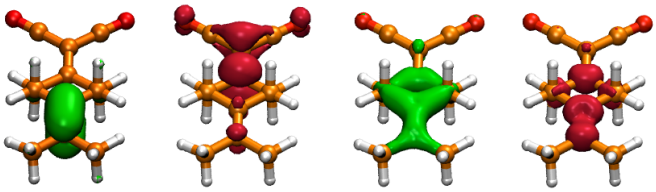

Figure 4.8: Detachment and attachment plots of t and θ for the CT state for PYCM.

4.2.2. Relation with TDHF

In broad terms, the VOA-CIS 'X' option stipulates that, by considering the set of CIS states, one can introduce wavefunctions into the electronic basis that help to capture the dynamical correlation of the ground state. For the sophisticated quantum chemist, this language bears the signature of TDHF, and indeed there is a close connection between TDHF and the VOA-CIS-X(n, m) algorithm. We will now demonstrate as much.

Using the language of Ref. [81] for this section only, the TDHF [80, 81] excitation energies and quasi-wavefunctions are defined via:

$$\begin{pmatrix} \mathbf{A} & \mathbf{B} \\ \mathbf{B}^* & \mathbf{A}^* \end{pmatrix} \begin{pmatrix} \mathbf{X} \\ \mathbf{Y} \end{pmatrix} = \omega \begin{pmatrix} 1 & 0 \\ 0 & -1 \end{pmatrix} \begin{pmatrix} \mathbf{X} \\ \mathbf{Y} \end{pmatrix}, \tag{4.5}$$

in which $\omega = E_{\mathrm{CIS}} - E_{\mathrm{HF}}$ is the excitation energy, and the corresponding matrix elements are:

$$\begin{aligned} \mathbf{A}_{ia,jb} &= \delta_{ij}\delta_{ab}(\epsilon_a - \epsilon_i) + \langle aj \,||\, ib \rangle \\ \mathbf{B}_{ia,jb} &= \langle ab \,||\, ij \rangle \end{aligned} \tag{4.6}$$

Now, let us write out Eqn. 4.5 as two separate equations:

$$\begin{cases} \mathbf{AX} + \mathbf{BY} = \omega \mathbf{X} \\ \mathbf{B}^*\mathbf{X} + \mathbf{A}^*\mathbf{Y} = -\omega \mathbf{Y} \end{cases} \tag{4.7}$$

Setting B=0 corresponds to standard CIS theory (or the Tamm-Dancoff approximation for TD-DFT).

If we now stipulate that the B matrix should be a first order perturbation in the Hamiltonian relative to CIS, while the Y vector should be the first order correction to the wavefunction, we notice that in Eqn. 4.7, the first equation is second order in $\mathbf{Y}$, while the second one is first order in $\mathbf{Y}$. At this point, one can solve for $\mathbf{Y}$ in a straightforward manner via perturbation

theory. If one further approximates that $\mathbf{A}$ is diagonally-dominant when computing $\mathbf{A}^{-1}$ matrix, one arrives at the final form:

$$Y_{ai} \approx -\sum_{bj} \frac{\langle ab \,||\, ij \rangle \, X_{bj}}{\omega + \epsilon_a - \epsilon_i} = -\frac{\left\langle \Phi_{\mathrm{HF}} \left| H a_a^\dagger a_i \right| \Psi_{\mathrm{CIS}} \right\rangle}{\epsilon_a - \epsilon_i + E_{\mathrm{CIS}} - E_{\mathrm{HF}}} \tag{4.8}$$

Eqn. 4.8 is identical to Eqn. 3.3 (up to a constant factor). This connection is a strong endorsement of our VOA-CIS algorithm. The usual interpretation of the $\mathbf{Y}$ is a "de-excitation" of the ground state relative to a singles wavefunction, or in other words, a doubly excited contribution to the ground-state. Thus, it would appear that the VOA-CIS algorithm is an extension of TDHF to include the electron-electron correlations that excited states inflict on each other (not just on the ground state). In the future, it would be interesting to compare the ground-state correlation energy produced by VOA-CIS-X(n, m) with the TDHF(or RPA) correlation energy.

4.3. Conclusions and Future Directions

In this article, we have presented the VOA-CIS algorithm and benchmarked its performance across a series of interesting photoexcitable organic molecules. VOA-CIS is a variational post-CIS electronic structure theory method that generates smooth and (usually) accurate potential energy surfaces; it works well for isolated energies or when there are degeneracies present. The method will not work well for molecules where Rydberg states dominate the excited state spectrum. The essential input for the VOA-CIS algorithm is the number of CIS states requested n; otherwise, the algorithm can be viewed as a blackbox approach. In many cases, VOA-CIS achieves energetic accuracy comparable to much more expensive methods and with a much cheaper cost.

Looking forward, our next goals in developing the VOA-CIS algorithm are threefold. 1. We plan to optimize our VOA-CIS code, and implement a completely parallelizable algorithm. 2. We will explore the possibilities of incorporating triples excitations into the VOA-CIS

algorithm for extra accuracy. 3. We will develop analytic gradients and derivate coupling for VOA-CIS. In the end, we believe the VOA-CIS algorithm can become a robust algorithm for studying electronic relaxation in almost all organic chromophores.

4.4. Appendix

4.4.1. Table for Benchmark Molecules

We now list the individual excited state energies that were calculated and averaged together to make up Figs. 4.6- 4.7. 28 molecules are included in the benchmark set of Thiel *et al.*

name	#mol	#S	#CIS	#V*	CASPT2	CASPT2	CC2	CCSD	CC3	Best	E_{CIS}	E_V^*
Ethene	0	0	0	1	7.98	8.62	8.40	8.51	8.37	7.80	8.01	7.64
E-Butadiene	1	0	0	0	6.23	6.47	6.49	6.72	6.58	6.18	6.44	5.90
	1	1	6	3	6.27	6.83	7.63	7.42	6.77	6.55	9.22	7.76
all-E-	2	0	0	0	5.01	5.31	5.41	5.72	5.58	5.10	5.47	4.96
Hexatriene	2	1	6	2	5.20	5.42	6.67	6.61	5.72	5.09	8.24	6.92
all-E-	3	0	3	1	4.38	4.64	5.87	5.99	4.97	4.47	7.50	6.32
Octatetraene	3	1	0	0	4.42	4.70	4.72	5.07	4.94	4.66	4.83	4.19
Cyclopropene	4	0	1	0	6.36	6.76	6.96	6.96	6.90	6.76	7.34	6.21
	4	1	0	1	7.45	7.06	7.17	7.24	7.10	7.06	6.92	6.59
Cyclopentadiene	5	0	0	0	5.27	5.51	5.69	5.87	5.73	5.55	5.54	5.09
	5	1	3	3	6.31	6.31	7.05	7.05	6.61	6.31	8.42	7.49
	5	2	5	9	7.89	8.52	8.86	8.95	6.69	-0.00	8.92	8.86
Norbornadiene	6	0	0	0	5.28	5.34	5.57	5.80	5.64	5.34	5.67	5.18
	6	1	1	1	6.20	6.11	6.37	6.69	6.49	6.11	7.25	6.50
	6	2	3	5	6.48	7.32	7.65	7.87	7.64	-0.00	8.04	7.70
	6	3	4	4	7.36	7.44	7.66	7.87	7.71	-0.00	8.27	7.57
Benzene	7	1	0	0	6.30	6.45	6.68	6.74	6.68	6.54	6.10	4.99
Naphthalene	8	0	1	1	4.03	4.24	4.45	4.41	4.27	4.24	5.24	4.70
	8	1	0	0	4.56	4.77	4.96	5.21	5.03	4.77	5.09	4.50
	8	2	5	6	5.39	5.90	6.22	6.23	5.98	5.90	7.34	6.96
	8	3	2	2	5.53	6.00	6.21	6.53	6.07	6.00	6.77	6.42
	8	3	2	4	5.53	6.00	6.21	6.53	6.07	6.00	6.77	6.69

	8	4	3	3	5.54	6.07	6.25	6.55	6.33	6.07	7.08	6.44
	8	6	4	5	5.93	6.33	6.57	6.77	6.57	6.33	7.27	6.72
Furan	9	0	0	0	6.04	6.43	6.75	6.80	6.60	6.32	6.53	6.26
	9	1	2	1	6.16	6.52	6.87	6.89	6.62	6.57	8.16	6.57
	9	2	7	7	7.66	8.22	8.78	8.83	8.53	8.13	9.15	8.97
Pyrrole	10	0	2	1	5.92	6.31	6.61	6.61	6.40	6.37	7.65	6.43
	10	1	0	2	6.00	6.33	6.83	6.87	6.71	6.57	6.78	6.70
	10	2	8	8	7.46	8.17	8.44	8.44	8.17	7.91	8.89	8.63
Imidazole	11	0	1	0	6.52	6.81	6.86	7.01	6.82	6.81	7.21	6.23
	11	1	0	1	6.72	6.19	6.73	6.80	6.58	6.19	7.07	6.52
	11	2	3	3	7.15	6.93	7.28	7.27	7.10	6.93	7.96	7.15
	11	3	2	2	7.56	7.91	8.00	8.15	7.93	-0.00	7.90	6.79
	11	4	9	9	8.51	8.15	8.62	8.70	8.45	-0.00	9.33	8.78
Pyridine	12	0	1	1	4.84	5.02	5.32	5.27	5.15	4.85	6.19	5.48
	12	1	0	0	4.91	5.14	5.12	5.25	5.05	4.59	6.13	5.44
	12	2	6	6	5.17	5.47	5.39	5.73	5.50	5.11	8.61	8.08
	12	3	2	3	6.42	6.39	6.88	6.94	6.85	6.26	6.51	6.68
	12	4	4	5	7.23	7.46	7.72	7.94	7.70	7.18	8.42	7.99
	12	5	5	4	7.48	7.29	7.61	7.81	7.59	7.27	8.44	7.86
Pyrazine	13	0	0	0	3.63	4.12	4.26	4.42	4.24	3.95	5.13	4.01
	13	1	4	2	4.52	4.70	4.95	5.29	5.05	4.81	7.03	4.92
	13	2	1	1	4.75	4.85	5.13	5.14	5.02	4.64	5.98	4.76
	13	3	3	3	5.17	5.68	5.92	6.02	5.74	5.56	6.70	5.35
	13	4	11	5	6.13	6.41	6.70	7.13	6.75	6.60	9.81	6.58
	13	5	2	4	6.70	6.89	7.10	7.18	7.07	6.58	6.65	6.37
	13	6	5	6	7.57	7.79	8.13	8.34	8.06	7.72	8.75	7.80
	13	7	6	7	7.70	7.65	8.07	8.29	8.05	7.60	9.07	7.85
Pyrimidine	14	0	0	0	3.81	4.44	4.49	4.70	4.50	4.55	5.87	4.88
	14	1	2	1	4.12	4.81	4.84	5.12	4.93	4.91	6.56	5.52
	14	2	1	2	4.93	5.24	5.51	5.49	5.36	5.44	6.50	5.87
	14	3	3	4	6.72	6.64	7.12	7.17	7.06	6.95	6.90	7.15

	14	4	7	7	7.32	7.64	8.08	8.24	8.01	-0.00	8.88	8.48
	14	5	6	6	7.57	7.21	7.79	7.97	7.74	-0.00	8.61	8.06
Pyridazine	15	0	0	0	3.48	3.78	3.90	4.11	3.92	3.78	4.91	3.59
	15	1	1	1	3.66	4.32	4.40	4.76	4.49	4.32	6.10	4.78
	15	2	2	2	4.86	5.18	5.37	5.35	5.22	5.18	6.32	5.24
	15	3	4	3	5.09	5.77	5.81	6.00	5.74	5.77	7.29	5.61
	15	4	6	5	5.80	6.52	6.40	6.70	6.41	-0.00	8.43	7.00
	15	5	3	4	6.61	6.31	7.00	7.09	6.93	-0.00	6.56	6.34
	15	6	5	6	7.39	7.29	7.57	7.79	7.55	-0.00	8.32	7.43
	15	7	7	7	7.50	7.62	7.90	8.11	7.82	-0.00	8.67	7.83
s-Tetrazine	17	0	0	0	1.96	2.24	2.47	2.71	2.53	2.24	3.52	1.83
	17	1	1	1	3.06	3.48	3.67	4.07	3.79	3.48	5.67	3.61
	17	2	2	2	4.51	4.73	5.10	5.32	4.97	4.73	6.08	4.53
	17	3	3	4	4.89	4.91	5.20	5.27	5.12	4.91	6.24	4.76
	17	4	4	3	5.05	5.18	5.53	5.70	5.34	5.18	6.56	4.72
	17	6	5	5	5.28	5.47	5.50	5.70	5.46	5.47	6.65	5.12
	17	7	9	6	5.48	6.07	6.32	6.76	6.23	-0.00	9.36	6.12
	17	8	11	8	5.99	6.38	6.91	7.25	6.87	-0.00	9.79	6.77
	17	10	8	9	6.37	6.77	6.70	6.99	6.67	-0.00	8.68	6.97
	17	11	6	7	7.13	6.96	7.60	7.66	7.45	-0.00	6.88	6.52
	17	12	7	10	7.54	7.43	7.75	8.06	7.79	-0.00	8.58	7.28
	17	13	10	11	7.94	8.15	8.65	8.88	8.51	-0.00	9.53	8.35
Formaldehyde	18	0	0	0	3.91	3.98	4.09	3.97	3.95	3.88	4.46	2.93
	18	1	1	2	9.09	9.14	9.35	9.26	9.18	9.10	9.62	9.04
	18	2	2	3	9.77	9.31	10.34	10.54	10.45	9.30	9.67	9.05
Acetone	19	0	0	0	4.18	4.42	4.52	4.43	4.40	4.40	5.10	3.78
	19	1	3	3	9.10	9.27	9.29	9.26	9.17	9.10	9.77	9.31
	19	2	2	2	9.16	9.31	9.74	9.87	9.65	9.40	9.69	8.89
Formamide	21	0	0	0	5.61	5.63	5.76	5.66	5.65	5.63	6.42	5.25
	21	1	2	1	7.41	7.44	8.15	4.52	8.27	7.44	8.82	6.84

	21	2	4	3	10.50	10.54	11.24	11.34	10.93	-0.00	10.57	8.37
Acetamide	22	0	0	0	5.54	5.80	5.77	5.71	5.69	5.80	6.58	5.26
	22	1	2	2	7.21	7.27	7.66	7.85	7.67	7.27	9.02	7.07
	22	2	4	3	10.08	10.09	10.71	10.77	10.50	-0.00	9.86	7.65
Propanamide	23	0	0	0	5.48	5.72	5.78	5.74	5.72	5.72	6.62	5.20
	23	1	2	2	7.28	7.20	7.56	7.80	7.62	7.20	9.00	7.22
	23	2	4	3	9.95	9.94	10.33	10.34	10.06	-0.00	9.82	7.73
Cytosine	24	0	0	0	4.39	4.68	4.80	4.98	-0.00	4.66	6.07	5.26
	24	1	1	1	5.00	5.12	5.13	5.45	-0.00	4.87	6.85	5.39
	24	2	2	2	6.53	5.54	5.01	5.99	-0.00	5.26	7.21	5.59
	24	3	3	3	5.36	5.54	5.71	5.95	-0.00	5.62	7.45	6.21
	24	4	5	6	6.16	6.40	6.65	6.81	-0.00	-0.00	7.99	7.30
	24	5	10	9	6.74	6.98	6.94	7.23	-0.00	-0.00	9.04	7.82
Thymine	25	0	0	0	4.39	4.94	4.94	5.14	-0.00	4.82	6.23	4.80
	25	1	1	1	4.88	5.06	5.39	5.60	-0.00	5.20	6.31	5.88
	25	2	4	4	5.88	6.15	6.46	6.78	-0.00	6.27	8.24	7.17
	25	3	3	2	5.91	6.38	6.33	6.57	-0.00	6.16	7.67	6.12
	25	4	6	5	6.10	6.52	6.80	7.05	-0.00	6.53	8.65	7.45
	25	5	7	6	6.15	6.86	6.73	7.67	-0.00	-0.00	8.88	8.09
	25	6	5	7	6.70	7.43	7.18	7.87	-0.00	-0.00	8.58	8.15
	25	7	8	8	7.13	7.43	7.71	7.90	-0.00	-0.00	9.59	8.63
Uracil	26	0	0	0	4.54	4.90	4.91	5.11	-0.00	4.80	6.22	4.81
	26	1	1	1	5.00	5.23	5.52	5.70	-0.00	5.35	6.49	6.03
	26	2	4	4	5.82	6.15	6.43	6.76	-0.00	6.26	8.36	7.16
	26	3	2	2	6.00	6.27	6.73	7.68	-0.00	6.10	7.61	6.09
	26	4	3	3	6.37	6.97	6.26	6.50	-0.00	6.56	7.82	7.13
	26	5	5	5	6.46	6.75	6.96	7.19	-0.00	6.70	8.76	7.58
	26	6	7	8	6.95	7.28	7.12	7.74	-0.00	-0.00	9.33	8.83
	26	7	8	7	7.00	7.42	7.66	7.81	-0.00	-0.00	9.47	8.48
Adenine	27	0	0	0	5.13	5.20	5.28	5.37	-0.00	5.25	6.23	5.76
	27	1	1	2	5.20	5.30	5.42	5.61	-0.00	5.25	6.37	5.89

	27	2	2	1	6.15	5.21	5.27	5.58	-0.00	5.12	7.05	5.80
	27	3	4	3	6.86	5.97	5.91	6.19	-0.00	5.75	7.50	6.78
	27	4	5	7	6.24	6.35	6.58	6.83	-0.00	-0.00	7.69	7.28
	27	5	8	8	6.72	6.64	6.93	7.17	-0.00	-0.00	8.16	7.55
	27	6	10	10	6.99	6.88	7.49	7.72	-0.00	-0.00	8.37	8.01

Table 4.4: A comparison of VOA-CIS energies with results from other excited-state approaches. Benchmark molecules and reference data taken from Ref. [4]. "Best" refers to the data which Thiel *et al* estimated to be most reliable Ref. [4].

*: "V" means VOA-CIS results.

CHAPTER 5 : The Fully Variatonal Orbital Adapted Configuration Interaction Singles Method

This chapter is adapted from Ref. [97].

5.1. Introduction

Calculating accurate excited states for photochemistry is a difficult problem, in no small part because of the many practical requirements. For photochemistry, an accurate model cannot be perturbative because state crossings are crucial for modeling relaxation; conical intersections are of great interest. Furthermore, photochemistry requires sampling a large configuration space of geometries, so that any useful must be very cheap. Finally, the daemons of electron-electron correlation theory are always exposed in excited state calculations, where one must calculate the relative energies of excited state with very different character (some local excitations, some charge transfer (CT)) to within a kcal/mol. Altogether, these requirements make up a significant challenge.

5.1.1. Overview of the Variational Orbital Adapted CIS (VOA-CIS)

In the previous chapters, we have proposed a new protocol for treating excited states based on the concept of orbital adaptation. We will now briefly review the concept of orbital adaptation in the context of wavefunctions theory. Recall that, according to configuration intersection singles (CIS), one builds an excited state by making the ansatz that the state should be an arbitrary combination of single excitations on top of a ground state reference. Thus, a typical CIS wavefunction can be written as $\left|\Psi^I_{\text{CIS}}\right\rangle = \sum_{ai} t_i^{aI} \left|\Phi_i^a\right\rangle$. Usually, CIS wavefunctions are qualitatively correct, but the energies of CIS states are not close to chemical accuracy. In the context of photoexcitation experiments, whenever charge transfer states arise, CIS fails miserably due to its overestimation of CT state excitation energies of 1-2 eV.[29]

With this in mind, in Chapter 2, we proposed a simple Orbital Optimized CIS (OO-CIS) perturbative correction to CIS. The main idea of the OO-CIS correction was to correct the molecular orbitals to better account for excited state density, rather than the HF ground state. Recall that, according to the usual CIS procedure, the molecular orbitals are optimized for the HF ground state only and then frozen for all subsequent CIS excited states.

According to OO-CIS one can rotate the occupied space slightly in the virtual space (with an amount depending on the specific state), and thus achieve a better representation of the final wavefunction. For charge-transfer states, OO-CIS energies can be comparable to [30] CIS(D)[2] energies (which are also perturbative).

Unfortunately, we have found that the perturbative nature of OO-CIS prevents any wide applicability in photochemistry. First, for charge transfer states, we now believe that the OO-CIS correction, while large, is *still not big enough!* Second, as a perturbative method, OO-CIS is not appropriate for modeling any curve crossings. For these reasons, we have come to realize that, to describe the electronic relaxation after photoexcitation, there may be no substitute for a variational approach. Such a reasoning has led us to construct a Variational Orbital Adapted CIS (VOA-CIS) ansatz. VOA-CIS is somewhat similar in spirit both to Head-Gordon's CIS(D_n)[62], Jorgensen's CC(2)[64] and Matsika's CIS(2)[74]. The basic premise is to "perturb-and-then-diagonalize", rather than diagonalize and then perturb (which is more common). VOA-CIS requires the diagonalization of the Hamiltonian in a reduced subspace of single and double excitations.

As detailed Ref. [7, 55], there are several options available for a typical VOA-CIS calculation. A VOA-CIS calculation can be specified by the notation VOA-CIS-C(n, m), where C, n, m must be specified. Here, n is the number of CIS states to be included in a variational calculation; one can consider this CIS subspace effectively an **active** space. m refers to the number of double excitations included in our variational space, and C refers to treatment of the ground state. In practice, in Ref. [7], we found that VOA-CIS-G(n, 2) yield the consistently best results among all different options, and this will be the only method against which we compare below. For a VOA-CIS-G(n, 2) calculation, one diagonalizes the Hamiltonian in the following basis:

$$\left\{ \left|\Phi_{\mathrm{HF}}\right\rangle, \left|\Psi^I_{\mathrm{CIS}}\right\rangle, \sum_{ai} \theta^{IJ}_{ai} a^\dagger_a a_i \left|\Phi^J_{\mathrm{CIS}}\right\rangle \right\} \tag{5.1}$$

Here, the basis of double excitations are obtained by performing perturbation theory (similar to those in OO-CIS). The θ^{IJ}s are defined as:

$$\begin{aligned} -\frac{1}{2}Y_{ai}^{IJ} &\equiv +\sum_{bcjk} t_k^{cI} \left\langle \Phi_k^c \left| \hat{H}\ a_a^\dagger a_i \right| \Phi_j^b \right\rangle\ t_j^{bJ} \qquad (5.2) \\ &= +\sum_{bcj} \left(t_i^{cI} t_j^{bJ} \langle cj \,||\, ab \rangle + t_j^{cI} t_j^{bJ} \langle ci \,||\, ba \rangle \right) \\ &\quad +\sum_{bjk} \left(t_k^{aI} t_j^{bJ} \langle ij \,||\, bk \rangle + t_k^{bI} t_j^{bJ} \langle ij \,||\, ka \rangle \right) \\ \theta_{ai}^{IJ} &\equiv -\frac{Y_{ai}^{IJ}}{\epsilon_a - \epsilon_i + E^J - E^I} \qquad (5.3) \end{aligned}$$

The total dimensionality of the basis is $1 + n + n^2$. All matrix elements necessary for the diagonalization can be easily evaluated through second-quantization, as shown in Chapter 3.

5.1.2. Shortcomings of VOA-CIS

Despite our efforts, the VOA-CIS still has several shortcomings. First, the VOA-CIS algorithm depends not only on the CIS subspace, but also on the specific choice of CIS wavefunctions. Thus, the algorithm is not well-defined whenever there is a degeneracy of CIS states. Second, because a set of CIS states (as ordered by energy) can change dramatically as a function of nuclear geometry, it would necessarily be difficult to construct a stable gradient or derivative coupling for a set of VOA-CIS states (where amplitude response would likely lead to numerical instabilities [98]).

5.1.3. Outline of This Chapter

With this history in mind, in Sec. 5.2 will introduce a fully variational VOA-CIS (FVOA-CIS) algorithm, including all technical and computational details. The fundamental difference between FVOA-CIS and VOA-CIS is the choice of doubles space: whereas VOA-CIS includes only a small set of doubles (as calculated by perturbation theory in Eqn. 5.1), FVOA-CIS includes a more a larger (and thus more flexible) space of doubles; see Eqn. 5.4.

Moreover, FVOA-CIS is fully variational–it depends only on the CIS subspace (rather than on the individual of CIS eigenvectors) – so that a gradient and derivative coupling should be possible. In Sec. 5.3, we will present an application to a model system. In Sec. 5.4, we show FVOA-CIS computational cost might be reduced by starting with TDDFT orbitals and amplitudes. Sec. 5.5 is a brief discussion and conclusion.

5.2. FVOA-CIS method

To construct a more general ansatz for the post-CIS wavefunction (which depends only on the initial choice of CIS subspace), we will make the following Fully Variational Orbital Adapted CIS (FVOA-CIS) ansatz:

$$\begin{aligned} \left|\Psi^{\text{FVOA-CIS}}\right\rangle = \quad & +c_{\text{HF}} \left|\Phi_{\text{HF}}\right\rangle + \sum_{I} c^{I}_{\text{CIS}} \left|\Psi^{I}_{\text{CIS}}\right\rangle \\ & + \sum_{aiI} c^{aiI} a^{\dagger}_{a} a_{i} \left|\Psi^{I}_{\text{CIS}}\right\rangle \end{aligned} \tag{5.4}$$

As constructed, the FVOA-CIS ansatz depends only the subspace of CIS states $\left\{\left|\Psi^{I}_{\text{CIS}}\right\rangle\right\}$. The FVOA-CIS wavefunction is determined by diagonalizing the Hamiltonian in in a reduced basis $\left\{ \left|\Phi_{\text{HF}}\right\rangle, \left|\Psi^{I}_{\text{CIS}}\right\rangle, a^{\dagger}_{a} a_{i} \left|\Psi^{I}_{\text{CIS}}\right\rangle \right\}$ and determining the $\vec{c}$ coefficients.

Let NOV be the number of occupied orbitals multiplied by the number of virtual orbitals, NOV= NO×NV; in other words, NOV is the dimensionality of the singles block of the Hamiltonian. And let n be the number of CIS wavefunctions that we include in our basis. With this ansatz, it is obvious that the dimension of the FVOA-CIS variational ansatz is $1 + n + n \times \text{NOV}$. Thus, even within our reduced post-CIS scheme, one is *not* able to diagonalize the Hamiltonian directly. Instead, one must invoke an iterative Davidson or Davidson-Jacobi [72, 99, 100, 101, 102, 103] algorithm, and focus only on the lowest few excited states (which are, after all, the only relevant states).

5.2.1. Matrix Elements

In terms of analytical expressions, the necessary matrix element for FVOA-CIS are identical to the matrix elements necessary for VOA-CIS. The latter matrix elements have already been published in details elsewhere [7, 55] and are reproduced in the Appendix. In practice, one requires matrix elements of the form $\left\langle \Psi^J_{\rm CIS} a^\dagger_j a_b \left|H\right| a^\dagger_a a_i \Psi^I_{\rm CIS} \right\rangle$. Now,the only meaningful algorithmic difference between a calculation of FVOA-CIS versus VOA-CIS wavefunctions comes from the iterative nature of the former. While a VOA-CIS algorithm permits one to calculate all necessary elements of the form $\langle \Psi^{\rm L} \left|H\right| \Psi^{\rm R} \rangle$ only once (before a large diagonalization), FVOA-CIS works iteratively–so that one must repeated form matrix-vector products of the form $H \left|\Psi^{\rm R}\right\rangle$.

5.2.2. Nonorthogonal Davidson Algorithm

One of the interesting details of the FVOA-CIS algorithm is the need to perform iterative diagonalization in a nonorthogonal basis.

Given hermitian matrices H and S, a generalized (nonorthogonal) diagonalization must satisfy the following equation: $HU = SUE$. In an ideal situation, where H and S are diagonal dominant– i.e. absolute values of the off-diagonals are much smaller compared with the difference of the diagonals– one can achieve cubic convergence with a generalized Davidson Algorithm. The basic idea is the following.

One starts off, somehow, with a trial vector v_i, which is (hopefully) not too far from the true eigenvector y_i of H. Let δ_i be the error. Then, the Rayleigh quotient θ_i and then the residue vector r_i can be written as:

$$\begin{aligned} \theta_i &= \frac{v_i^T H v_i}{v_i^T S v_i} \\ r_i &= H v_i - \theta_i S v_i \\ &= -(H - \theta_i S)\delta_i \end{aligned} \tag{5.5}$$

To find the correction vector δ_i, one must construct the matrix inverse $(H - \theta_i S)^{-1}$, which is why Davidson is called a "shift-and-invert" method. Assuming H and S are diagonal dominant, one can safely approximate $\delta_i \approx -(H_d - \theta_i S_d)^{-1} r_i$, where $H_d(S_d)$ are only the diagonal elements of the $H(S)$ matrix with all off-diagonals set to be zero. If H and S are indeed diagonal dominant, the Davidson method converges cubically and is an effective approach to diagonalization.

The above math assumed we were searching for only one root. To find multiple eigenvectors, one can effectively retain the same procedure. Just as above, one builds and updates a search subspace $\mathcal{V}_k$. Within $\mathcal{V}_k$, one must keep all trial eigenvectors orthogonal. If the dimension of $\mathcal{V}_k$, $\dim(\text{span}(\mathcal{V}_k))$ ever increases to the full dimensionality of the whole space d, one is guaranteed to calculate the exact result but, in practice, convergence is usually achieved far before $\dim(\text{span}(\mathcal{V}_k))$ gets close to d. For the case of the many eigenvectors, the generalized Davidson algorithm in a *nonorthogonal* basis is shown in Alg. 5.1.

Algorithm 5.1 Davidson diagonalization

1: ▷ a set of orthonormal trial vectors

2: Guess the search space $\mathcal{V}_k \equiv \{v_i; i = 1 \cdots n\}$.

3: Interaction matrices H' and S':

$$\begin{cases} H' &= v^T H v \\ S' &= v^T S v \end{cases} \tag{5.6}$$

4: ▷ In the reduced space

5: Generalized diagonalization: $H'y = S'y\Theta$.

6: ▷ Expand the trial vectors in the original (full) basis

7: Ritz vectors: $u = vy$.

8: **for** i= $1 : n$ **do**

9: Residual vector: $r_i \equiv Hu_i - \theta_i S u_i$. ▷ $\theta_i = \Theta_{ii}$

10: **if** $||r_i|| \geq \epsilon$ **then**

11: Correction vector: $t_i = -(H_d - \theta_i S_d)^{-1} r_i$.

12: **end if**

13: **end for**

14: ▷ Check for convergence

15: **if** dim(span($\mathcal{T}_k \equiv \{t_j, j = 1 \cdots m, m \leq n\}$))= 0 **then**

16: exit. ▷ Converged

17: **else**

18: **if** dim(span($\{\mathcal{V}_k, \mathcal{T}_k\}$)) > max(span($\mathcal{V}_k$)) **then**

19: ▷ Shrink the space as needed

20: $\mathcal{V}_k = \{u_i; i = 1 \cdots n\}$.

21: **end if**

22: **end if**

23: New trial space: $\mathcal{V}_k^{'} = \{\mathcal{V}_k, \mathcal{T}_k\}$.

24: Go back to line 3 with $\mathcal{V}_k^{'}$, until convergence on line 16.

Now, the Davidson algorithm is very efficient with the "shift-and-invert" trick, when H and S matrices are diagonal dominant; convergence can be painful otherwise. For a FVOA-CIS calculation, one might wonder about how the Davidson algorithm would perform. After all, the basis vectors in a FVOA-CIS calculation are strongly linearly dependent– so that the absolute value of off-diagonal elements can be comparable or even much bigger than the difference of the diagonal elements. Fortunately, in practice, we have consistently found that convergence is not problematic and from our experience, FVOA-CIS is able to converge in roughly 15 iterations.

5.2.3. FVOA-CIS-G vs FVOA-CIS-O

Before showing the results of FVOA-CIS calculations, there is one final nuance to be discussed, namely how to treat the ground state. There are effectively two possible options. On the one hand, according to Eqn. 5.4, one option is optimize the ground state together with the excited states. Unfortunately, for such an option, we find that vertical excited state energies are usually too large; the ground state is somewhat overstabilized. This result is not surprising, given the spectacular failures of CISDexcited state energies[55]. That being said, the raw errors in FVOA-CIS excitation energies are not terrible (and nothing compared to CISD energies). Henceforward, if the ground state is optimized iteratively along with the excited states (i.e. the Hamiltonian is diagonalized in the basis $\left\{\left|\Phi_{\mathrm{HF}}\right\rangle, \left|\Psi^I_{\mathrm{CIS}}\right\rangle, a^\dagger_a a_i \left|\Psi^I_{\mathrm{CIS}}\right\rangle\right\}$), we will refer to such an algorithm the FVOA-CIS-G option.

Now, a second option is to optimize the excited states alone (i.e. diagonalize the Hamiltonian in the basis $\left\{\left|\Psi^I_{\mathrm{CIS}}\right\rangle, a^\dagger_a a_i \left|\Psi^I_{\mathrm{CIS}}\right\rangle\right\}$), and then, after such optimization, perform one more diagonalization where we include the ground HF state. Such a procedure does ensure that the excited states are orthogonalized relative to the ground state. We will refer to such an algorithm as the FVOA-CIS-O option.

Empirically, we find that FVOA-CIS-G and FVOA-CIS-O excited states are almost always identical, but FVOA-CIS-G and FVOA-CIS-O ground states can be significantly different.

5.3. Results

The FVOA-CIS algorithm just proposed has been implemented in a developmental version of the quantum chemistry package, Q-Chem[75]. As a test, we now report results for a key model system (PYCM) that will stress the ability of the method to recover the correct ratio between charge transfer and non-CT excited states. The molecule PYCM [2-(4-(Propan-2-Ylidene) Cyclohexylidene)Malononitrile] is shown in Fig. 5.1. According to Ref. [54], one can expect a low-lying CT state (where charge is transferred from the methylene unit to the cyano groups) and another low-lying CT state (where the excitation is local to the cyano groups).

5.3.1. Absorption

PYCM can be considered a donor-bridge-acceptor (DBA) system, where the donor (D) is the alkene group and the acceptor (A) is the dicyano group. At the ground state geometry, the lowest excitation (S_1) in PYCM is a HOMO $\rightarrow$ LUMO transition. Since the HOMO sits on the D site and LUMO on the A site, S_1 is a CT state and can be detected experimentally by an absorption peak at 36800 cm^{-1} or 4.56 eV.[54] The locally excited state $A \rightarrow A^*$ is slightly higher, peaking at 43900 cm^{-1} or 5.44 eV. The reported measurements were made at 20°C in n-hexane, which is a nonpolar solvent, so the solvent effect should be minimal.[54]

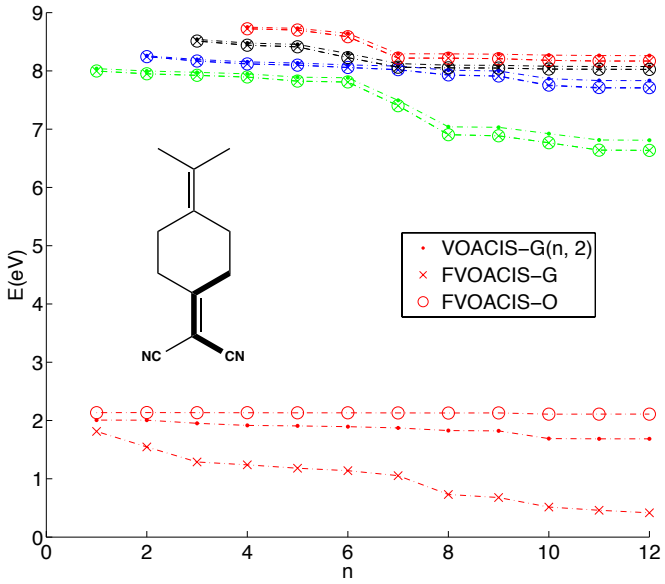

Figure 5.1: FVOA-CIS-G(n), FVOA-CIS-O(n) and VOA-CIS-G(n, 2) energies for PYCM, as a function of n (the number of CIS states included in our active space [see Eqn. 5.4]). The reference energy is $E = -571.5$ a.u.. Each color represents a singlet state $S_i, i \in [0, 3]$. In the limit that $n \to \infty$, all methods will recover the CISD energies. Note that, for all methods, one recovers the correct S_1 state only when we include at least 7 CIS states.

In Fig. 5.1, we plot the FVOA-CIS energies as function of the number of CIS states n included in the active space. For comparison, we also plot VOA-CIS-G(n, 2) energies, which were previously reported in Ref. [55]. The nuclear geometry has been optimized at the MP2 level, For this calculation, and all subsequent calculations, we use the 6-31G* basis and two-electron matrix elements are evaluated through the resolution of the identity [57, 58], with the auxiliary rimp2-cc-pvdz basis set. In Ref. [55] we showed that, for this system, the CIS excited state orderings are completely unreliable. Whereas the CT state S_7 according to CIS, VOA-CIS-G(n, 2) and TD-DFT (functional ωB97x) both (correctly) assert that the CT state should be S_1. Thus, in Fig. 5.1, one can observe a sharp dip in the VOA-CIS S_1 energy around $n = 7$. Moreover, also according to Ref. [55], CISD gives abysmal excitation energies (38.41 eV)[7], because the ground state energy recovers a disproportionate share of the correlation energy; by contrast, VOA-CIS-G(n, 2) achieves a good balance between the ground state and excited states and the excitation energies (5.12 eV)[7] are pretty good. Let us now discuss the new FVOA-CIS results.

A comparison of ground states

From Fig. 5.1, it is clear that, in the treatment of the ground state, VOA-CIS, FVOA-CIS-G, and FVOA-CIS-O all predict different structure. Empirically, it would appear that: $E_g^{\text{FVOA-CIS-G}(n)} < E_g^{\text{VOA-CIS-G}(n,\,2)} < E_g^{\text{FVOA-CIS-O}(n)}$. We believe the first inequality should always hold (for any molecular system): after all, FVOA-CIS-G fully optimizes the ground state energy using all possible double excitations on top of the CIS active space ($a_a^\dagger a_i \left|\Psi_{\text{CIS}}^I\right\rangle$); see Eqn. 5.4. At the same time, for VOA-CIS-G(n, 2), one optimizes using only a much smaller fraction of the doubles space. For this reason, raw excitation energies according to FVOA-CIS-G will (unfortunately) depends strongly on the number of CIS states included in the active space (n), while VOA-CIS-G(n, 2) and FVOA-CIS-O excitation energies will be far less sensitive. Next, for the second inequality, it is not obvious why one should expect $E^{\text{VOA-CIS-G}} < E^{\text{FVOA-CIS-O}}$; both methods would appear to contain very similar amounts of

correlation energy. As such, we are hesitant to make any universal conclusions (from this limited data set).

A comparison of excited states

With regards to excited state energies, FVOA-CIS-G and FVOA-CIS-O energies are almost identical, which is a strong indication that the HF ground state does *not* interact strongly with any one excited state; by contrast, the ground state correlation energy is entirely dynamical in nature. Interestingly, VOA-CIS and FVOA-CIS are also parallel to each other for all values of n and quite close in energy, so that one may conclude that full versus partial orbital adaptation does not significantly affect the quality of the excited states. Thus, the quality of the vertical excitations is defined by the quality the ground state and one's ability to generate a balanced description of the ground state. For $n = 12$, the calculated absorption energies of S_1 are 4.52 eV, 5.12 eV and 6.21 eV according to FVOA-CIS-O, VOA-CIS and FVOA-CIS-G(compared with the experimental value 4.56 eV). For the $S_2 - S_1$ energy gap, all methods give the same value (1.07 eV).

Finally, as we mentioned above, one obvious problem with all of the methods just discussed is the need to include at least 8 CIS states in the calculation ($n \geq 8$) in order to recover a reliable result for S_1. The need for many CIS states can represent a significant computational cost; an alternative approach (based on TD-DFT) will be discussed in Sec. 5.4.

5.3.2. Smooth PES and Emission

PYCM emission spectra are very interesting. Whereas the locally excited state decays radiationlessly, CT state shows a broad structureless fluorescence, whose position and intensity are sensitive to the polar or nonpolar solvents.[54] Verhoeven *et al* expected PYCM to show an avoided crossing between the S_1 and S_2 states, with a cis-trans transformation τ along the ethylenic double bond with reaction coordinate τ (the angle of rotation). Thereafter, around near $\tau = 90°$, Verhoeven *et al* predicted a crossing between the S_1 and S_0 states (as

is the case for ethylene [3, 77]), thus allowing a complete (radiationless) decay back to the ground state. See Figure 7 in Ref. [54] for the intuitive details predicted by Verhoeven.

In Ref. [7], by building an accurate PES along the torsional angle τ (from 0° to 90°), we largely verified the Verhoeven view of electronic relaxation in PYCM. The previously published VOA-CIS data[7] is shown in Fig. 5.2. To construct this graph, we used a nuclear geometry optimized for the S_1 excited state, (at the level of CIS and basis set of 6-31G*), and then, after fixing all other molecular coordinates, we rotated only the dihedral angle τ. The data is shown in Fig. 5.2 for τ ranging from 0° to 100°. As one can see, according to VOA-CIS there is a simple crossing between S_2 and S_1, and a very complicated crossing between S_1 and S_0. We will now follow the same procedure for FVOA-CIS.

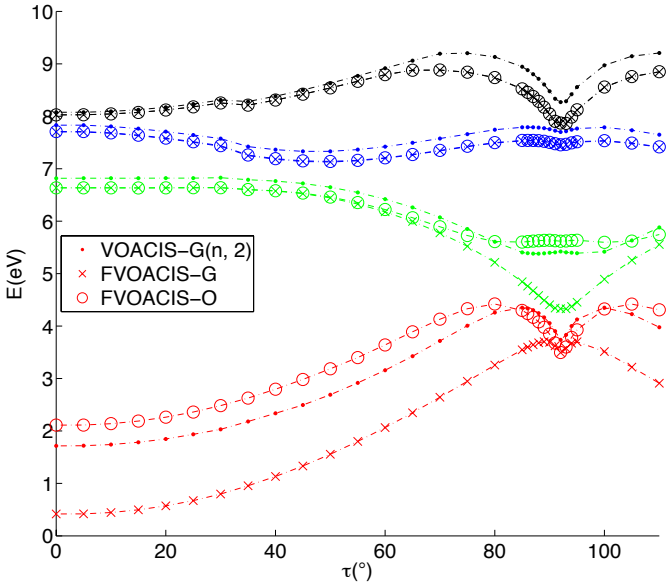

Figure 5.2: VOA-CIS-G(12, 2), FVOA-CIS-G(12) and FVOA-CIS-O(12) energies for PYCM, as a function of torsional angle τ. The reference energy is $E = -571.5$ a.u.. Each color represents a singlet state $S_i, i \in [0, 3]$. Note that only FVOA-CIS-G recovers the correct shape of the $S_1 - S_0$ avoided crossing around $\tau = 90°$.

Ground state - excited state crossing

Fig. 5.2 shows the $S_0 - S_3$ PESs as a function of τ, as predicted from FVOA-CIS-G, FVOA-CIS-O and VOA-CIS. As would be expected, FVOA-CIS-G energies are strictly lower than VOA-CISand FVOA-CIS-Oenergies, and FVOA-CIS-O energies can be larger or smaller than VOA-CIS energies,

Focusing first on the ground state, we find (as before) the FVOA-CIS-G and FVOA-CIS-O can differ a lot– the difference is roughly 1eV far away from the $S_1 - S_0$ crossing. As stated earlier, this difference stems for the overstabiliziation of the CISD ground state. At the same time, the FVOA-CIS-O ground state energy is very close to E_{HF} far away from the $S_1 - S_0$ crossing; the FVOA-CIS-O approach does not significantly add correlation energy if the ground state is well separated from the excited states.

Let us now focus on the crossing region, where $E_1 - E_0$ is very small (around $\tau = 90$). At this geometry, there is a very strong interaction between S_0, S_1 and the ground-state picks up static (and not just dynamic) correlation. Unfortunately, here we find that VOA-CIS and FVOA-CIS-O fail mostly because neither method introduces enough correlation energy to the ground state. Both methods predict an erroneous local minimum in the ground state energy at $\tau = 90$ and the topology does not resemble a typical crossing (as would be expected). Both methods also fail to predict a strong minimum in the S_1 excited state energy at $\tau = 90$. By contrast, when we fully optimize the ground and excited state energies, with FVOA-CIS-G, we find a relatively simple avoided crossing between S_0 and S_1. Overall, this data highlights the fact that, near a $S_1 - S_0$, there is no substitute for full optimization (FVOA-CIS-G).

Relative Excitation Energies

It is important to note that, although FVOA-CIS-G and FVOA-CIS-O S_0 can differ by nearly $1.5eV$, both methods give almost identical predictions for raw excited state energies.

This agreement confirms our intuition that the G/O distinction should *not* affect the relative energies in the excited space. In fact, we find that both FVOA-CIS algorithms are almost always parallel to and thus consistent with VOA-CIS as before. In particular, both FVOA-CIS methods do recover the simple $S_2 - S_1$ crossing around $\tau \approx 40°$.

Thus, in the end, we can make the following conclusions: (i) only the FVOA-CIS-G PESs are fully consistent with the Verhoeven picture of electronic relaxation [54] and recover both the $S_2 - S_1$ and $S_1 - S_0$ crossings; (ii) near the ground-state geometry, the FVOA-CIS-O option gives the best vertical excitation energies ($E_1 - E_0$).

5.4. Discussion: FVOA-CIS with DFT orbitals and TDDFT amplitudes

One of the biggest drawbacks of any post-CIS excited state method is that CIS often yields completely unreliable excited state orderings and, thus, any post-CIS rediagonalization must include a large number of CIS states. For instance, as discussed above, for PYCM the CT enters as S_7 according to CIS. Thus, we must use at least $n \geq 7$ (and $n \geq 10$ is better) for convergence, and the computational cost of FVOA-CIS scales sharply with n. Given this drawback and given the fact that TD-DFT often does a better job in state-ordering (certainly, for PYCM [7]), it is appealing to apply a FVOA-CIS rediagonalization on top of a set of TD-DFT states. In other words, one can simply run the FVOA-CIS algorithm with DFT orbitals (instead of HF orbitals) and TD-DFT amplitudes (in the Tamm-Dancoff approximation) rather than CIS amplitudes. Here, the motivation would be that long-range TDDFT corrections usually do a better job of describing CT states than almost all other options, and thus, with a good functional, TD-DFT states are more likely to be a better starting point for further optimization. For example, Davidson showed long ago that DFT orbitals are closer to Dyson orbitals than HF orbitals[104].

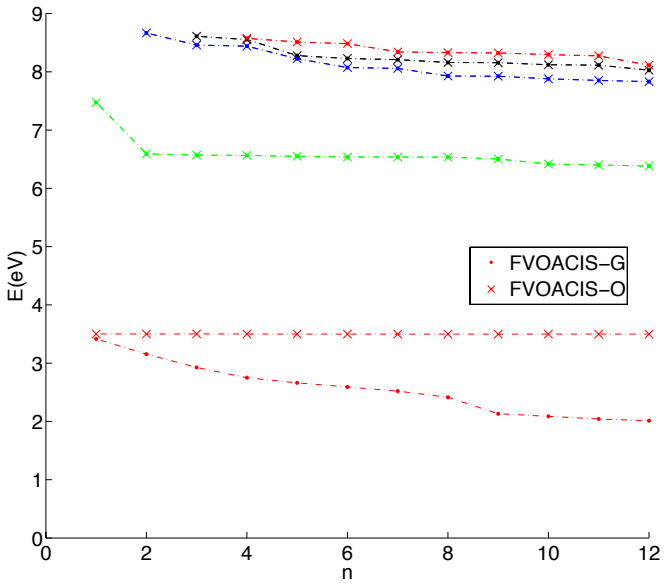

Figure 5.3: FVOA-CIS-G(n) and FVOA-CIS-O(n) energies for PYCM from TDDFT molecular orbitals (ωB97x) and singles amplitudes, as a function of torsional angle n. The reference energy is $E = -571.5$ a.u.. Each color represents a singlet state $S_i, i \in [0, 3]$. Note that, unlike the case of CIS (see Fig. 5.1), there is no state reordering if we use TD-DFT excited states with DFT molecular orbitals to form an active space.

In Fig. 5.3, we graph the FVOA-CIS energies as a function of n, only now using DFT molecular orbitals and TD-DFT/TDA singles amplitudes. Several conclusions are immediate from this graph. First, the FVOA-CIS-G and FVOA-CIS-O ground states do differ for the ground state, just as was discussed above for the case of HF orbitals/CIS amplitudes. Second, and more interestingly, one finds very different behavior when comparing FVOA-CIS excited states. In contrast to the case of HF/CIS, when we use DFT orbitals and TD-DFT/TDA singles amplitudes (with the ωB97x pseudopotential), we clearly do not see any sharp features that indicate state reordering. Within the FVOA-CIS doubles space, rediagonalization using TD-DFT states (rather than CIS states) gives reasonably converged excited state energies with only $n = 2$ (where CIS requires $n \geq 7$). If such improved convergence is general, one might consider replacing a CIS subspace with a TD-DFT/TDA subspace more generally for the computational savings. However, that being said, one should note that the final FVOA-CIS-O energy (as calculated with TD-DFT) is better with HF orbitals rather than TD-DFT orbitals (which is not surprising – TD-DFT states are calculated with pseudopotentials rather than the exact Hamiltonian). Thus, replacing CIS with TD-DFT for a post-TDDFT correction may not be as simple as a free lunch.

5.5. Conclusion

We have presented two slightly different variations of a fully variational orbital adaptation scheme to improve upon CIS excited state energies. The results of our efforts are mixed. Let $\Delta E_1 = E_1 - E_0$. On the one hand, given that FVOA-CIS-G is the only accurate method near a $S_1 - S_0$ avoided crossing (ΔE_1 small), one might recommend the G algorithm for studying photochemistry. On the other hand, given FVOA-CIS-O reproduces better vertical excitation energies for near the equilibrium ground state geometry (ΔE_1 large), one might prefer the O algorithm. In general, neither method is completely satisfactory. With this in mind, it is very tempting to interpolate between these two extreme methods using ΔE_1 as

a guide:

$$\left|\Psi^I_{\text{FVOA-CIS}}\right\rangle = \alpha(\Delta E_1)\left|\Psi^I_{\text{FVOA-CIS-G}}\right\rangle + \beta(\Delta E_1)\left|\Psi^I_{\text{FVOA-CIS-O}}\right\rangle \tag{5.7}$$

Here, one would choose α and β as functions of the energy gap $\Delta E_1 = E_1 - E_0$, such that $\alpha(\Delta E_1) + \beta(\Delta E_1) = 1$. We should then require:

$$\begin{cases} \lim_{\Delta E_1 \to 0} \quad \alpha \quad = 1, & \lim_{\Delta E_1 \to 0} \quad \beta \quad = 0 \\ \lim_{\Delta E_1 \to \infty} \quad \alpha \quad = 0, & \lim_{\Delta E_1 \to \infty} \quad \beta \quad = 1 \end{cases} \tag{5.8}$$

Obviously, fitting FVOA-CIS data with an empirical parameter would make the method no longer strictly *ab initio*. That being said, however, such interpolation might be a good idea in general, given the difficulty of finding a good size-extensive method that is also able to correctly treat ground-excited state crossings. Clearly, the gradient of such an interpolated scheme would be easy to calculate, but a derivative coupling would be difficult. Given the difficulty of reproducing accurate and cheap excited state PESs for photochemistry, future work may well investigate such an interpolated approach.

CHAPTER 6 : Conclusion and Future Directions

In this thesis, we have proposed a series of three different *ab initio* quantum chemistry methods for modelling molecular excited states, especially in the context of photochemistry, and balancing non-charge transfer and charge transfer states:

- Orbital Optimized Configuration Interaction Singles (OO-CIS): Perturbative;
- Variatonal Orbital Adapted Configuration Interaction Singles (VOA-CIS) with 9 options: Variational;
- Fully Variatonal Orbital Adapted Configuration Interaction Singles (FVOA-CIS) with 2 options: Variational.

Each method has been carefully studied and benchmarked in order to assess speed vs. accuracy. We have shown the second and third options are able to balance non-CT vs CT excited state energies. We hope that these methods will play important roles in future electronic structure calculations, and will certainly inspire other post-CIS corrections for wavefunction theory. In addition to any success we have had, there are many low-lying fruits to be seized upon for these current projects:

- **Parallelization.** We have already implemented pieces of code for the algorithms above with OpenMP [105], and we can reduce the wall time needed for medium-sized molecules. We are reasonably confident, however, that the total wall time can be further optimized, either with OpenMP or MPI.
- **Analytic Gradient.** As mentioned in Chapter 5, perhaps *the* primary motivation for a *fully* variational FVOA-CIS method is the need for globally smooth PESs with analytical gradient. With a fully variational method, constructing a gradient should now be both practical and numerically stable.
- **Conical Intersections.** Though Chapter 4 and Chapter 5 provide a demonstration of the VOA-CIS and FVOA-CIS algorithms near an avoided crossing, no applications have been made yet regarding true conical intersections. Such calculations might be

very instructing as far as assessing how the location of conical intersections change when correlation energy is included at a higher level.

- **Chemical Dynamics.** Finally, our group has done a lot of work in the realm of chemical dynamics, but thus far all *ab initio* work has been done only at the CIS theoretical level– presumably limited by the huge computational cost of electronic structure. Once better parallelization is realized, one would love to explore chemical dynamics with optimal PESs. Our instinct is that, using VOA-CIS or FVOA-CIS, one might well discover some rich new physics.

BIBLIOGRAPHY

[1] D. Casanova, Y. M. Rhee, and M. Head-Gordon, *J. Chem. Phys.* **128**, 164106 (2008).

[2] M. Head-Gordon, R. J. Rico, M. Oumi, and T. J. Lee, *Chem. Phys. Lett.* **219**, 21 (1994).

[3] M. Barbatti, J. Paier, and H. Lischka, *J. Chem. Phys.* **121**, 11614 (2004).

[4] M. Schreiber, M. R. Silva-Junior, S. P. Sauer, and W. Thiel, *J. Chem. Phys.* **128**, 134110 (2008).

[5] D. Casanova and M. Head-Gordon, *J. Chem. Phys.* **129**, 064104 (2008).

[6] Because of its large size, we were unable to obtain the exact CISD energies for the PYCM molecule in Sec. 4.1.1. However, we estimated the CISD energies for $S_i, i \in \{0, 1, 2\}$ in two different (and consistent) ways. First we ran exact CISD calculations with Q-Chem; the residuals of these calculations have not converged even after 30 iterations, even though the energies "appear converged" to within 0.01 eV. Second, with the GAMESS program, we ran three different CISD calculations, each with a different number of frozen (inactive) occupied orbitals: namely, $40, 35$ and 30. These numbers can be fit quite well with a linear fit. Since the true number of core orbitals for the PYCM molecule is 14, we extrapolated our frozen core values to the case of 14 core orbitals. Both approaches above gave very similar results (differing by less than 0.6 eV). In Fig. 4.1, we plot the (as of yet not fully converged) Q-Chem data.

[7] X. Liu and J. E. Subotnik, *J. Chem. Theory Comp.* **10**, 1004 (2014).

[8] A. Szabo and N. Ostlund, *Modern Quantum Chemistry: Introduction to Advanced Electronic Structure Theory* (Dover, New Jersey, 1996).

[9] J. J. Sakurai, *Modern Quantum Mechanics* (Addison Wesley, 1993).

[10] I. N. Levine, *Quantum Chemistry* (Prentice Hall; 7 edition, 2013).

[11] A. Nitzan, *Chemical Dynamics in Condensed Phases* (Oxford University Press, USA, 2006).

[12] C. A. Mead and D. G. Truhlar, *J. Chem. Phys.* **77**, 6090 (1982).

[13] M. D. Newton, *Chem. Rev.* **91**, 767 (1991).

[14] M. Baer, *Chem. Phys. Lett.* **35**, 112 (1975).

[15] T. V. Voorhis, T. Kowalczyk, B. Kaduk, L. P. Wang, C. L. Cheng, and Q. Wu, *Ann. Rev. Phys. Chem.* **61**, 149 (2010).

[16] J. E. Subotnik, S. Yeganeh, R. J. Cave, and M. A. Ratner, *J. Chem. Phys.* **129**, 244101 (2008).

[17] R. J. Cave and M. D. Newton, *Chem. Phys. Lett.* **249**, 15 (1996).

[18] A. A. Voityuk and N. Rosch, *J. Chem. Phys.* **117**, 5607 (2002).

[19] C. P. Hsu, Z. Q. You, and H. C. Chen, *J. Phys. Chem. C* **112**, 1204 (2008).

[20] H. C. Chen, Z. Q. You, and C. P. Hsu, *J. Chem. Phys.* **129**, 084708 (2008).

[21] C. P. Hsu, Acc. of Chem. Res. **42**, 509 (2009).

[22] Q. Wu and T. VanVoorhis, *J. Chem. Theory Comp.* **2**, 765 (2006).

[23] J. E. Subotnik, R. J. Cave, R. P. Steele, and N. Shenvi, *J. Chem. Phys.* **130**, 234102 (2009).

[24] C. Edmiston and K. Ruedenberg, Reviews of Modern Physics **35**, 457 (1963).

[25] J. M. Foster and S. F. Boys, Reviews of Modern Physics **32**, 300 (1960).

[26] S. F. Boys, in *Quantum Theory of Atoms, Molecules and the Solid State*, edited by P. Lowdin (Academic Press, NY, 1966), p. 253.

[27] S. Fatehi, E. Alguire, and J. E. Subotnik, *J. Chem. Phys.* **139**, 124112 (2013).

[28] E. Alguire, S. Fatehi, Y. Shao, and J. E. Subotnik, *J. Phys. Chem. A* **118**, 11891 (2014).

[29] J. E. Subotnik, *J. Chem. Phys.* **135**, 071104 (2011).

[30] X. Liu, S. Fatehi, Y. Shao, B. S. Veldkamp, and J. E. Subotnik, *J. Chem. Phys.* **136**, 161101 (2012).

[31] L. Goerigk and S. Grimme, *J. Chem. Phys.* **132**, 184103 (2010).

[32] J. E. Subotnik, J. Vura-Weis, A. Sodt, and M. A. Ratner, *J. Phys. Chem. A* **114**, 8665 (2010).

[33] Z. Q. You and C. P. Hsu, *J. Chem. Phys.* **133**, 074105 (2010).

[34] A. Dreuw, J. L. Weisman, and M. Head-Gordon, *J. Chem. Phys.* **119**, 2943 (2003).

[35] M. Casida, in *Recent Advances in Density Funtional Methods*, edited by D. P. Chong (World Scientific, 1995), vol. 1, pp. 155–192.

[36] A. Dreuw and M. Head-Gordon, *J. Am. Chem. Soc.* **126**, 4007 (2004).

[37] R. J. Magyar and S. Tretiak, *J. Chem. Theory Comp.* **3**, 976 (2007).

[38] J. Neugebauer, M. J. Louwerse, E. J. Baerends, and T. A. Wesolowski, *J. Chem. Phys.* **122**, 094115 (2005).

[39] A. W. Lange and J. M. Herbert, *J. Chem. Theory Comp.* **3**, 1680 (2007).

[40] L. Bernasconi, M. Sprik, and J. Hutter, *J. Chem. Phys.* **119**, 12417 (2003).

[41] A. Hesselmann, A. Ipatov, and A. Görling, *Phys. Rev. Rev. A* **80**, 012507 (2009).

[42] N. T. Maitra and D. Tempel, *J. Chem. Phys.* **125**, 184111 (2006).

[43] M. J. G. Peach, P. Benfield, T. Helgaker, and D. J. Tozer, *J. Chem. Phys.* **128**, 044118 (2008).

[44] P. Wiggins, J. A. G. Williams, and D. J. Tozer, *J. Chem. Phys.* **131**, 091101 (2009).

[45] R. M. Richard and J. M. Herbert, *J. Chem. Theory Comp.* **7**, 1296 (2011).

[46] T. M. Henderson, B. G. Janesko, and G. E. Scuseria, *J. Chem. Phys.* **128**, 194105 (2008).

[47] J. D. Chai and M. Head-Gordon, *J. Chem. Phys.* **128**, 084106 (2008).

[48] M. A. Rohrdanz and J. M. Herbert, *J. Chem. Phys.* **129**, 034107 (2008).

[49] R. Baer, E. Livshits, and U. Salzner, *Ann. Rev. Phys. Chem.* **61**, 85 (2010).

[50] M. Head-Gordon, A. M. Graña, D. Maurice, and C. A. White, *J. Phys. Chem.* **99**, 14261 (1995).

[51] P. Pulay, in *Modern Electronic Structure Theory Part II*, edited by D. Yarkony (World Scientific Publishing, Singapore, 1995), p. 1191.

[52] D. Maurice, *Single electron theories of excited states* (University of California, Berkeley, 1998).

[53] N. C. Handy and H. F. Schaefer, *J. Chem. Phys.* **81**, 5031 (1984).

[54] P. Pasman, F. Rob, and J. W. Verhoeven, *J. Am. Chem. Soc.* **104**, 5127 (1982).

[55] X. Liu, Q. Ou, E. Alguire, and J. E. Subotnik, *J. Chem. Phys.* **138**, 221105 (2013).

[56] J. B. Foresman, M. Head-Gordon, J. A. Pople, and M. J. Frisch, *J. Phys. Chem.* **96**, 135 (1992).

[57] O. Vahtras, J. Almlöf, and M. W. Feyereisen, *Chem. Phys. Lett.* **213**, 514 (1993).

[58] M. Feyereisen, G. Fitzgerald, and A. Komornicki, *Chem. Phys. Lett.* **208**, 359 (1993).

[59] B. Helmich and C. Hattig, *J. Chem. Phys.* **135**, 214106 (2011).

[60] R. A. Marcus, *J. Phys. Chem.* **67**, 853 (1963).

[61] R. A. Marcus and N. Sutin, Biochimica et Biophysica Acta **811**, 265 (1985).

[62] M. Head-Gordon, M. Oumi, and D. Maurice, *Mol. Phys.* **96**, 593 (1999).

[63] C. Hattig, **50**, 37 (2005).

[64] O. Christiansen, H. Koch, and P. Jorgensen, *Chem. Phys. Lett.* **243**, 409 (1995).

[65] D. Kats, T. Korona, and M. Schutz, *J. Chem. Phys.* **125**, 104106 (2006).

[66] B. Helmich and C. Hattig, *J. Chem. Phys.* **139**, 084114 (2013).

[67] J. Schirmer, *Phys. Rev. Rev. A* **26**, 2395 (1981).

[68] J. H. Starcke, M. Wormit, and A. Dreuw, *J. Chem. Phys.* **130**, 024104 (2009).

[69] J. Schirmer and A. B. Trofimov, *J. Chem. Phys.* **120**, 11449 (2004).

[70] A. D. Dutoi, L. S. Cederbaum, M. Wormit, J. H. Starcke, and A. Dreuw, *J. Chem. Phys.* **132**, 144302 (2010).

[71] A. B. Trofimov and J. Schirmer, **28**, 2299 (1995).

[72] S. R. Langhoff and E. R. Davidson, International Journal of Quantum Chemsitry **8**, 61 (1974).

[73] H. Koch, H. Jensen, P. Jorgensen, and T. Helgaker, *J. Chem. Phys.* **93**, 3345 (1990).

[74] D. Laikov and S. Matsika, *Chem. Phys. Lett.* **448**, 132 (2007).

[75] Y. Shao, L. Fusti-Molnar, Y. Jung, J. Kussmann, C. Ochsenfeld, S. T. Brown, A. T. B. Gilbert, L. V. Slipchenko, S. V. Levchenko, D. P. O'Neill, et al., *Phys. Chem. Chem. Phys.* **8**, 3172 (2006).

[76] N. J. Turro, V. Ramamurthy, and J. C. Scaiano, *Principles of Molecular Photochemistry* (University Science Books, 2008).

[77] T. Mori, W. J. Glover, M. S. Schuurman, and T. J. Martinez, *J. Phys. Chem. A* **116**, 2808 (2012).

[78] R. Crespo, H. Teramae, D. Antic, and J. Michl, Chemical Physics **244**, 203 (1999).

[79] H.-J. Werner and P. J. Knowles, *J. Chem. Phys.* **89**, 5803 (1988).

[80] A. D. Mclachlan and M. A. Ball, Reviews of Modern Physics **36**, 844 (1964).

[81] A. Dreuw and M. Head-Gordon, *Chem. Rev.* **105**, 4009 (2005).

[82] M. Bixon, J. Jortner, and J. W. Verhoeven, *J. Am. Chem. Soc.* **16**, 7349 (1994).

[83] A. I. Krylov, *Ann. Rev. Phys. Chem.* **59**, 433 (2008).

[84] A. D. Becke, *J. Chem. Phys.* **98**, 1372 (1993).

[85] A. Savin, in *Recent Advances in Density Funtional Methods*, edited by D. P. Chong (World Scientific, 1995), pp. 129–154.

[86] A. Savin and H. J. Flad, International Journal of Quantum Chemsitry **56**, 327 (1995).

[87] P. M. W. Gill, R. D. Adamson, and J. A. Pople, *Mol. Phys.* **88**, 1005 (1996).

[88] H. Iikura, T. Tsuneda, T. Yanai, , and K. Hirao, *J. Chem. Phys.* **120**, 8425 (2004).

[89] J. W. Song, T. Hirosawa, T. Tsuneda, and K. Hirao, *J. Chem. Phys.* **126**, 154105 (2007).

[90] T. Yanai, D. P. Tew, and N. C. Handy, *Chem. Phys. Lett.* **393**, 51 (2004).

[91] O. A. Vydrov, J. Heyd, A. V. Krukau, and G. E. Scuseria, *J. Chem. Phys.* **125**, 234109 (1006).

[92] M. A. Rohrdanz, K. M. Martins, and J. M. Herbert, *J. Chem. Phys.* **130**, 054112 (2009).

[93] A. W. Lange, M. A. Rohrdanz, and J. M. Herbert, *J. Phys. Chem. B* **112**, 6304 (2008).

[94] T. J. Martinez, M. Ben-Nun, and R. D. Levine, *J. Phys. Chem.* **100**, 7884 (1996).

[95] M. Ben-Nun and T. J. Martinez, *J. Chem. Phys.* **112**, 6113 (2000).

[96] S. Saebo and P. Pulay, *Ann. Rev. Phys. Chem.* **44**, 213 (1993).

[97] X. Liu and J. Subotnik (2015), unpublished data.

[98] S. Fatehi, E. Alguire, and J. E. Subotnik, *J. Chem. Phys.* **139**, 124112 (2013).

[99] E. R. Davidson, J. Comp. Phys. **17**, 87 (1975).

[100] M. L. Leininger, C. D. Sherrill, W. D. Allen, , and H. F. Schaefer, Journal of Computational Chemistry **22**, 1574 (2001).

[101] Y. Notay, SIAM J. Matrix Anal. Appl. **26**, 522 (2006).

[102] E. R. Davidson, *J. Chem. Phys.* **46**, 3320 (1967).

[103] R. J. Cave, in *Modern Electronic Structure Theory and Applications in Organic Chemistry*, edited by E. R. Davidson (World Scientific, Singapore, 1997), pp. 197–256.

[104] P. R. Koren, F. W. Chen, and E. R. Davidson, *Mol. Phys.* **99**, 1329 (2001).

[105] B. Chapman, G. Jost, and R. van van der Pas, *Using OpenMP: Portable Shared Memory Parallel Programming (Scientific and Engineering Computation)* (The MIT Press, MA, 2007).